Springer Theses
Recognizing Outstanding Ph.D. Research

Davide Michieletto

Topological Interactions in Ring Polymers

Springer

Springer Theses

Recognizing Outstanding Ph.D. Research

Aims and Scope

The series "Springer Theses" brings together a selection of the very best Ph.D. theses from around the world and across the physical sciences. Nominated and endorsed by two recognized specialists, each published volume has been selected for its scientific excellence and the high impact of its contents for the pertinent field of research. For greater accessibility to non-specialists, the published versions include an extended introduction, as well as a foreword by the student's supervisor explaining the special relevance of the work for the field. As a whole, the series will provide a valuable resource both for newcomers to the research fields described, and for other scientists seeking detailed background information on special questions. Finally, it provides an accredited documentation of the valuable contributions made by today's younger generation of scientists.

Theses are accepted into the series by invited nomination only and must fulfill all of the following criteria

- They must be written in good English.
- The topic should fall within the confines of Chemistry, Physics, Earth Sciences, Engineering and related interdisciplinary fields such as Materials, Nanoscience, Chemical Engineering, Complex Systems and Biophysics.
- The work reported in the thesis must represent a significant scientific advance.
- If the thesis includes previously published material, permission to reproduce this must be gained from the respective copyright holder.
- They must have been examined and passed during the 12 months prior to nomination.
- Each thesis should include a foreword by the supervisor outlining the significance of its content.
- The theses should have a clearly defined structure including an introduction accessible to scientists not expert in that particular field.

More information about this series at http://www.springer.com/series/8790

Davide Michieletto

Topological Interactions in Ring Polymers

Doctoral Thesis accepted by
the University of Warwick, Coventry, UK

Springer

Author
Dr. Davide Michieletto
School of Physics and Astronomy
University of Edinburgh
Edinburgh
UK

Supervisor
Prof. Matthew S. Turner
Department of Physics
University of Warwick
Coventry
UK

ISSN 2190-5053 ISSN 2190-5061 (electronic)
Springer Theses
ISBN 978-3-319-41041-8 ISBN 978-3-319-41042-5 (eBook)
DOI 10.1007/978-3-319-41042-5

Library of Congress Control Number: 2016942899

Printed on acid-free paper

This Springer imprint is published by Springer Nature
The registered company is Springer International Publishing AG Switzerland

Publications related to this thesis:

(1) D. Michieletto, D. Marenduzzo, E. Orlandini, G.P. Alexander, M.S. Turner, *Threading Dynamics of Ring Polymers in a Gel*, ACS Macro Lett., **3**, 255–259 (2014)

(2) D. Michieletto, D. Marenduzzo, E. Orlandini, G.P. Alexander, M.S. Turner, *Dynamics of Self-Threading Polymers in a Gel*, Soft Matter, **10**, 5936–5944 (2014)

(3) D. Michieletto, E. Orlandini, M.S. Turner, *Rings in Random Environments: Sensing Disorder Through Topology*, Soft Matter, **11**, 1100–1106 (2015)

(4) D. Michieletto, D. Marenduzzo, E. Orlandini, *Is the Kinetoplast DNA a Percolating Network of Linked Rings at its Critical Point?.,* Phys. Biol., **12**, 036001 (2015)

(5) D. Michieletto, D. Marenduzzo, E. Orlandini, *Topological Patterns in Two-dimensional Gel Electrophoresis of DNA Knots*, Proc. Natl. Acad. Sci. USA, **112** (40), E5471–E5477 (2015)

(6) D. Michieletto and M.S. Turner, *A Topologically Driven Glass in Ring Polymers,* Proc. Natl. Acad. Sci. USA, doi:10.1073/pnas.1520665113 (2016)

Supervisor's Foreword

The theoretical methods needed to describe long, flexible polymers started to be developed in the middle of the twentieth century with great names like Flory, Edwards and de Gennes all making important contributions. The arrival of powerful computer simulations in recent decades has allowed us to make further progress by a combination of coarse-graining and either brute-force solution of dynamical equations or ensemble-averaging. Much of the field is now mature and, broadly speaking, the physics of polymers is fairly well understood. However, there is one important island of intellectual difficulty still stubbornly resisting erosion and that is the physics of ring polymers. Rings are polymers that are closed into a long, cyclic macromolecule with no ends and are an important archetype of topological complexity in polymers in general. Ring polymers can be synthesised in the lab or isolated from living systems, such as the plasmids found in bacteria or the exotic chain mail-like genetic material of *Kinetoplastida*. What makes understanding rings difficult is the topological constraint associated with their uncrossability. That is to say that the global topological state of the system at synthesis, with whatever knots and/or links that might then be present, must be maintained for all later times if the polymers cannot break, fuse or cross through one another. An important special case, that is the primary focus of this thesis is that when the polymers all remain unknotted with themselves and unlinked from each other. This is the ensemble most often studied in the literature and, like linear polymers (but in contrast with chain-mail-like topologies), it is ultimately liquid-like, i.e. as it has no zero frequency shear modulus, at least for temperatures above a glass transition temperature, depending (only) on the chain chemistry, below which microscopic molecular motion is lost. What is difficult about topological constraints is that they are highly non-local. If one wants to determine whether two ring polymer conformations are topologically permitted or not, e.g. for inclusion in an ensemble average, one needs information on the entire spatial configuration of both of them. While this makes analytical progress challenging we can still turn to computer simulations.

If one reads the literature from the 80s and 90s one starts to find the first few references of the possibility that inter-ring threadings could occur and that, were

these threading to proliferate, an unusual "tangled" state of matter might arise. This possibility greatly intrigued me when I was still a graduate student in the group at the Cavendish Laboratory in Cambridge led by Sir Sam Edwards. The subsequent development of more efficient computers might partially excuse the fact that it took 20 years for this interest to find an outlet! It is particularly pleasing to see a similar interest in these systems sparked in Davide Michieletto who has produced a thesis that is a *tour de force* for the field. At the risk of sentimentality it is also satisfying to see the baton of polymer theory from the Halcyon days in Cambridge handed down at least one more generation.

This thesis is mainly concerned with computer simulation of unlinked, unknotted ring polymers in various ensembles, these being ring polymers in neutral solvent, ring polymers in perfectly ordered gels and ring polymers in imperfect gels. Why bring gels into the picture? One reason is that they model the environment present in the ubiquitous separation technique known as gel electrophoresis. A more compelling reason is discussed in this thesis: The gel meshwork allows for the formulation of a mathematically precise definition of inter-ring threading, in which one long ring penetrates through another, in much the same way as when one rubber band is threaded through a second; the threaded, or "passive", ring is pinned for as long as the threading, or "active" ring, remains in place. The active ring can diffuse freely while the passive ring can make any (topology-preserving) move provided it does not cross through the active polymer at the site of the penetration. These kinds of threadings have been notoriously difficult to pin down mathematically since, by construction, they do not alter the topological state of the system. It has therefore been difficult to say what the essence of a threading really is and hence which rearrangements produce (or remove) them and which do not.

There are many interesting results in this thesis but, in the interests of keeping this introduction to a modest length, I will focus on the two that were most exciting for me. The first of these is related to exactly this matter—the definition of a threading. Davide's brilliant insight was to use the gel architecture to define cells, through which the rings must lie. When one ring threads a second this alters the topological state of a proxy system: the polymer contours that lie within the cell, truncated at the walls of the cell and then appropriately extended so as to be closed outside the cell. This allows a rigorous definition of threading and, therefore, threading to be counted and tracked in computer simulations of rings moving inside gels. Davide was able to show that threadings do indeed occur and that they proliferate in long rings with a number per ring that appears to be almost exactly proportional to the ring polymer contour length. Combined with evidence for slowing down, due to the requirement that threadings be undone in a particular order, this is perhaps the best evidence to date for the emergence of a highly interpenetrating state in which the longest relaxation times might ultimately scale exponentially in, rather than as a power of, the polymer length. We refer to such a system as a *topological glass* as they would have the extremely unusual property of having exponentially slow (somewhat glassy) relaxation times but show no slowing down in the microscopic dynamics, as the temperature is assumed to remain well above the classical glass transition temperature throughout.

The second really important result in this thesis is concerned with long ring polymers in neutral solvent at high concentrations where the polymer coils are strongly overlapping. Do the threading that were observed in the presence of the gel also occur in this ensemble? A new approach was required as the gel is no longer present and its architecture cannot therefore be exploited as before. Davide's second really brilliant insight was to realise that threading can be identified by artificially immobilising ("freezing") a fraction of the ring polymers in an equilibrated simulation of rings so that they have no microscopic freedom to move at all. If threading are present then some of them will involve a ring in the frozen fraction threading through one that is unfrozen. In this case the unfrozen chain will effectively experience a permanent threading and be pinned at the site of that threading throughout the simulation. The pinned chain can still move but can only diffuse away a distance that is of the order of the equilibrium coil size as the pinning delivered by the frozen ring must remain somewhere within its contour. Davide then showed that such confined diffusion can be observed in these systems of rings and, by construction that such threading would have been present, at least transiently, in the equilibrated system prior to (partial) freezing. This essentially proves, for the first time, the existence of threadings in concentrated ring systems and opens up an entire field of study concerned with the properties of these threaded systems and the topological glass that might eventually emerge from them.

Coventry, UK
April 2016

Prof. Matthew S. Turner

Abstract

Ring polymers offer a richness of behaviours that are of broad interest and have deep consequences in many fields of Science. In this thesis I investigate some general and universal properties, i.e. independent of the chemical nature of the polymers, emerging from systems made of a collection of rings. These will be studied by using methods of equilibrium and non-equilibrium Statistical Mechanics together with Molecular Dynamics simulations of coarse-grained models for the systems under investigation. Within these frameworks, important questions regarding the macroscopic behaviour of ring-shaped polymers have yet to find a satisfactory answer. The work presented in this Thesis finds its principal motivations in problems arising in Material Science, the so-called "melt" of rings, and in Biology, such as the organisation of mitochondrial DNA in some organisms and the mechanisms governing the electrophoretic separation of DNA samples in gels. There are several theoretical challenges in these fields which represent state-of-the-art scientific research and whose partial answers are provided in the work presented in this Thesis. One of the major achievements of the work presented is the general understanding of the role played by topological properties, i.e. those invariant under smooth deformations of the polymer contour, on the macroscopic behaviour of the investigated systems. Finally, the conclusions drawn from the presented work can have important scientific consequences as they may ultimately lead to a more complete understanding of complicated issues in Biology and to the design of next-generation soft materials.

Acknowledgments

There is a number of people that I would like to thank and for a number of reasons. It is very likely that the following acknowledgements will not do justice to all of them, but I will try.

I believe that the first to be thanked, both emotionally and chronologically, should be my family. No matter the difficulties and preoccupations throughout the (long) period of my education, they always offered their indefatigable support, and for that I am glad and grateful. I would like to thank in particular my parents, grandparents and uncles who spent a considerable part of their life with me since when I was very young and had therefore shaped my character and attitude towards life. I am satisfied with the person that I have become and I owe a big part of this to you.

Second, I would like to warmly thank Stefania for her talent to bring out the best in me. You have a mysterious ability of being both, a pillow to my mind and a fire that kindles my soul and that drives me towards new goals and adventures. I most certainly would not be the person I am if it wasn't for you, and I am exceedingly pleased that you have become my best friend and partner since very early in my life.

I would also like to thank the many brilliant persons who I am honoured to call friends. I am glad that the physical distance separating us has not weakened our bonds.

Finally, I would like to thank my supervisor Matthew for his supporting and always too kind words throughout the Ph.D.; Gareth for having taught me to look for the beauty in all the little things; Davide and Enzo for their positive and constant support and for acting not only as mentors but also as friends and fellow countrymen. I thank all of them for sharing their time and precious insight when I was in need of ideas and seeking inspiration.

Contents

Chapter 1
Introduction

Io stimo piú il trovar un vero, benché di cosa leggiera, che'l disputar lungamente delle massime questioni senza conseguir veritá nissuna.

G. Galilei

Polymers are ubiquitous in Nature. They consist of a collection of many simple units (from the Greek word for "many" *poly* and for "unit" *mer*) and because of this, they are among the most simple examples of physical cooperativity. Polymers are made of repetitive patterns which make them easy to design, while their length can reach the million of units. Polymers can be thought of as very early examples of self-replicating objects: Given a single unit (a monomer) and enough substrate to form more units, a long sequence of monomers is bound to appear and eventually this can even break up forming many copies of itself. Nature has exploited this self-replicating ability by giving polymers a central role in Biology.

Examples of biopolymers, or polymers produced by living organisms, are virtually endless: polysaccharides such as cellulose, starch and glycogen and, in general, carbohydrates are polymers made of repeating units which originate from the chemical group of monosaccharides such as glucose and are used as energy storage in mammals or scaffolding in plants. Filaments made of actin are polymers made up of proteins which, acting in concert with myosin, allow muscles to contract and extend. Microtubules are hollow and chiral polymers found throughout the cytoplasm formed as a long and dynamic self-assembly of tubulin which are crucial for intracellular transport and mitosis. Finally, possibly the most famous biopolymer in Nature is the deoxyribonucleic acid, or DNA, which is made as a collection of four nucleotides.

I prefer finding something true, although of small importance, rather than keep debating on the major issues failing to achieve any truth.

D. Michieletto, *Topological Interactions in Ring Polymers*, Springer Theses,
DOI 10.1007/978-3-319-41042-5_1

DNA is an unparalleled example of polymers ability to self-replicate and to store information (Hurst and Dawkins 1992; Alberts et al. 2014).

The self-replicating property of polymers is one of the many features which are fascinating about them. Ancient mesoamericans had already harnessed one of their other crucial properties. They discovered that the liquid sap extracted from the hevea tree would become elastic and resist tension once dried. From a microscopic point of view, they were witnessing the first instances of vulcanisation, which is nowadays widely used to make, among other things, shoes and tyres. The process for which cross-linking a polymeric liquid would confer elastic properties to it would have been fully understood only 3500 years later, around 1850 (Hosler et al. 1999).

Another pivotal feature of polymers is that some of them are easy to design and cheap to synthesise. As a consequence, their artificial realisation soon started to attract economic interest. During the Second World War the production of synthetic fibres such as nylon and polyester received an important incentive in order to substitute natural counterparts such as silk, cotton and wool. At the same time, countries strongly encouraged and generously financed scientific research on polymers in order to produce more advanced forms of artificial polymers and materials. This resulted in the first Nobel price in Polymer Science given to Hermann Studinger in 1953 for understanding that polymers were made of atoms held together by covalent bonds (Staudinger 1920).

Two of the polymers that are nowadays most abundantly produced in the world are polyethylene and polystyrene. These are made by long sequences of the simple repeating units shown in Fig. 1.1. A common problem in synthesising these long chains is branching: sometimes multi-functional units such as that in Fig. 1.1c appear and create unwanted side-chains. When this problem is avoided, *linear* chains such as that in Fig. 1.1d are produced. Other times, more complex topologies such as *branched*, *star* or *comb* polymers are generated (Fig. 1.2).

In the last fifty years a number of important scientists spent part of their careers trying to understand macroscopic properties of systems made of polymers. Two of these, Paul Flory and Pierre-Gilles de Gennes have been awarded with Nobel prices for their theoretical work in 1974 and 1991, respectively. Others, such as Sir Sam Edwards and Masao Doi, are worldly renowned for their contributions to Polymer Physics.

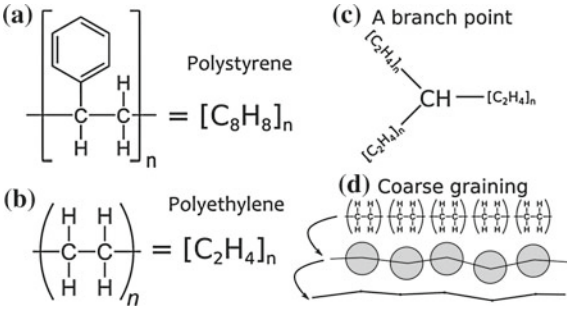

Fig. 1.1 **a**, **b** Examples of artificial polymers: skeletal and chemical formulae for polyethylene and polystyrene molecules. **c** Example of a branch point in polyethylene. **d** A linear polyethylene chain and coarse graining of its chemical details

Fig. 1.2 Polymers with different topologies. From *left* to *right*: linear, star, branched (quenched), circular or ring, linked and knotted

One of the first steps toward the formulation of a polymer theory is selecting the right level of description. While understanding the role of chemical and local details is crucial whenever one wants to optimise the production of a specific material or enhance a feature of a given polymer, global and general properties are the only ones truly necessary for understanding universal polymer features (Gennes 1971). This process is often known with the general name of "coarse-graining" (Fig. 1.1d) and will be extensively employed in this thesis as mean to simplify the computational modelling and achieve more general and universal results. Details such as chemical bonds or type of atoms forming the chains are often neglected in physical descriptions of polymers, while the polymerisation index, i.e. the length of the sequence of monomers, or the stiffness of the chain are taken into account accurately, as they have an universal, i.e. system independent, effect on the properties of a polymer.

The largest part of the theoretical work in the past decades has been focused on systems made of linear polymers. The behaviour of linear polymers in good solvent and sparse solutions is well captured by the Rouse-Zimm polymer model (Gennes 1971) while the case of dense solutions, or melts, has been very successfully understood in terms of the *reptation* model (Doi and Edwards 1998), sketched in Fig. 1.3.

According to this theory, a linear polymer in a dense solution of other chains is constrained by the neighbouring polymers in an effective "tube", its transversal motion being restricted all along its contour. The dynamics of the chain is then allowed by the "curvilinear" diffusion of defects that can flow up and down the polymer backbone (Fig. 1.3a). As a result of such motion, the polymer itself diffuses along the tube and its ends free themselves from the transversal constraints, exploring new regions of the surrounding space (Fig. 1.3b). This leads the chain to "reptate" (from the Latin *reptare*, to creep), through the obstacles and eventually renew the tube (Fig. 1.3c). While this motion takes place, a smaller and smaller section of the original chain will still be confined within the initial tube (Fig. 1.3d), finally leading to a completely renewed and uncorrelated configuration. Any stress that had been applied at the initial time is now completely relaxed through the curvilinear motion of the defects.

The time required for the chain to undergo this process is called the "reptation time" and it is proportional to the system viscosity η, readily measurable in experiments. According to the reptation theory, these two quantities obey the scaling $\eta \sim \tau_{\text{rep}} \sim M^3$, with M being the chains polymerisation length. Experimental findings instead suggest a slightly higher value of $M^{3.4}$. This behaviour was captured through a further refinement of the reptation theory, also referred to as "double reptation", which takes into account the reorganisation of the tubes surrounding any

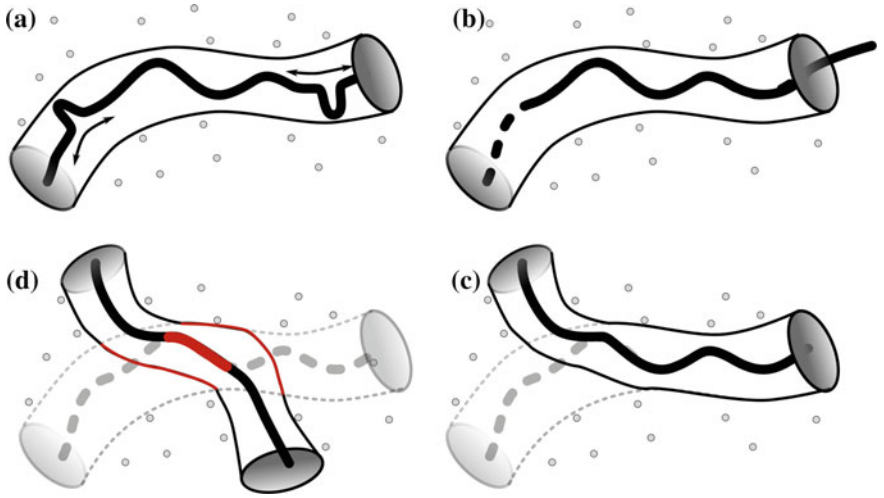

Fig. 1.3 Reptation mechanism for linear polymers in dense solutions. **a** A linear polymer is surrounded by neighbouring chains (*grey dots*) which act as an effective "tube" forcing the polymer to perform a 1D diffusion along its backbone. **b** The polymer can retract the tube by freeing its ends. **c** The tube is renewed whenever the chain explores new regions of space. **d** Both ends contribute to the tube renewal. As time passes, the section still contained in the original tube (highlighted in *red*) becomes smaller and smaller and the chain de-correlates from its starting configuration

given chain, leading to an effective constraint release (Viovy 1985). One of the most important advances brought by the reptation theory is the fact that seemingly different systems, such as dense solution of linear, branched or star polymers and even cross-linked polymer systems, can be described in a unified theory (Doi and Edwards 1998).

For this reason, the realisation that the behaviour of ring polymers in solution could not be captured by the tube model came as a shock (McLeish 2002). The reptation theory in fact heavily relies on the presence of loose ends to describe the disentanglement process. On the contrary, the basic assumptions on which this theory relies are not met by rings, or circular polymers, given their lack of ends. Because of this, the macroscopic properties of systems of un-linked and un-knotted ring polymers in solution present some big open questions and are far from being fully captured. For all other polymer architectures, the presence of ends is pivotal for the chains to renew their configurations; ring polymers, having no ends, markedly depart from such relaxation pathway. This is why ring polymers are perhaps one of the last big mysteries in Polymer Physics (McLeish 2008).

Adding further topological constraints such as, linking between rings or knotting (see Fig. 1.2), complicates the picture even more. In these cases, in fact, the scientific community is not even equipped with the right mathematical tools to classify these objects: At present, a quantity does not exist that can unambiguously distinguish every knot or link (Adams 1994).

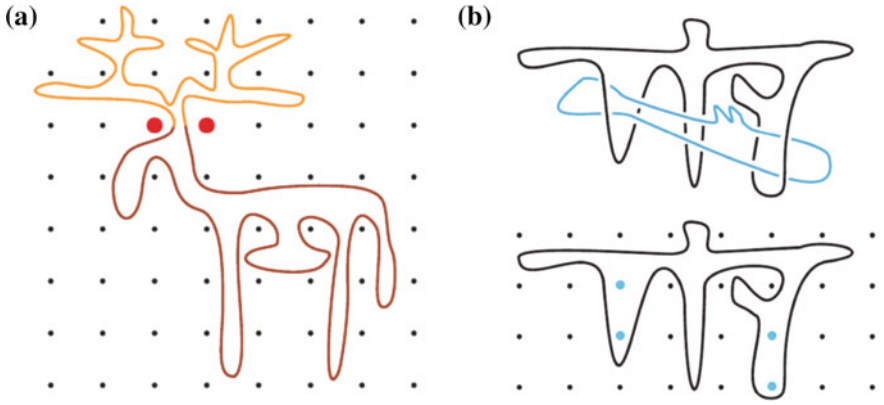

Fig. 1.4 **a** A ring polymer that is not threaded by its neighbours (*black dots*) and assuming a lattice animal (moose) configuration. **b** A ring that is threaded by a neighbour. Its contour can be thought of as encircling points (*blue*) that cannot be crossed until the blue ring has diffused away (from Ref. Kapnistos et al. (2008) with permission from Macmillan Publishers Ltd: Nature Materials, copyright 2008)

Joining the two ends of an open chain would seem, at first sight, to be a relatively trivial change; In reality, it has a profound impact on the static and dynamic properties of a polymer (Bates and Maxwell 2005). This procedure in fact changes its topological state, i.e. the state that is preserved under smooth deformations of its contour, and introduces long-ranged constraints on the allowed conformations.

Whereas ring polymers have no ends to retract or protrude, they can generate any number of temporary double-folded segments which can explore the space as if they were terminal segments. These conformations are sometimes referred to as "lattice animals", or annealed branched polymers, as the branch points are free to move along the polymer contour and they sometimes recall familiar animal shapes (see Fig. 1.4a). From this, one can understand that although lacking of ends, ring polymers do not necessarily display a reduced ability to explore space. Rather, they follow unique pathways through which relax the stress. Ring polymers have, in some sense, a greater freedom of movement with respect to their linear or quenched branched polymers, although they suffer of much stronger topological constraints due to the fact that they have to preserve their topological state at all times. Because of all this, ring polymers in solution are, at present, a topic of intense debate and lively interest among the Polymer Physics community (Kapnistos et al. 2008; Halverson et al. 2011a; Mirny 2011; Pasquino et al. 2013; Rosa and Everaers 2014; Grosberg 2014).

In spite of our difficulties in capturing their behaviour, ring polymers are abundant in Nature, who seems to have no difficulty at all to regulate their properties and topology, often in very delicate and life-depending conditions, such as in the case of bacterial DNA or inside the eukaryotic cell nucleus (Calladine et al. 1997; Alberts et al. 2014). For instance, bacterial DNA, which is circular, has to be kept un-knotted

and un-linked at all times during mitosis; failing to do so would lead to the death of the organism as its replicated genetic material cannot be separated into the two daughter cells. DNA knots and links have been frequently observed in the genetic material of bacteria, viruses and eukaryotes, since their discovery in the late '70s (Liu et al. 1976, 1981; Fairlamb et al. 1978), and because they are so ubiquitous, all organisms have developed special enzymes—called topoisomerases (Berger et al. 1996)—whose function is to help untie DNA knots and links. This indicates how the topological regulation in systems of bio-polymers is a serious issue, and learning how Nature deals with it might provide us with fresh means to design next-generation soft materials or to understand and detect genetic diseases (Cavalli and Misteli 2013; Marini et al. 2015).

One of the most studied ensembles involving ring polymers is the so-called "melt" of rings which consists of a dense solution of rings above its glass and/or crystallization temperatures, i.e. a polymer liquid. The reasons for which this system has received much attention in the last years are twofold: firstly, it has been found to share some properties with the organisation of chromosomes inside the cell nucleus (Cremer and Cremer 2001; Rosa and Everaers 2008; Vettorel et al. 2009; Mirny 2011; Halverson et al. 2011a, b; Grosberg 2014; Rosa and Everaers 2014; Halverson et al. 2014), and secondly, recent experimental advances allowed, for the first time, its purification from linear contaminants which allowed us to study directly the pure melt of rings using artificial polymers such as polyisoprene or polystyrene chains (Kapnistos et al. 2008; Pasquino et al. 2013).

Despite the intense scientific effort spent characterising the dynamics of ring polymers, a full satisfactory description has not yet been achieved. In particular, understanding the conformations assumed by the rings in the melt is of great contemporary interest. Although these show some features reminiscent of a collapsed globule (Grosberg et al. 1993; Rosa and Everaers 2014), they also display some deviations from a fully crumpled conformation (Halverson et al. 2011a), and in particular, they show intra- and inter-chain protrusions, also known as "threadings" (Lo and Turner 2013). A ring is said to be passively threaded by another, actively threading, ring when the contour of the former is pierced through by the contour of the latter, very much like the rings in Fig. 1.4b.

These threadings represent serious, although not permanent, constraints on the diffusion of the rings and it has been conjectured that when the number of such constraints is large enough, a spanning cluster of inter-threaded rings might arise and form what has been called a "topological glass" (Lo and Turner 2013). The first part of this Thesis will be devoted to understanding and reproducing (*in silico*) this peculiar and unique state of matter. The main objectives will be the detection of threadings in melt and dense solutions of ring polymers and their consequent employment as a driving element to tune the physical properties of the system and induce a (topological) kinetically arrested state.

The second and third parts of this Thesis will be focused on more biologically-oriented applications. As mentioned before, knotted and linked ring polymers are abundant in Nature under the form of bio-polymers such as DNA, RNA and proteins. In order to understand the mechanisms through which their formation and

simplification is regulated inside the cell, Molecular Biologists often face the challenge of identifying knots and links topological state. This is nowadays achieved via gel electrophoresis techniques which can efficiently and beautifully separate charged biopolymers having different length, molecular weight and topology. In the case of DNA this technique is even able to separate molecules with different amount of supercoiling or at different replication stages (Calladine et al. 1997; Viovy 2000; Trigueros et al. 2001; Arsuaga et al. 2002; Olavarrieta et al. 2002). Nonetheless, a physical picture capturing the behaviour of knotted and linked bio-polymers moving through gels in response to external fields as a function of their topological state is still lacking a satisfactory theoretical model. This problem will be tackled in this Thesis from a physical perspective and by focusing on the role of topology in the entangling and disentangling properties of knotted polymers driven by external fields and interacting with random and complex media, such as physical gels.

Another important biological example in which Nature has to deal with polymers displaying topologically complex features is in the case of the mitochondrial genome of organisms of the class *Kinetoplastida*, also called the "Kinetoplast DNA" (Jensen and Englund 2012). This is made of thousands of short loops forming a spanning linked network resembling a medieval chain-mail (Chen et al. 1995). The correct assembly and disassembly of this network during the replicating phase and the corresponding topological regulation is crucial for the survival of this unique species whose evolutionary survival is a long-standing issue in evolutionary biology (Borst 1991). How these organisms can master this complicated task is not at all clear. Although this system presents many complicated biological issues, I will provide a minimal coarse-grained model in order to capture the key elements of the problem and understand the role of topology in this biological system. I will show that, in this case, such simple coarse-grained bio-physical model can, not only contribute toward the understanding of how the Kinetoplast is formed and regulated, but also provide us with some insight into the evolutionary success of these organisms.

Finally, from the aforementioned examples, one can appreciate that I write this Thesis with the aim of understanding how topology affects the general macroscopic behaviour of systems made of ring (bio-)polymers. In particular, I will focus on three types of topological "interactions", namely threading, knotting and linking, and from each one I will draw and examine specific examples mainly inspired from Material Science and Biology.

It is worth pointing out at this stage that although real-life polymers can be various and have the most different roles in our every-day life, ranging from polystyrene which makes common plastics to DNA which contains the information of life itself, they all share some universal physical properties, which are independent of their chemical composition. This is the reason why it is possible to capture the behaviour of such diverse systems within the same coarse-grained physical models. Focussing on the general physical properties of the systems and discarding, as much as possible, any chemical or biological detail can often help us understanding the general underlying mechanisms regulating such systems and pinpoint more general and universal questions.

The work presented in this Thesis will be structured as follows:

In Chap. 2 I will provide the reader with a brief theoretical background on the static and dynamic properties of polymers in solution.

In Chap. 3 I will give a brief general overview of the computational details and numerical schemes used in the rest of the Thesis and will describe the computational models employed.

Chapter 4 will be divided into two sections: First, I will introduce an algorithm to unambiguously detect and identify a peculiar type of topological interaction: threading of un-knotted and un-linked ring polymers. The system I will investigate is a dense solution of ring polymers immersed in gel which will provide me with a way to unambiguously define these elusive kind of inter-chain interactions. In addition, I will investigate the effect of threadings on the relaxation dynamics of the rings and provide an explanation of the observed, both in experiments (Doi et al. 2015) and simulations (Halverson et al. 2011b), slowing down in terms of emergence of system-spanning connected clusters of inter-threaded rings, thereby relating the increase of spatial correlations with the increase of relaxation time.

In the second part of the Chapter I will tackle a melt of un-knotted and un-linked ring polymers, possibly one of the most studied systems by the Polymer Physics community in recent years. It has been conjectured (Lo and Turner 2013) that the main topological interaction affecting the polymers behaviour in this system is that of threading. On the other hand, currently there is no way to unambiguously identify threadings in a melt of rings, in contrast to the case described before. For this reason I will probe their existence dynamically, i.e. by imposing some external artificial constraints on the rings' motion and by studying the *in silico* response of the system to this external perturbation. I will introduce a protocol that can provide us with a way to identify the presence of threadings and ultimately show that a melt of rings can, in fact, generate a dynamically arrested state under certain conditions.

In Chap. 5 I will study another type of topological interaction: linking between ring polymers. In order to investigate the properties inherited by a system of rings interacting via linking I will focus on biological organisms whose viability relies on the effectiveness of this topological interaction: the *Kinetoplastidae*. These organisms possess a unique mitochondrial DNA that is made of thousands of linked DNA loops, the "Kinetoplast DNA". I will investigate its structure and provide a simple biophysical model to explain its stability and topological organisation, both of which are still source of intense debate in the biological community. I will tackle these issues with a philosophy of extreme simplification and the results that I will present will shed some light into the evolutionary advantage of the Kinetoplast and might provide us with some fresh insight into how to artificially generate an "Olympic gel".

In Chap. 6 I will study an intra-chain topological interaction: knotting. As mentioned before, one of the most successful and broadly used techniques to separate knots in biological material is by using gel electrophoresis, although its theoretical understanding is far from complete. For this reason I will focus on understanding how knots interact with the surrounding environment and in particular I will compare linear, circular un-knotted and knotted polymers dragged by an external field through a disordered environment, such as that of a physical gel. I will investigate

their behaviour depending on different field strengths, environmental disorder and knot type. The results I will present will be particularly important as they can directly inform biological experiments such as DNA gel electrophoresis and enlighten some recent unexplained experimental outcomes.

Finally, in Chap. 7 I will draw some conclusions, summarise the main findings and attempt to provide a unifying view over the topics treated in this Thesis.

References

Adams, C.C.: The Knot Book: An Elementary Introduction to the Mathematical Theory of Knots. W H Freeman and Company, New York (1994)

Alberts, B., Johnson, A., Lewis, J., Morgan, D., Raff, M.: Molecular Biology of the Cell. Taylor & Francis, New York (2014)

Arsuaga, J., Vázquez, M., Trigueros, S., Sumners, D., Roca, J.: Knotting probability of DNA molecules confined in restricted volumes: DNA knotting in phage capsids. Proc. Natl. Acad. Sci. USA **99**(8), 5373 (2002)

Bates, A., Maxwell, A.: DNA topology, Oxford University Press, Oxford (2005)

Berger, J., Gamblin, S., Harrison, S., Wang, J.: Structure and mechanism of DNA topoisomerase II. Nature **379**, 225 (1996)

Borst, P.: Why kinetoplast DNA networks? Trends Genet. **7** (1991)

Calladine, C. R., Drew, H., Luisi, F. B., and Travers, A. A.: Understanding DNA: The Molecule and How it Works, Elsevier Academic Press, New York (1997)

Cavalli, G., Misteli, T.: Functional implications of genome topology. Nat. Struct. Mol. Biol. **20**(3), 290 (2013)

Chen, J., Rauch, C.A., White, J.H., Englund, P.T., Cozzarelli, N.R.: The topology of the kinetoplast DNA network. Cell **80**(1), 61 (1995)

Cremer, T., Cremer, C.: Chromosome territories, nuclear architecture and gene regulation in mammalian cells. Nat. Rev. Genet. **2**(4), 292 (2001)

de Gennes, P.G.: Reptation of a Polymer Chain in the Presence of Fixed Obstacles. J. Chem. Phys. **55**(2), 572 (1971)

Doi, M., Edwards, S.: The Theory of Polymer Dynamics, Oxford University Press, Oxford (1988)

Doi, Y., Matsubara, K., Ohta, Y., Nakano, T., Kawaguchi, D., Takahashi, Y., Takano, A., Matsushita, Y.: Melt Rheology of Ring Polystyrenes with Ultrahigh Purity. Macromolecules **48**(9), 3140 (2015)

Fairlamb, A.H., Weislogel, P.O., Hoeijmakers, J.H., Borst, P.: Isolation and characterization of kinetoplast DNA from bloodstream form of Trypanosoma brucei. J. Cell Biol. **76**(2), 293 (1978)

Grosberg, A.: Annealed lattice animal model and Flory theory for the melt of non-concatenated rings: towards the physics of crumpling. Soft Matter **10**, 560 (2014)

Grosberg, A.Y., Rabin, Y., Havlin, S., Neer, A.: Crumpled globule model of the three-dimensional structure of DNA. Europhys. Lett. **23**(5), 373 (1993)

Halverson, J.D., Lee, W.B., Grest, G.S., Grosberg, A.Y., Kremer, K.: Molecular dynamics simulation study of nonconcatenated ring polymers in a melt. I. Statics. J. Chem. Phys. **134**(20), 204904 (2011a)

Halverson, J.D., Lee, W.B., Grest, G.S., Grosberg, A.Y., Kremer, K.: Molecular dynamics simulation study of nonconcatenated ring polymers in a melt. II. Dynamics. J. Chem. Phys. **134**(20), 204905 (2011b)

Halverson, J.D., Smrek, J., Kremer, K., Grosberg, A.: From a melt of rings to chromosome territories: the role of topological constraints in genome folding. Rep. Prog. Phys. **77**, 022601 (2014)

Hosler, D., Burkett, S.L., Tarkanian, M.J.: Prehistoric Polymers: Rubber Processing in Ancient Mesoamerica. Science **284**(June), 1988 (1999)
Hurst, L.D., Dawkins, R.: Life in a test tube. Nature **357**, 198 (1992)
Jensen, R.E., Englund, P.T.: Network news: the replication of kinetoplast DNA. Annu. Rev. Microbiol. **66**, 473 (2012)
Kapnistos, M., Lang, M., Vlassopoulos, D., Pyckhout-Hintzen, W., Richter, D., Cho, D., Chang, T., Rubinstein, M.: Unexpected power-law stress relaxation of entangled ring polymers. Nat. Mater. **7**(12), 997 (2008)
Liu, L., Perkocha, L., Calendar, R., Wang, J.C.: Knotted DNA from bacteriophage capsids. Proc. Natl. Acad. Sci. USA **78**(9), 5498 (1981)
Liu, L.F., Depew, R.E., Wang, J.C.: Knotted single-stranded DNA rings: A novel topological isomer of circular single-stranded DNA formed by treatment with Escherichia coli ω protein. J. Mol. Biol. **106**, 439 (1976)
Lo, W.-C., Turner, M.S.: The topological glass in ring polymers. Europhys. Lett. **102**(5), 58005 (2013)
Marini, B., Kertesz-Farkas, A., Ali, H., Lucic, B., Lisek, K., Manganaro, L., Pongor, S., Luzzati, R., Recchia, A., Mavilio, F., Giacca, M., Lusic, M.: Nuclear architecture dictates HIV-1 integration site selection. Nature **521**(7551), 227 (2015)
McLeish, T.: Polymers without beginning or end. Science **297**(5589), 2005 (2002)
McLeish, T.C.B.: Floored by the rings. Nature **7**, 933 (2008)
Mirny, L.A.: The fractal globule as a model of chromatin architecture in the cell. Chromosome Res. **19**(1), 37 (2011)
Olavarrieta, L., Martínez-Robles, M.L., Sogo, J.M., Stasiak, A., Hernández, P., Krimer, D.B., Schvartzman, J.B.: Supercoiling, knotting and replication fork reversal in partially replicated plasmids. Nucleic Acids Res. **30**(3), 656 (2002)
Pasquino, R., Vasilakopoulos, T., Jeong, C., Lee, H., Rogers, S., Sakellariou, G., Allgaier, J., Takano, A., Bras, A., Chang, T., Goossen, S., Pyckhout-Hintzen, W., Wischnewski, A., Hadjichristidis, N., Richter, D., Rubinstein, M., Vlassopoulos, D.: Viscosity of Ring Polymer Melts. ACS Macro Lett. **2**, 874 (2013)
Rosa, A., Everaers, R.: Structure and dynamics of interphase chromosomes. PLoS Comput. Biol. **4**(8), 1 (2008)
Rosa, A., Everaers, R.: Ring polymers in the melt state: The physics of crumpling. Phys. Rev. Lett. **112**, 118302 (2014)
Staudinger, H.: Über polymerisation. Berichte der deutschen chemischen Gesellschaft (A and B Series) **53**(6), 1073 (1920)
Trigueros, S., Arsuaga, J., Vazquez, M.E., Sumners, D., Roca, J.: Novel display of knotted DNA molecules by two-dimensional gel electrophoresis. Nucleic Acids Res. **29**(13), E67 (2001)
Vettorel, T., Grosberg, A.Y., Kremer, K.: Statistics of polymer rings in the melt: a numerical simulation study. Phys. Biol. **6**(2), 025013 (2009)
Viovy, J.: Constraint release in the slip-link model and the viscoelastic properties of polymers. J. Phys. **46**, 847 (1985)
Viovy, J.: Electrophoresis of DNA and other polyelectrolytes: Physical mechanisms. Rev. Mod. Phys. **72**(3), 813 (2000)

Chapter 2
Predicting the Behaviour of Rings in Solution

> *No man is obliged to learn and know every thing;* [...]*; yet all persons are under some obligation to improve their understanding; otherwise it will be a barren desert, or a forest with overgrown weed and brambles.*
>
> I. Watts

Polymeric systems offer an incredible richness of behaviour. Depending on the solution concentration, its temperature or its quality and the polymers length, or topology, every system made of polymers can be categorised into a "universality class", within which it finds a physical characterisation (scaling) of its macroscopic properties.

The physical properties of polymers have been pioneered by Flory in the '50s, by Edwards in the '60s and '70s and by de Gennes in the '70s and '80s. The theories that they developed were mainly concerned with linear polymers and helped the understanding and realisation of many polymer compounds used nowadays. Both Edwards and de Gennes became, at some stage, interested in studying polymers displaying more complicated topologies. They mainly focused on branched and star polymers, although both of them turned their attention to ring polymers, sooner or later, during their lifetime. Edwards (1967, 1968) chose to tackle the matter from a field-theoretic point-of-view while de Gennes (1979), Raphael et al. (1997) chose a more practical "gedankenexperiment" in which he studied a gel made of linked polymer rings, broadly known as "Olympic gel". Both these series of attempts were far from being the most successful and important contributions brought forward by these two giants which indicates the difficulty of the topic (and partially excuses the diffident approach that I will assume in tackling the matter). Even though understanding ring polymers is a difficult task, important advances in the field have been achieved in the past decades (Cates and Deutsch 1986; Rubinstein 1986; Grosberg et al. 1993; Obukhov and Rubinstein 1994): Ring polymers are nowadays well known for behaving very differently from their linear counterparts, although a full theoretical description of their static and dynamic properties is far from achieved.

D. Michieletto, *Topological Interactions in Ring Polymers*, Springer Theses,
DOI 10.1007/978-3-319-41042-5_2

In this chapter I will briefly review the main theoretical findings regarding systems of ring polymers in dense solutions, melts and embedded in gels. In particular, I will separately treat static and dynamic properties, and I will introduce the key observables that I will use to characterise and investigate the systems in the following chapters.

2.1 Statics

2.1.1 The Size of a Crumpled Coil

The size of a polymer coil has been investigated in various solvents and different concentrations in the past decades. The general assumption is that the size R of a polymer coil depends on the degree of polymerisation M as

$$R \sim M^{\nu} \tag{2.1}$$

where ν is also known as the entropic exponent and is related to the fractal dimension of the coil via $\nu = d_F^{-1}$. The Gaussian, or ideal, approximation for the end-to-end size R_e of a polymer coil results in the scaling

$$R_e^2 = \sum_{i,j}^{M} \langle \boldsymbol{r}_i \boldsymbol{r}_j \rangle = \sum_{i}^{M} \langle \boldsymbol{r}_i^2 \rangle + \sum_{i \neq j}^{M} \langle \boldsymbol{r}_i \boldsymbol{r}_j \rangle = M\sigma^2, \tag{2.2}$$

where $\boldsymbol{r}$ is the vector joining two consecutive segments along the chain, $|\boldsymbol{r}_i| = \sigma$ is the size of a segment and segments $\boldsymbol{r}_i, \boldsymbol{r}_j$ are correlated only if $i = j$.[1] This gives the value of $\nu = 1/2$ for ideal coils and applies to polymers in dimension d above the upper critical dimension $d_c = 4$, for which the ideal polymer picture breaks down and self-avoiding (steric) constraints become too important to be neglected.

One of the most famous and important schemes to infer the value of ν for self-avoiding polymer coils in $d < d_c$ has been advanced by Flory (1953): Given the monomer concentration of a coil

$$c_{int} \simeq \frac{M}{R^d} \tag{2.3}$$

the steric repulsion inside a polymer coil of volume R^d can be given in a mean-field picture, i.e. neglecting the inter-monomer correlations, as a virial term

$$F_{\text{steric}} \simeq k_B T v c_{int}^2 R^d \simeq k_B T v \frac{M^2}{R^d}, \tag{2.4}$$

[1] Local (short-ranged) correlations, do not affect the scaling.

where v takes the role of excluded volume parameter ($v > 0$ for good solvents) and has dimensions of a d-dimensional length. This repulsive term is balanced by an entropic term which contrasts the coil expansion much further than the ideal size (with $\nu = 1/2$). This entropic term can be written as

$$F_{\text{elastic}} \simeq k_B T \frac{R^2}{M\sigma^2}. \tag{2.5}$$

Summing both terms, the free energy of a coil can be written as

$$\frac{F}{k_B T} = \frac{F_{\text{steric}} + F_{\text{elastic}}}{k_B T} \simeq v\frac{M^2}{R^d} + \frac{R^2}{M\sigma^2}. \tag{2.6}$$

After minimisation in terms of the size R, this formula leads to the famous scaling for self-avoiding coils in d dimensions

$$R \simeq \left[v\sigma^2 N^3\right]^{1/(d+2)} \tag{2.7}$$

which gives $\nu_{1D} = 1$, $\nu_{2D} = 3/4$ and $\nu_{3D} = 3/5$, which surprisingly[2] well agrees with experimental observations (in particular numerical estimates give $\nu_{3D} = 0.588$).

The size of a ring polymer, because of its lacking of ends, is better captured by the radius of gyration, defined as

$$R_g^2 = \frac{1}{2M^2}\sum_{i,j}\left[\boldsymbol{R}_i - \boldsymbol{R}_j\right]^2 = \frac{1}{M}\sum_i [\boldsymbol{R}_i - \boldsymbol{R}_{CM}]^2 \tag{2.8}$$

where $\boldsymbol{R}_i$ is the position of segment i and $\boldsymbol{R}_{CM}$ is the position of the ring's centre of mass. Nonetheless, the same Flory theory applies to rings, which follow the scaling $R_g \sim \sigma M^{\nu}$ with $\nu = 3/5$ in 3D and in good solvent in dilute conditions.

When rings are placed inside a gel structure the picture changes dramatically. In fact, while linear polymers remain in the same universality class, i.e. retain the same ν when placed inside a gel, rings have been shown to completely change their behaviour. Rings embedded in a gel whose lattice spacing is less than or comparable to the rings persistence length l_P (i.e. the length needed to de-correlate the tangent vector or, equivalently, to observe spontaneous bending due to thermal fluctuations) assume lattice animal (LA) configurations. Examples of these have been shown in the Introduction (Fig. 1.4). The rings assume double-folded configurations to preserve their topology and by doing this they protrude through the gel pores via temporary loops, or branches. The first prediction of the scaling exponent in d dimensions of such random, or annealed, branched structures was given by Lubensky and Isaacson (1979), Isaacson and Lubensky (1980) and, subsequently, by Parisi and Sourlas

[2] "Surprisingly" because Flory's theory actually overestimates the repulsive term by neglecting monomer-monomer correlations, but also overestimates the elastic term, thereby balancing out the errors and leading to a very accurate estimation of the scaling of the real size R (de Gennes 1979).

(1981) in terms of the exponent of the Lee–Yang edge singularity of the Ising model in $d-2$ dimensions and it is, to my knowledge, one of the few (if not the only) exact field-theoretic result in 3 dimensions, and gives

$$R_g \sim \sigma M^{5/[2(d+2)]}. \tag{2.9}$$

This prediction, which holds for isolated self-avoiding ring polymers in gels, or lattice animals, in dimensions $d < d_c = 8$, is (in 3D: $\nu = 1/2$) incidentally the same as that for ideal chains, although the statistics of the conformations is completely different. It is also worth noting that annealed and quenched branched polymers are in different universality classes (Gutin et al. 1993). This means that branched polymers with fixed, i.e. quenched, functional units (or branching points), do not behave like lattice animals, for which the branching point are temporary, i.e. can be annealed.

What happens when the coils are instead in concentrated conditions, i.e. many different chains are overlapping and $c > c^* \simeq M/R^d$? In this case, it is well known (de Gennes 1979; Doi and Edwards 1988) that the steric interaction between different coils screens the coils self-avoidance. This means that in a melt of polymers, i.e. a dense solution of polymers from which the solvent has been drained, the statistics of the polymers is ideal once again, i.e. as if $d \geq d_c$. In this case linear polymers return to assume $\nu = 1/2$, but what happens to the rings? One could argue that a ring polymer in the melt should assume the size of an ideal ring polymer, in agreement with the behaviour of linear polymers in melt. This is not true. In fact, the size of an ideal annealed branched polymer can be described in terms of ideal tree-like structures and its scaling is given by the Kramers theorem (Daoud and Joanny 1981; Rubinstein and Colby 2003)

$$R_g^2 = \frac{\sigma^2}{M} \frac{\sum_k M_1(k)[M - M_1(k)] Z_{M_1(k)} Z_{M-M_1(k)}}{\sum_k Z_{M_1(k)} Z_{M-M_1(k)}} \sim \sigma^2 M^{1/2}, \tag{2.10}$$

where the sum is over all the bonds k which separate the branched tree into two sub-trees (always the case as there are no loops in lattice animals) of sizes M_1 and $M - M_1$ weighted by the corresponding probability $Z_{M_1(k)} Z_{M-M_1(k)}$, and which gives $R_g \sim \sigma M^{1/4}$. On the other hand, this prediction is only valid for dimensions $d \geq d_c = 8$ (de Gennes 1979; Isaacson and Lubensky 1980) and, in particular, in $d = 3$ generates a clear artificial singularity in the coil mass as the degree of polymerisation M increases. For this reason Daoud and Joanny (1981) conjectured that the limiting scaling for a randomly annealed structure in d dimensions and in concentrated conditions might be obtained from a free energy that contains all the n-body terms

$$\frac{F}{k_B T} = v \frac{M^2}{R^d} + w \frac{M^3}{R^{2d}} + \cdots + t_n \frac{M^n}{R^{d(n-1)}} + \cdots \tag{2.11}$$

and whose minimisation (with respect to R) leads to

$$R_g \sim \sigma M^{1/d}, \tag{2.12}$$

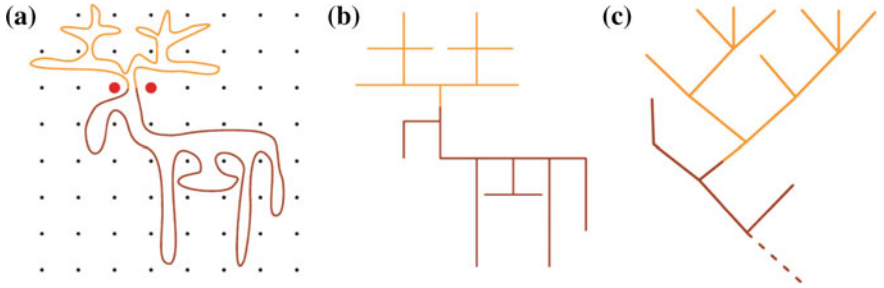

Fig. 2.1 **a** The moose-like configuration of a ring polymer in gel and its tree representation **b** which can be also mapped to a Cayley-tree (partially showed in **c**) whose nodes have maximum valence equal to 4. Adapted from Ref. (Kapnistos et al. 2008) with permission from Macmillan Publishers Ltd: Nature Materials, copyright 2008

once $n \to \infty$. This scaling has been found, both numerically (see Chap. 4 and Halverson et al. 2011) and experimentally (see Gooßen et al. 2014; Brás et al. 2014; Doi et al. 2015), to correctly describe the size of ring polymers in melt, or dense solutions, in the limit of large polymerisation M.

More recently, Grosberg (2014) provided a Flory-like theory in order to specifically address and describe the scaling of ring polymers in the melt in terms of their spatial size R and their "Cayley-tree representation" size L_c. The latter represents the extension of the Cayley tree, or graph, representation of the lattice animal (see Fig. 2.1). If $L_c \sim M/2$ then the ring is fully stretched and all the segments belong to the backbone L_c. On the other hand, if $L_c \sim \ln M$, then the ring resembles a dendritic polymer (Grosberg 2014). By assuming the existence of a further scaling exponent ρ_c such that $R \sim \sigma M^{\nu}$ and $L_c \sim \sigma M^{\rho_c}$ (or $R \sim \sigma^{1-\nu/\rho_c} L^{\nu/\rho_c}$), one can introduce two Flory-like free energies: $F_{\text{elastic}} \sim k_B T R^2/\sigma^2 L_c$ which penalises the stretching of the backbone, and a second $F_{\text{branching}} \sim k_B T L_c^2/M\sigma^2$ which penalises insufficient branching on the Cayley tree. After a rescaling due to the presence of an entanglement length-scale M_e, which defines a blob size below which the statistics is Gaussian, and that maps to an edge of the Cayley tree representation,[3] one obtains:

$$\frac{F}{k_B T} \sim \frac{R^2}{L_c \sqrt{M_e}\sigma} + \frac{L_c^2}{M\sigma^2} \tag{2.13}$$

which, after minimisation with respect to L_c, gives

$$L_c \sim \sigma M_e^{1/2} \left(\frac{R}{M^{1/3} M_e^{1/6}}\right)^{2/3} \left(\frac{M}{M_e}\right)^{5/9}. \tag{2.14}$$

[3] This means that $M \to M/M_e$, $\sigma \to \sigma M_e^{1/2}$ and $L_c \to L_c/M_e^{1/2}$.

For this value of L_c, the resulting free energy is a monotonic function of R and one can therefore argue that it will attain its minimum at the minimum (physical) value of R, i.e. $R \sim \sigma M^{1/3}$. This therefore leads to

$$R \sim \begin{cases} \sigma M^{1/2} & \text{for } M \ll M_e \\ \sigma M_e^{1/6} M^{1/3} & \text{for } M \gg M_e \end{cases} \quad \text{or } \nu = 1/3 \tag{2.15}$$

and

$$L_c \sim \begin{cases} \sigma M^{1/2} & \text{for } M \ll M_e \\ \sigma M_e^{-1/18} M^{5/9} & \text{for } M \gg M_e \end{cases} \quad \text{or } \rho_c = 5/9. \tag{2.16}$$

Equivalently, one finds $R \sim \sigma^{1-\nu/\rho_c} L_c^{\nu/\rho_c} = \sigma^{2/5} L_c^{3/5}$ in the limit of large rings. In summary, within this picture rings in melt can be thought of as fractal globules $R \sim \sigma M^{1/3}$ whose backbone is governed by self-avoiding statistics $R \sim \sigma^{2/5} L_c^{3/5}$. While R can easily be obtain, via, for instance, the radius of gyration R_g, measuring the size of the backbone L_c presents much more difficulties and has never been done in the literature. This is because there exists no algorithm able to detect a tree-like structure that is not clearly visible with naked eye, and even primitive-path analysis fails in this case (Halverson et al. 2011).

A further attempt to capture the behaviour of rings in the melt via a Flory-like framework is worth mentioning here. Cates and Deutsch in the '80s (Cates and Deutsch 1986) advanced a model that simply assumes that rings in the melt are topologically constrained by their neighbours and this leads them to adopt a double folded configuration. The constraint experienced by the rings can be associated with an entropic loss of roughly one entropy unit, or degree of freedom ($k_B T$), per neighbour. Since every chain has roughly R^d/M neighbours, one obtains:

$$\frac{F}{k_B T} \sim \frac{R^d}{M\sigma^d} + \frac{M\sigma^2}{R^2} \tag{2.17}$$

where the second term is the elastic energy required to extend a chain. After the usual minimisation in terms of R one obtains:

$$R \sim \sigma M^{2/(d+2)} \tag{2.18}$$

which gives, in particular, $\nu_{3D} = 2/5$. In Chap. 4 I will show that this prediction is recovered as a crossover between the short chain regime, $R \sim \sigma M^{1/2}$, and the long chain limit, $R \sim \sigma M^{1/3}$.

Even though ring polymers only differ from their linear counterparts in having a closed contour, they display markedly distinct behaviour. Understanding this, represents one of the most challenging tasks remaining in Polymer Physics. In addition, the so-called "fractal globule" structure often associated with the scaling collapsed state of rings in the melt has raised also some interest in the Biology community. This is because it represents a strongly collapsed state which displays a weak level

of entanglement among parts of the sub-chain; as a consequence, it has been identified as a good candidate to explain the structure of chromatin (Mirny 2011) and to describe the formation and the stability of chromosome territories (Cremer and Cremer 2001; Rosa and Everaers 2008).

2.1.2 Contact Exponents for the Crumpled Globule

Although the collapsed conformation assumed by rings in the melt is broadly accepted, it is far from clear what their internal arrangement is. In fact, although $\nu = 1/3$ resembles a collapsed coil, such as one that could be observed in poor solvent, there are many types of internal arrangements consistent with $\nu = 1/3$ (Rosa and Everaers 2014). Perhaps the most important candidates in this case are (i) the equilibrium globule: a disordered dense packing of coil confined within a sphere of radius $R \sim M^{1/3}$ and possessing a core filled with segments (of length $s < M^{2/3}$) following ideal statistics, i.e. $r(s) \sim s^{1/2}$; and (ii) the fractal globule: a recursive coiling of mass which appears like a collapsed globule at any length scale (larger than the entanglement length M_e) within the globule (Grosberg et al. 1993), i.e. $r(s) \sim s^{1/3}$ (see Fig. 2.2). One of the key differences between these two conformations is the probability of contact $P_c(s)$ of two segments distant s segments along the contour and defined as

$$P_c(s) = \left\langle \frac{1}{M} \sum_{i=1}^{M-1} \sum_{j=i+1}^{M} \Theta(a - |\boldsymbol{r}_i - \boldsymbol{r}_j|) \right\rangle \tag{2.19}$$

with a a chosen cut-off for the interaction and $\Theta(x)$ the Heaviside function. A mean-field estimate of this probability leads to

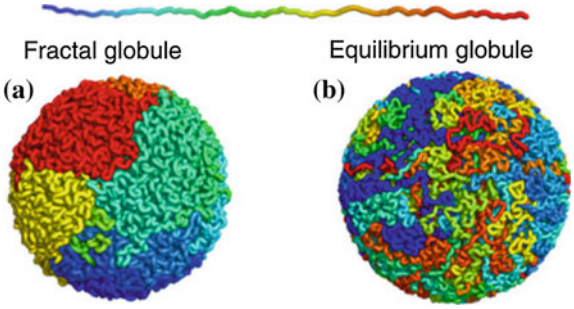

Fig. 2.2 Pictorial representation of **a** fractal and **b** equilibrium, globules. While the former displays internal segregation of the segments, the latter displays a larger degree of mixing. These different features are reflected by the different values assumed by the contact exponent, which is $\gamma = 1$ for the former and $\gamma = 3/2$ for the latter (from Ref. Mirny 2011 with permission of Springer)

$$P_c(s) \simeq \frac{\sigma^d}{r(s)^d} \sim s^{-\nu d} \equiv s^{-\gamma} = \begin{cases} s^{-3/2} & \text{equilibrium globule and } s < M^{2/3} \\ s^{-1} & \text{fractal globule,} \end{cases} \tag{2.20}$$

where γ is called the contact exponent. The mean-field value of $\gamma = 1$ for the fractal globule case is un-physical, since the number of neighbours per segment would, in this case, diverge as $\sum_s s^{-1} \to \infty$. Numerical (Halverson et al. 2011, 2013) and experimental (Lieberman-Aiden et al. 2009; Mirny 2011) observations in fact report a contact exponent close to, but slightly greater than, unity.

Another useful quantity is how "rough" the coil surface is. This can also be understood in terms of number of contacts n_c or inter-blobs[4] contacts n_g. Let us assign to these two quantities the exponents β_c and β_g regulating the scaling of the contacts for an s-monomer long sub-chain as

$$n_c(s) \sim s^{\beta_c} \tag{2.21}$$

being the number of contacts of a given segment with any other segment and

$$n_g(s) \sim s^{\beta_g} \tag{2.22}$$

being the number of contacts between blobs sitting near one another in space. The surface exponents β_c and β_g have to be related to one another by the fact that only a number $r(s)^d/s$ of blobs can be neighbours to a given blob, and therefore:

$$s^{\beta_c} \sim \frac{r(s)^d}{s} s^{\beta_g} = s^{\nu d - 1} s^{\beta_g} \tag{2.23}$$

which gives

$$\beta_c = \beta_g + \nu d - 1 \tag{2.24}$$

or in the case of a globule ($\nu = 1/d$):

$$\beta_c = \beta_g. \tag{2.25}$$

On the other hand, the contact exponent γ is itself related to the surface exponent β_c as the number of contacts of a given monomer with other monomers is $\sum_{s'>s}^{\infty} P_c(r)$, which gives the total number of contacts of an s-monomer long segment as

$$s^{\beta_c} \sim s \sum_{s'=s}^{\infty} \left(s'\right)^{-\gamma} \sim s^{-\gamma+2} \tag{2.26}$$

[4] A blob being a polymer segment made of several (g) monomers where $1 \ll g \ll M$ and assuming a size described by the scaling $R(g) \sim g^{\nu}$ with $\nu = 3/5$, being not interacting with other chains (de Gennes 1979).

or

$$\beta_c + \gamma = 2. \tag{2.27}$$

It is worth stressing that Eqs. (2.24) and (2.27) are general relations which hold for any fractal structure and do not rely on the fractal globule assumption. Also, from Eqs. (2.24) and (2.27) one can infer some restrictions for the values of these exponents, in particular $\beta_c \geq \beta_g$ and $1 \leq \gamma \leq 1 + 1/d$.[5] It is also worth noting that for Hilbert curves in 3D for which $R \sim M^{1/3}$ (being space filling), the contact surface scales with $\beta = \beta_c = \beta_g = 2/3$ which implies $\gamma = 4/3$, while, by contrast, the numerical estimation of β for the fractal globule case (see Chap. 4 and Halverson et al. 2011) seems to be close to unity, $\beta \simeq 0.95 - 0.98$, implying $\gamma = 1.02 - 1.05$ compatible with the results from Hi-C contact maps (Lieberman-Aiden et al. 2009; Zhang et al. 2012) and the findings reported in Chap. 4.

2.1.3 The Structure Factor

Another observable that is worth investigating in order to probe the internal fractal structure of polymer coils is the single-chain static structure factor, $S_1(q)$. Experimentally, this quantity can be measured via light or neutron scattering (refer to Rubinstein and Colby 2003 for experimental realisation details). This is defined as

$$S_1(q) = \left\langle \frac{1}{M} \sum_i^M \sum_j^M e^{i\boldsymbol{q}(\boldsymbol{r}_i - \boldsymbol{r}_j)} \right\rangle \tag{2.28}$$

where the average is taken over polymers, monomer positions $\boldsymbol{r}_i$ and over orientations of the scattering wave-vector $\boldsymbol{q}$ (when the system is isotropic). For wave-vectors $|\boldsymbol{q}|$ much smaller than R_g^{-1} (or length-scales $|\boldsymbol{q}|^{-1}$ much larger than R_g), the scattering function gives

$$S_1(q) \simeq M, \tag{2.29}$$

since all monomers within the coil contribute to the sum. When $2\pi R_g^{-1} < q < 2\pi\sigma^{-1}$, one finds that all monomers n_q within the volume q^{-3} contribute to $S_1(q)$. In this case, the static structure factor relates to the fractal dimension of the chain as

$$S_1(q) \simeq n_q \simeq \left(\frac{1}{q^d \sigma^d}\right)^{1/\nu d} = (q\sigma)^{-1/\nu} = (q\sigma)^{-d_F}. \tag{2.30}$$

In the case of linear polymers in melt the structure factor correctly returns $d_F = 2$ for the whole range $2\pi R_g^{-1} < q < 2\pi\sigma^{-1}$ (Kremer and Grest 1990). In the case of

[5] These are obtained by using $1/d \leq \nu \leq 1$, $1 - 1/d \leq \beta_c = \beta_g \leq 1$, in Eqs. (2.24) and (2.27).

ring polymers in dense solutions the scaling of Eq. (2.28) is less unambiguous and it has been conjectured (Halverson et al. 2011) that it displays signatures of more complex internal arrangement of the coils (see also Chap. 4).

2.2 Dynamics

2.2.1 Diffusion Coefficient and Relaxation Time

The first theories describing how ring polymers diffuse through either other chains or a gel have been advanced separately by Cates and Deutsch (1986), Rubinstein (1986), Klein (1986). They share the same spirit, i.e. describing the diffusion of rings in the melt assuming that rings can move in an amoebae fashion through the surrounding (static) obstacles by successive protrusions mediated by kink-gas diffusion along the polymer contour (de Gennes 1979). Within this framework, "kinks" or "defects" (or excess of mass along the chain) can diffuse independently along the polymer contour until they stop their diffusion on a segment of the randomly branched ring structure and contribute to the extension of that segment. By assuming that the kinks perform a 1D random walk along the contour, the time required to span a distance R_g corresponds to the Rouse time and is computed as

$$\tau_{\text{Rouse}} \sim M^2. \tag{2.31}$$

The ring can therefore renew its configuration by consecutive kinks diffusion. For a ring made by M segments this takes a time

$$\tau \sim M\tau_{\text{Rouse}} = M^3 \tag{2.32}$$

or, equivalently, a diffusion coefficient

$$D_{CM} \sim \frac{R_g^2}{\tau} = M^{2\nu-3}. \tag{2.33}$$

Using the field-theoretic exponent in Eq. (2.9), i.e. $\nu = 5/(2d+4)$, one finally obtains

$$D_{CM} \sim M^{-(3d+1)/(d+2)}, \tag{2.34}$$

which, in 3D, gives $D_{CM} \sim M^{-2}$ roughly compatible with numerical evidence (see Chap. 4 and Cates and Deutsch 1986; Halverson et al. 2011). Incidentally, this result is the same for linear polymers in melt, since the overall size of isolated self-avoiding rings in a background of obstacles (or gels) is described by $\nu = 1/2$ in 3D which is numerically equal to the exponent for linear polymers in melt. If one were to use

the fractal globule exponent $\nu = 1/3$, Eq. (2.33) would give $D_{CM} \sim M^{-7/3}$ which is weaker than the experimentally and computationally observed scaling.

More recently, Milner, Iyer and then Grosberg (Iyer and Arya 2012; Smrek and Grosberg 2015) advanced several other theories for the diffusion of a ring polymers among other chains, or "fixed obstacles". Milner and Newhall (2010) proposed an approach based on the "centrality" of a node in the lattice animal representation of the ring defined as

$$\zeta_k = \min\left(M_1(k), M - M_1(k)\right) \tag{2.35}$$

where $M_1(k)$ is the size of one of the two sub-trees generated by cutting the k-th bond of the tree-representation (see Fig. 2.1). They proposed that, analogously to the reptation mechanism in linear polymers, rings undergo diffusion by vacating bonds via the "evaporation" of one of the two sub-trees across that bond. This means that if the centrality ζ_k of bond k is small, one expects its relaxation to be quick. On the other hand, bonds whose removal produce two sub-trees with similar sizes are expected to take the longest to disappear. Kramers theorem can be used to show that the probability distribution of the nodes' centrality $P(\zeta)$ is given by the weights in Kramers theorem in Eq. (2.10) (Rubinstein and Colby 2003), appropriately normalised:

$$P(\zeta) = \frac{Z_\zeta Z_{M-\zeta}}{\sum_\zeta Z_\zeta Z_{M-\zeta}} \simeq \sqrt{\frac{n_v - 1}{8\pi(n_v - 2)}} \left(\frac{M}{\zeta(M-\zeta)}\right)^{3/2}, \tag{2.36}$$

where n_v is the valence of the nodes. This distribution has the feature that most of the nodes have low centrality and therefore relax quickly. One can then proceed by assuming that rings must arrange themselves in order to satisfy such a centrality distribution, and therefore this acts as an effective entropic potential for the rings biasing the mass diffusion as

$$\beta U_\zeta = -\log P(\zeta). \tag{2.37}$$

By performing Monte-Carlo simulations of trees diffusing on Bethe lattices, Milner and Newhall finally concluded that the mass accumulated within i generations from a given high-centrality bond scaled as $M(i) \sim i^a = i^{1.5-1.7}$ and, as a consequence, the variance of the centrality should scale as the mass diffused in a time $\tau_\zeta \sim t^2$ or

$$\langle \Delta\zeta^2 \rangle \sim t^{a/2} = t^{0.75-0.85}, \tag{2.38}$$

which leads to a total relaxation time for a tree formed by M nodes, corresponding to the time required for the centrality to diffuse a "distance" of order M, of

$$\tau_{\text{relax}} \sim M^{2/(a/2)} \simeq M^{8/3}. \tag{2.39}$$

Their result is again roughly compatible with recent findings (Kapnistos et al. 2008; Halverson et al. 2011), although completely neglects the motion of other chains

and, in particular, inter-chain interactions which can explain the even more recent findings (Pasquino et al. 2013; Gooßen et al. 2014; Doi et al. 2015) (see also to Chap. 4).

Smrek and Grosberg (2015) based on the novel description of a ring as an annealed tree made of crumpled branches decorating a self-avoiding path on a Cayley tree, i.e. $R \sim \sigma M^{1/3}$ and $R \sim \sigma^{2/5} L^{3/5}$ with $L \sim \sigma M^{5/9}$ (or $\nu = 1/3$, $\rho = 5/9$ and $\nu/\rho = 3/5$), advanced an alternative picture for the dynamics of rings in the melt. By assuming the existence of an "entanglement length" M_e below which the chain is Gaussian, i.e. $R_{\text{blob}} \sim \sigma M_e^{1/2}$, which is taken as the "blob size", the Rouse time for a blob can be written as

$$\tau_{\text{blob}} \sim \frac{\zeta_e M_e^2 \sigma^2}{k_B T} \tag{2.40}$$

where ζ_e is the effective friction of a blob. The chain is formed by $g = M/M_e$ blobs and every time a blob moves by R_{blob} a fraction $1/g$ of mass contributes to the overall diffusion of the centre of mass. The displacement of the chain center of mass, defined as

$$\langle \delta r_{CM}^2 \rangle \equiv g_3(t) = \left\langle [\boldsymbol{r}_{CM}(t + t_0) - \boldsymbol{r}_{CM}(t_0)]^2 \right\rangle_{t_0} \tag{2.41}$$

where $\langle \dots \rangle_{t_0}$ indicates average over different initial time-steps, can therefore be written as the displacement of g^ρ blobs of size R_{blob} forming the backbone L:

$$\langle \delta r_{CM}^2 \rangle \equiv g_3 \simeq g^\rho \left(\frac{\sigma M_e^{1/2}}{g} \right)^2 = M_e g^{\rho-2} \sigma^2 \tag{2.42}$$

that gives a diffusion coefficient of the blobs along the backbone of $D_{\text{bb}} \sim g_3/\tau_{\text{blob}}$. The full relaxation of the chain can be achieved once the centre of mass has travelled the ring's size L, i.e.

$$\tau_{\text{relax}} \sim \frac{L^2}{D_{\text{bb}}} = \tau_{\text{blob}} g^{\rho+2} \tag{2.43}$$

where one uses the fact that $L \sim M_e^{1/2} g^\rho \sigma$ giving

$$\tau_{\text{relax}} \sim \frac{\zeta_e \sigma^2}{k_B T} M^{23/9}. \tag{2.44}$$

The diffusion coefficient of the whole ring can be found by imposing that the ring is displaced a distance equal to its own size ($R = \sigma M_e^{1/2} g^\nu$) in the relaxation time τ_{relax}, i.e.

$$D_{CM} \equiv \frac{R^2}{\tau_{\text{relax}}} \sim \frac{M_e \sigma^2}{\tau_{\text{blob}}} g^{2\nu-\rho-2} \simeq D_{\text{blob}} M^{-17/9}. \tag{2.45}$$

All these findings are roughly compatible with numerical and experimental evidence, although they predict exponents that underestimate the observed ones. In particular, none of these explain why the sub-diffusion of the rings can be observed on length-scales many times the ring's gyration radius (Halverson et al. 2011, 2014). This may be due to chains moving and interacting non-trivially with one-another. The main reason for this is that mean-field theories analyse the behaviour of chains among other "fixed" chains. This is not the case in ring polymer melts where inter-chain interactions are important (see Chap. 4 and Halverson et al. 2011) and lead to collective behaviour. In order to correctly capture the dynamics of rings in the melt one should take into account the collective re-arrangements and configurational fluctuations, which makes the problem much harder to tackle.

2.2.2 How Rings Relax Stress

How rings relax their stress is perhaps one the key questions that I will try address. Recently there have been quite a few attempts to quantify the stress relaxation of rings in a background of obstacles (Milner and Newhall 2010) and in the melt (Kapnistos et al. 2008; Pasquino et al. 2013; Smrek and Grosberg 2015). All the theoretical effort has been focused on describing rings as amoebae (Rubinstein 1986) moving through obstacles situated around the ring double-folded configuration, i.e. not threading its contour. This strong assumption seems now ubiquitous when tackling the ring melt problem. On the contrary, I will show for the first time that this is instead not a correct assumption: Rings do protrude through one-another, and this has strong consequences on the dynamics, which should be considered when formulating a theory of their stress relaxation (see Chap. 4).

Experimentally there is several evidence that melts of rings display a very low stress-relaxation modulus $G(t)$ which never exhibits a plateau (Kapnistos et al. 2008; Pasquino et al. 2013). One the other hand, their slow overall relaxation to free diffusion (Halverson et al. 2011) as well as a dramatic viscosity enhancement observed in more recent findings (Doi et al. 2015) indicate that inter-coil interactions are important but hard to quantify.

It is very likely, that rings can relax their "internal" (or "configurational"), i.e. intra-coil, stress much faster than they can relax their inter-coil correlations. This conjecture will be supported by computational evidence in Chap. 4. Although achieving an analytical description of this behaviour is not an easy task, I believe that numerically probing the decoupling between relaxation time-scales related to different length-scales can help the theoretical community to formulate a more appropriate description for the motion of rings in the melt or dense solutions. In addition, the possibility that additional "relevant length-scales" exist and directly control the motion of rings in the melt has been raised in the past by Cates and collaborators (Müller et al. 1996; Muller et al. 2000) and might have found a direct proof in the results that I will present in Chap. 4.

While the internal relaxation of linear polymers is intimately related to the persistence of their neighbours forming the surrounding tube, this cannot be said for ring polymers, which can create new protrusion anywhere along their contour, being not limited by the presence of fixed ends. On the other hand, threadings, which are only possible between ring polymers, might affect the overall relaxation, i.e. the diffusion of the centre of mass of the polymers, leaving the internal stress relaxation mechanisms unaffected. In light of this I propose to focus on measuring the long-time inter-coil correlations which can be most readily done via scattering methods, and in particular via the coherent scattering function $S_c(q,t)$, defined below.

2.2.3 *Inter-Coil Correlations Probed by Dynamic Scattering*

Intra-coil correlations on length-scales $l = 2\pi q^{-1}$ are commonly probed by the coherent (or in-coherent) dynamic scattering function $S_c(q,t)$ (or $S_{in}(q,t)$ obtained setting $i = j$):

$$S_c(q,t) = \left\langle \frac{1}{M} \sum_{i}^{M} \sum_{j}^{M} e^{i\boldsymbol{q}(\boldsymbol{r}_i(t+t_0) - \boldsymbol{r}_j(t_0))} \right\rangle, \tag{2.46}$$

where the average is taken over the rings in the system and different t_0. In practice, one can imagine one probe chain in the solution scattering the incident light and then repeating the measurement over many different probe chains. This function is also sometimes called the "self-intermediate scattering function" and its Fourier transform the "self-part of the Van Hove function" in the glass-transition community (Berthier and Biroli 2011), where it is one of the main tools used to capture density-density correlations in a glass-forming systems. This scattering function was also studied by de Gennes (1981) to capture the behaviour of one reptating linear chain among other fixed chains.

In some cases, especially when dealing with molecular liquids or liquids made of simple constituents, the dynamic scattering function can give some information regarding inter-objects correlations, being internal degrees of freedom not included in the picture. In the case of polymer liquids, characterising inter-coil correlations via the dynamic scattering function can be less straightforward (Aichele and Baschnagel 2001; Frey et al. 2015). In particular, it is sometimes necessary to extend the computation of Eq. (2.46) to all the atoms in the system, rather than the ones forming the chains.[6] In this case the function is also known as the (dynamic) "pair-correlation" function, which is rarely studied as numerically infeasible to compute throughout the simulation.

In light of this one is often limited to the computation of Eq. (2.46) over the beads forming a single chain and to take the average over many chains. This means that

[6] In this case the computation can scale as $(NM)^2$, for a system of N chains M beads long, rather than NM^2.

$S_c(q,t)$ formally captures intra-coil correlations, and does not give direct evidence of inter-coil correlations. On the other hand, it is possible to infer some information on the inter-coil correlations when q becomes greater than the inter-coil distance 2λ, where λ is defined as

$$\lambda = \phi^{-1/3} R_g \tag{2.47}$$

where ϕ is the coils volume concentration, i.e.

$$\phi = \frac{4N\pi R_g^3}{3\sigma^3 L^3}. \tag{2.48}$$

The free volume available to the coils is $1/\phi$ and hence the free length (in units of the radius of gyration of the polymers) is $\phi^{-1/3}$. This means that above overlap the inter-coil distance is smaller than $2R_g$.

The information that one can obtain from $S_c(q,t)$ on the collective behaviour of the rings is based on the following reasoning: the dominant contribution to $S_c(q,t)$ comes from beads j that have not travelled (much) further than $2\pi/q$ from the other bead i within t time-steps. Therefore if there was a length-scale above which the independent motion of the beads was somehow constrained, that would appear when probing the system with the right q. In particular, one can imagine that if a ring was permanently pinned down by a frozen obstacle threading through its contour then one should expect

$$\lim_{t\to\infty} S_c(q \simeq \pi R_g^{-1}, t) = S_c^{\infty}(q \simeq \pi R_g^{-1}) > 0 \tag{2.49}$$

where $S_c^{\infty}(q)$ is a constant greater than zero and near one, as most of the beads forming the chain would be forever trapped in a region of linear size $l \simeq 2R_g$. On the other hand, if one was to probe larger q's, i.e. shorter length scales, one should in principle observe a more unconstrained relaxation, and in particular

$$\lim_{t\to\infty} S_c(q \gtrsim \pi R_g^{-1}, t) \simeq 0. \tag{2.50}$$

Although it is worth bearing in mind that this scattering function would not decay strictly to zero, as presence of permanent obstacles, i.e. regions that the beads are not free to explore, has the effect of suppressing the full de-correlation of the monomers.

Even in the case of multiple threadings, the cage formed by the penetrations represent a severe obstacle only for the overall diffusion, while internal modes, shorter than the average distance between threadings, are left unhindered. This suggests that in the case that the threadings are sparse enough, the ring should display a slow decorrelation of the dynamic scattering function on length-scales comparable to the diameter of the ring, but a faster de-correlation on shorter length scales. Extending this reasoning to the case where the pinning ring is itself mobile, one can, in any case, expect the passively threaded ring to be slower (again on length-scales $2\pi q^{-1} \gtrsim 2R_g$) compared to a ring that is instead not threaded. Both, threaded and non-threaded rings,

should instead relax their internal (i.e. $2\pi q^{-1} \lesssim 2R_g$) stress at roughly the same rate, i.e. having the same decay of $S_c(q \gtrsim \pi R_g^{-1}, t)$.

Investigating the differences/analogies in the behaviour of the dynamic scattering function at different length-scales can therefore give some insight into the presence of topological constraints in solutions of rings and can shed some light onto the dynamics of rings. This will be discussed in more detail in Chap. 4.

References

Aichele, M., Baschnagel, J.: Glassy dynamics of simulated polymer melts: coherent scattering and van Hove correlation functions. Eur. Phys. J. E **5**(2), 229 (2001)

Berthier, L., Biroli, G.: Theoretical perspective on the glass transition and amorphous materials. Rev. Mod. Phys. **83**(2), 587 (2011)

Brás, A., Gooßen, S., Krutyeva, M.: Compact structure and non-Gaussian dynamics of ring polymer melts. Soft Matter **10**, 3649 (2014)

Cates, M., Deutsch, J.: Conjectures on the statistics of ring polymers. J. Phys. Paris **47**, 2121 (1986)

Cremer, T., Cremer, C.: Chromosome territories, nuclear architecture and gene regulation in mammalian cells. Nat. Rev. Genet. **2**(4), 292 (2001)

Daoud, M., Joanny, J.: Conformation of branched polymers. J. de phys. **42**(10), 1359 (1981)

de Gennes, P.G.: *Scaling concepts in polymer physics*, Cornell University Press (1979)

de Gennes, P.G.: Coherent scattering by one reptating chain. J. Phys. (Paris) **42**(5), 735 (1981)

Doi, M., Edwards, S.: The Theory of Polymer Dynamics, Oxford University Press, Oxford (1988)

Doi, Y., Matsubara, K., Ohta, Y., Nakano, T., Kawaguchi, D., Takahashi, Y., Takano, A., Matsushita, Y.: Melt Rheology of Ring Polystyrenes with Ultrahigh Purity. Macromolecules **48**(9), 3140 (2015)

Edwards, S.: Statistical mechanics with topological constraints: I. Proc. Phys. Soc. **91**, 513 (1967)

Edwards, S.: Statistical mechanics with topological constraints: II. J. Phys. A: Math. Gen. **1**, 15 (1968)

Flory, P.J.: Principles of polymer chemistry, Cornell University Press. Ithaca, New York (1953)

Frey, S., Weysser, F., Meyer, H., Farago, J., Fuchs, M., Baschnagel, J.: Simulated glass-forming polymer melts: Dynamic scattering functions, chain length effects, and mode-coupling theory analysis. Eur. Phys. J. E **38**(11), 1 (2015)

Gooßen, S., Brás, A.R., Krutyeva, M., Sharp, M., Falus, P., Feoktystov, A., Gasser, U., Wischnewski, A., Richter, D.: Molecular Scale Dynamics of Large Ring Polymers. Phys. Rev. Lett. **113**, 169302 (2014)

Grosberg, A.: Annealed lattice animal model and Flory theory for the melt of non-concatenated rings: towards the physics of crumpling. Soft Matter **10**, 560 (2014)

Grosberg, A.Y., Rabin, Y., Havlin, S., Neer, A.: Crumpled globule model of the three-dimensional structure of DNA. Europhys. Lett. **23**(5), 373 (1993)

Gutin, A., Grosberg, A., Shakhnovich, E.: Polymers with annealed and quenched branchings belong to different universality classes. Macromolecules **26**(5), 1293 (1993)

Halverson, J.D., Lee, W.B., Grest, G.S., Grosberg, A.Y., Kremer, K.: Molecular dynamics simulation study of nonconcatenated ring polymers in a melt. I. Statics. J. Chem. Phys. **134**(20), 204904 (2011a)

Halverson, J.D., Lee, W.B., Grest, G.S., Grosberg, A.Y., Kremer, K.: Molecular dynamics simulation study of nonconcatenated ring polymers in a melt. II. Dynamics. J. Chem. Phys. **134**(20), 204905 (2011b)

Halverson, J.D., Kremer, K., Grosberg, A.Y.: Comparing the results of lattice and off-lattice simulations for the melt of nonconcatenated rings. J. Phys. A **46**(6), 065002 (2013)

Halverson, J.D., Smrek, J., Kremer, K., Grosberg, A.: From a melt of rings to chromosome territories: the role of topological constraints in genome folding. Rep. Prog. Phys. **77**, 022601 (2014)
Isaacson, J., Lubensky, T.C.: Flory exponents for generalized polymer problems. J. Phys. **41**, 469 (1980)
Iyer, B.V.S., Arya, G.: Lattice animal model of chromosome organization. Phys. Rev. E **86**(1), 011911 (2012)
Kapnistos, M., Lang, M., Vlassopoulos, D., Pyckhout-Hintzen, W., Richter, D., Cho, D., Chang, T., Rubinstein, M.: Unexpected power-law stress relaxation of entangled ring polymers. Nat. Mater. **7**(12), 997 (2008)
Klein, J.: Dynamics of entangled linear, branched, and cyclic polymers. Macromolecules **118**(33), 105 (1986)
Kremer, K., Grest, G.S.: Dynamics of entangled linear polymer melts: A molecular-dynamics simulation. J. Chem. Phys. **92**(8), 5057 (1990)
Lieberman-Aiden, E., van Berkum, N.L., Williams, L., Imakaev, M., Ragoczy, T., Telling, A., Amit, I., Lajoie, B.R., Sabo, P.J., Dorschner, M.O., Sandstrom, R., Bernstein, B., Bender, M.A., Groudine, M., Gnirke, A., Stamatoyannopoulos, J., Mirny, L.A., Lander, E.S., Dekker, J.: Comprehensive mapping of long-range interactions reveals folding principles of the human genome. Science **326**(5950), 289 (2009)
Lubensky, T., Isaacson, J.: Statistics of lattice animals and dilute branched polymers. Phys. Rev. A **20**(5), 2130 (1979)
Milner, S., Newhall, J.: Stress Relaxation in Entangled Melts of Unlinked Ring Polymers. Phys. Rev. Lett. **105**(20), 208302 (2010)
Mirny, L.A.: The fractal globule as a model of chromatin architecture in the cell. Chromosome Res. **19**(1), 37 (2011)
Muller, M., Wittmer, J., Cates, M.: Topological effects in ring polymers. II. Influence Of persistence length. Phys. Rev. E **61**(4), 4078 (2000)
Müller, M., Wittmer, J.P., Cates, M.E.: Topological effects in ring polymers: A computer simulation study. Phys. Rev. E **53**(5), 5063 (1996)
Obukhov, S., Rubinstein, M.: Dynamics of a ring polymer in a gel. Phys. Rev. Lett. **73**(9), 1263 (1994)
Parisi, G., Sourlas, N.: Critical behavior of branched polymers and the Lee-Yang edge singularity. Phys. Rev. Lett. **46**(14), 871 (1981)
Pasquino, R., Vasilakopoulos, T., Jeong, C., Lee, H., Rogers, S., Sakellariou, G., Allgaier, J., Takano, A., Bras, A., Chang, T., Goossen, S., Pyckhout-Hintzen, W., Wischnewski, A., Hadjichristidis, N., Richter, D., Rubinstein, M., Vlassopoulos, D.: Viscosity of Ring Polymer Melts. ACS Macro Lett. **2**, 874 (2013)
Raphael, E., Gay, C., de Gennes, P.G.: Progressive construction of an Olympic gel. J. Stat. Phys. **89**, 111 (1997)
Rosa, A., Everaers, R.: Structure and dynamics of interphase chromosomes. PLoS Comput. Biol. **4**(8), 1 (2008)
Rosa, A., Everaers, R.: Ring polymers in the melt state: The physics of crumpling. Phys. Rev. Lett. **112**, 118302 (2014)
Rubinstein, M.: Dynamics of ring polymers in the presence of fixed obstacles. Phys. Rev. Lett. **57**(24), 3023 (1986)
Rubinstein, M., Colby, H.R.: Polymer Physics, Oxford University Press, Oxford (2003)
Smrek, J., Grosberg, A.Y.: Understanding the dynamics of rings in the melt in terms of annealed tree model. J. Phys.: Condens. Matter **27**, 064117 (2015)
Zhang, Y., McCord, R.P., Ho, Y.-J., Lajoie, B.R., Hildebrand, D.G., Simon, A.C., Becker, M.S., Alt, F.W., Dekker, J.: Spatial organization of the mouse genome and its role in recurrent chromosomal translocations. Cell **148**(5), 908 (2012)

Chapter 3
Molecular Dynamics Models

It is nice to know that the computer understands the problem
…But I would like to understand it too.

E. Wigner

Computer simulations, or "experiments" (Frenkel and Smit 2001), are important tools for studying complex systems. This Thesis itself largely relies on computational methods, in particular Molecular Dynamics (MD) simulations. For this reason, I devote this chapter to describing the essence of the MD simulations employed here and the computational details of the models described in the subsequent chapters.

Molecular Dynamics simulations have been used for the first time in the late 50's (Alder and Wainwright 1959). They started as a method to investigate the properties of systems of hard spheres (Alder and Wainwright 1957) and simple liquids (Rahman 1964) and later became a fundamental technique to model the dynamics of biomolecules (McCammon et al. 1977; Karplus and Petsko 1990). As opposed to standard Monte-Carlo techniques, MD simulations offer the advantage of naturally probing the dynamical properties of the systems, such as transport coefficients, time-dependent responses and rheological properties. In addition, Molecular Dynamics models are very flexible in terms of the level of coarse-graining performed on the model. They can either be very accurate in describing microscopic molecular details or in evolving a more coarse-grained picture, depending on the level of detail needed. Usually, MD models lend themselves to a much higher level of molecular detail, than standard Monte-Carlo models. One of the key challenges of MD models is to include the appropriate inter-molecular potentials, and, in particular, find the right level of coarse-graining required to reach the best accuracy given practical constraints on their feasibility.

Because modelling microscopic chemical interactions are computationally expensive and much of the puzzling physical features of rings in solution are hidden in their long-time behaviour, my interest is in retaining only the key physical elements.

D. Michieletto, *Topological Interactions in Ring Polymers*, Springer Theses,
DOI 10.1007/978-3-319-41042-5_3

I therefore adopt coarse-grained models for the polymers in order to reach longer simulations time-scales. In particular, I will formulate a mesoscopic physical model of the polymers and neglect specific chemical details. Some of the problems discussed in the following chapters will be naturally associated with specific types of polymers. For instance, gel electrophoresis is very often performed on DNA samples, and therefore it is natural to start from a more physically faithful description for the DNA. On the other hand, the chemical details of the base-pair system is not necessary to capture the physics of gel electrophoresis and will, therefore, be coarse-grained out. In addition, addressing more coarse-grained models has often the advantage of delivering more general results, which might be valid for other systems, as long as they share similar physical and topological properties.

In what follows, I will firstly discuss some general elements of Molecular Dynamics simulations and secondly, I will give describe in detail the coarse-grained models used in the following chapters.

3.1 Molecular Dynamics Scheme

The aim of a Molecular Dynamics simulation is to integrate the classical equations of motion:

$$\begin{aligned} \frac{\partial \boldsymbol{r}_i}{\partial t} &= \boldsymbol{v}_i \\ m_i \frac{\partial \boldsymbol{v}_i}{\partial t} &= \boldsymbol{F}_i = -\frac{\partial \mathcal{U}}{\partial \boldsymbol{r}}, \end{aligned} \tag{3.1}$$

where m_i and $\boldsymbol{r}_i$ are, respectively, the mass and the position of the ith atom, often also referred to as "monomers". $\boldsymbol{F}_i$ is the force acting on the ith atom, which can be calculated by knowing the potential energy $\mathcal{U}$. This is, in general, dependent on all the other atoms in the system, and, of course, on external fields applied to the system from the outside. In order to reproduce the correct motion, one therefore needs to define what are the interactions between the atoms in the system under study. These can be classified as: non-bonded and bonded potentials. The former deal with interactions between atoms which are not connected at a molecular level, for instance atoms belonging to different polymers. The latter describe the interactions between atoms which do share a molecular connection, such as hydrogen and oxygen in a water molecule.

3.1.1 Non-bonded Potentials

Each atom in the simulation can interact via non-bonded potentials with all the other atoms in the system and, if present, a wall delimiting the simulation box. Because of

this, one needs to define the 1-body, 2-body, 3-body, *etc.* interactions as

$$\mathcal{U}_{nb} = \sum_{i}^{N} u(\boldsymbol{r}_i) + \sum_{i} \sum_{j>i} v(\boldsymbol{r}_i, \boldsymbol{r}_j) + \cdots \tag{3.2}$$

where $u(\boldsymbol{r}_i)$ is the potential describing the interaction between a single atom and, for instance, a wall and $v(\boldsymbol{r}_i, \boldsymbol{r}_j)$ the potential describing a 2-body interaction, e.g. a Lennard-Jones or Coulomb potential. For instance in the case of charged polymers, one should, in principle, include both steric and Coulomb interactions. It is also common, as long as the simulation reproduces the essential physics, to drop all the higher order terms.

The two-body repulsion can be efficiently modelled via the following shifted-truncated form of the Lennard-Jones (LJ) potential (or Weeks–Chandler–Andersen model Weeks et al. 1971):

$$\mathcal{U}_{LJ}(\boldsymbol{r}_i, \boldsymbol{r}_j) = 4\epsilon \left[\left(\frac{\sigma_c}{r_{ij}} \right)^{12} - \left(\frac{\sigma_c}{r_{ij}} \right)^{6} + \frac{1}{4} \right] \Theta(2^{1/6}\sigma_c - r_{ij}), \tag{3.3}$$

where $\Theta(x)$ is the usual Heaviside function, i.e. 1 for $x \geq 0$ and 0 otherwise, and σ_c is the minimum distance between beads. The potential depth is ϵ and $r_{ij} = |\boldsymbol{r}_i - \boldsymbol{r}_j|$ is the distance between the ith and jth atom. This version of the Lennard-Jones potential is chosen in order to broadly model only the steric repulsion between atoms, thereby avoiding (i) unwanted Van der Walls attractions and (ii) long-ranged interactions without introducing discontinuity in the potentials.

Another useful way of modelling steric interactions is via a "soft" potential. One of the most used forms of this potential is the following:

$$\mathcal{U}_{\text{soft}}(\boldsymbol{r}_i, \boldsymbol{r}_j) = \epsilon_s \left[1 + \cos\left(\frac{\pi r_{ij}}{r_c} \right) \right] \Theta(r_c - r). \tag{3.4}$$

Here, ϵ_s is the height of the potential at $r_{ij} = 0$ and r_c the cut-off. This potential is generally used for initialising a system possessing partially overlapping elements. These are in fact gently pushed apart by this potential without generating numerical divergences. This pre-equilibration step is very important to avoid "blow-ups" and it is usually done by performing a short run in which the parameter ϵ_s is slowly raised typically from $\epsilon_s = 0$ to $\epsilon_s = 50\epsilon$, before the LJ potential is turned on.

3.1.2 Bonded Potentials

Bonded potentials describe the interactions between atoms which share molecular bonds. The simplest potential describing the connection between two atoms is the harmonic potential that models the bond as a spring with stiffness κ_h and equilibrium length r_0:

$$\mathcal{U}_{\text{harm}}(\boldsymbol{r}_i, \boldsymbol{r}_j) = \frac{\kappa_h}{2}\left[r_{ij} - r_0\right]^2 . \tag{3.5}$$

This potential is usually inappropriate for use in polymer chains simulations, especially in dense conditions, as it can allow bonds to stretch and polymers to cross through one-other. More appropriate 2-body bonded potentials exist for system of polymers, such as the Finitely Extensible Non-linear Elastic (FENE) potential:

$$\mathcal{U}_{\text{FENE}}(\boldsymbol{r}_i, \boldsymbol{r}_j) = -\frac{\kappa_f}{2} R_0^2 \ln\left[1 - \left(\frac{r_{ij}}{R_0}\right)^2\right], \tag{3.6}$$

for $r_{ij} < R_0$ and $\mathcal{U}_{\text{FENE}}(\boldsymbol{r}_i, \boldsymbol{r}_j) = \infty$, otherwise. The values of the parameters chosen here in this Thesis are $R_0 = 1.6\,\sigma$ and $\kappa_f = 30\,\epsilon/\sigma^2$. These choices ensure that strand-crossing events are suppressed. This is of paramount importance when the topological state of a polymer, e.g. (un-)knotted or (un-)linked, needs to be preserved throughout the simulation.

In order to model the chains stiffness, the following 3-body bonded potential is commonly used:

$$\mathcal{U}_{\text{bend}}(\boldsymbol{r}_i, \boldsymbol{r}_j, \boldsymbol{r}_k) = \frac{k_B T l_p}{\sigma}\left[1 - \frac{\boldsymbol{r}_{ij}\cdot\boldsymbol{r}_{jk}}{r_{ij} r_{jk}}\right] = \frac{k_B T l_p}{\sigma}\left[1 - \cos\theta\right], \tag{3.7}$$

where the angle θ is defined as the angle between consecutive bonds (see Fig. 3.1). Here, $\boldsymbol{r}_{ij} \equiv \boldsymbol{r}_j - \boldsymbol{r}_i$ is the vector joining two bonded monomers and l_p is the persistence length which corresponds to half the Kuhn length l_K Doi and Edwards 1988. For instance, to correctly model hydrated double-stranded DNA (dsDNA) chain embedded in a solvent in physiological conditions, one should take its persistence length to be $l_p = l_K/2 \simeq 20\sigma$, i.e. roughly 20 times its thickness.

A 4-body bonded interaction can be used to capture the torsional stiffness of polymers: The most common choice in this case is a dihedral potential, which can

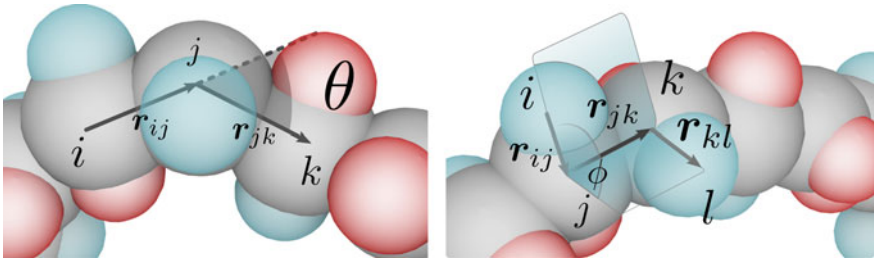

Fig. 3.1 The angle θ for the bending potential in Eq. (3.7) is defined as the angle between the vectors joining consecutive pairs along the polymer contour. The angle ϕ for the dihedral potential in Eq. (3.8) is defined as the angle between the planes defined by the pairs of vectors $\boldsymbol{r}_{ij}, \boldsymbol{r}_{jk}$ and $\boldsymbol{r}_{jk}, \boldsymbol{r}_{kl}$ connecting the polymer backbone (*grey beads*) to the *patches* to the sides (*blue* or *red*)

be modelled as a CHARMM (MacKerell et al. 1998) potential:

$$\mathcal{U}_{\text{dihedral}}(\boldsymbol{r}_i, \boldsymbol{r}_j, \boldsymbol{r}_k, \boldsymbol{r}_l) = \kappa_d \left[1 + \cos\left(n\phi - d\right)\right] \tag{3.8}$$

where κ_d is the spring energy, $n \geq 0$ is a free parameter, d an integer number of degrees and ϕ is defined as the angle between the planes defined by the triplets of atoms ijk and jkl (Fig. 3.1). The angle ϕ is defined as $\cos\phi = \hat{\boldsymbol{n}}_{ijk} \cdot \hat{\boldsymbol{n}}_{jkl}$ where $\boldsymbol{n}_{ijk} = \boldsymbol{r}_{ij} \times \boldsymbol{r}_{ik}$ and $\hat{\boldsymbol{n}} = \boldsymbol{n}/n$ is the unit vector. This model is particularly used when studying torsionally constrained polymers, e.g. non-nicked dsDNA, and its consequent supercoiling properties (Brackley et al. 2014).

3.1.3 Brownian Dynamics

When the subject of the "computer experiment" involves a solvent, and the hydrodynamic interactions can safely be neglected, it is common practice to model the solvent "implicitly". Instead of integrating the deterministic motion of the small solvent particles, one can couple the beads forming the solute with a bath at fixed temperature T: this implies that every atom in the system undergoes some motion which is no longer deterministic but includes a stochastic term. This is modelled as a force that represents the random (frequent) collision of the solute with the solvent (much smaller) particles. This method of simulating systems where the solute molecules are much heavier than the solvent ones is often referred to as "Brownian Dynamics". The equation describing the motion of the atoms is the Langevin equation:

$$m_i \frac{\partial^2 \boldsymbol{r}_i}{\partial t^2} = -\xi_i \frac{\partial \boldsymbol{r}_i}{\partial t} - \frac{\partial \mathcal{U}}{\partial \boldsymbol{r}} + \sqrt{2k_B T \xi_i}\, \boldsymbol{f}_i \tag{3.9}$$

where $\boldsymbol{f}_i$ is a delta correlated white noise with zero mean

$$\left\langle f_i^{\alpha}(t) f_j^{\beta}(s) \right\rangle = \delta(t-s)\delta_{ij}\delta_{\alpha\beta} \tag{3.10}$$

along each Cartesian component (Greek letters) and ξ_i is the friction coefficient of the ith atom. In the limit in which the term on the left hand side of Eq. (3.9) is neglected, i.e. in the long-time limit $t \gg m_i/\xi_i$, the Langevin equation takes the "over-damped" form:

$$\frac{\partial \boldsymbol{r}_i}{\partial t} = -\frac{1}{\xi_i}\frac{\partial \mathcal{U}}{\partial \boldsymbol{r}_i} + \sqrt{2D_i}\, \boldsymbol{f}_i \tag{3.11}$$

where the diffusion coefficient of the ith atom is $D_i = k_B T/\xi_i$. Equation (3.11) is a good approximation of the motion of atoms described by Eq. (3.9) only after an inertial time $\tau_{in} = m_i/\xi_i$. The friction ξ_i can be expressed as $\xi_i = m_i/\gamma_d$, where γ_d (having time units) is a damping factor that regulates the time-scale related to temperature relaxation. The time-scale τ_{in} can therefore be understood as the time

required for the temperature to equilibrate across the system, or for the kinetic energy to be redistributed. The parameter γ_d can be thought of as inversely proportional to the solution viscosity and is directly tuned by the user when integrating Eq. (3.9) in the LAMMPS (http://lammps.sandia.gov) engine, which I will employ below.

System Units

When performing Molecular Dynamics simulations it is often useful to express the properties of the system as multiples of unit-less fundamental quantities. All the results reported in this Thesis from MD simulations will be given in such units. In particular, distances will be measured in units of σ, masses in units of the monomer mass m, time in units of the Lennard-Jones (LJ) time $\tau_{LJ} \equiv \sigma\sqrt{m/\epsilon}$, energies in units of ϵ, temperatures in terms of ϵ/k_B and forces in units of ϵ/σ.

The LJ time can be understood as the time required by a particle of mass m to be repelled to a distance σ by a force ϵ/σ, and gives the time-scale for collisions between particles interacting via the Lennard-Jones potential in Eq. (3.3). The standard convention for Lennard-Jones reduced units sets $m = \sigma = \epsilon = k_B = 1$, therefore setting also the LJ time $\tau_{LJ} = 1$. The inertial time is related to this time by the choice of the damping parameter γ_d, which is units of LJ time. In what follows I will always set $\gamma_d = \tau_{LJ}$ which gives $\tau_{in} = \tau_{LJ} = m/\xi = 1$. This implies that the overdamped limit of the Langevin equation becomes a good approximation of Eq. (3.9) already after few timesteps.

Finally, the Brownian time $\tau_{br} = \sigma^2/D_b$, where $D_b = k_B T/\xi$ is the diffusion coefficient of a bead and can be interpreted as the time needed for an atom to diffuse its own size. With this choice of parameters, the Brownian time is equal to the LJ time and the inertial time. Summarising, with this choice of parameters, the relevant time-scales for the microscopic motion of the atoms are all set to 1 in LJ reduced units.

Mapping the reduced LJ units to real units can be easily done by fixing the fundamental quantities in the system, i.e. the length-scale σ and the temperature T. For instance, when the length-scale σ reflects the thickness of hydrated dsDNA, it can take values between 2 to 15 nm depending on the concentration of salt, or more generally, positive ions, in solution (Rybenkov et al. 1993). Here, I will often use the value of $\sigma = 2.5$ nm found near physiological conditions (NaCl concentration of 0.15 M). The temperature will be set, as usual, at $T = 300$ K. By using the Stokes formula for the friction of beads of diameter σ in a solution of viscosity η_{sol}

$$\zeta = 3\pi\eta_{sol}\sigma \tag{3.12}$$

together with $m/\xi = \tau_{LJ} = \sigma\sqrt{m/\epsilon}$ and $\epsilon = k_B T$ (see next section) one can obtain an expression for the LJ time independent of the mass:

$$\tau_{LJ} = \frac{3\pi\eta_{sol}\sigma^3}{k_B T} = \tau_{br} = \tau_{in}. \tag{3.13}$$

By using the nominal water viscosity $\eta = 1\ cP$ one finally obtains $\tau_{LJ} \simeq 36\ ns = \tau_{in} = \tau_{br}$. It is worth stressing that the simulation time in real-life units that can be achieved with this scheme scales as the cubic power of the monomer size σ. This implies that choosing the right level of detail is of paramount importance. In the case of a dsDNA, modelling the chain as a single chain of thickness σ, or as two spiralling helices, each of thickness σ, can dramatically reduce the typical simulation time-scale that can be achieved by a factor of about 5^3.

Time Integration

The integration is performed in the canonical ensemble, i.e. number (N), volume (V) and temperature (T) are conserved. The temperature is fixed by a Langevin thermostat, which couples the system to a bath at temperature T by regulating the magnitude of the thermal noise via the fluctuation-dissipation relation. Since the focus of this Thesis is on systems where the thermal noise plays an important role, the temperature T is chosen so that the thermal energy $k_B T$ equals the LJ interaction energy ϵ used in Eq. (3.3). The numerical integration is performed using the velocity-Verlet algorithm (Swope et al. 1982) using a time-step of $\Delta t = 0.01\tau_{LJ}$. The Verlet class of algorithms has the advantage of conserving the energy, or volume of phase space, during the time-evolution of the Hamilton equations, as opposite to, for instance, the Euler method, which does not ensure energy conservation (Frenkel and Smit 2001). The standard implementation of the velocity-Verlet scheme requires the storing of information for two time-steps. The "velocity-Verlet" version instead has the advantage of storing the information only for a single time-step. The standard Verlet algorithm in the case of systems in which there is no implicit solvent, i.e. in the case the system evolves according to Eq. (3.1), can be easily derived by looking at the Taylor expansion of the equations of motion around time t:

$$\boldsymbol{r}(t+\Delta t) = \boldsymbol{r}(t) + \boldsymbol{v}(t)\Delta t + \frac{\boldsymbol{a}(t)}{2}\Delta t^2 + \frac{\boldsymbol{b}(t)}{6}\Delta t^3 + \mathcal{O}(\Delta t^4) \tag{3.14}$$

$$\boldsymbol{r}(t-\Delta t) = \boldsymbol{r}(t) - \boldsymbol{v}(t)\Delta t + \frac{\boldsymbol{a}(t)}{2}\Delta t^2 - \frac{\boldsymbol{b}(t)}{6}\Delta t^3 + \mathcal{O}(\Delta t^4) \tag{3.15}$$

where $\boldsymbol{b}(t) = \dfrac{\partial^3 \boldsymbol{r}(t)}{\partial t^3}$, $\boldsymbol{a}(t)$ the acceleration and $\boldsymbol{v}(t)$ the velocity. By summing these two equations one obtains:

$$\boldsymbol{r}(t+\Delta t) = 2\boldsymbol{r}(t) - \boldsymbol{r}(t-\Delta t) + \boldsymbol{a}(t)\Delta t^2 \tag{3.16}$$

which is the standard form of the Verlet algorithm. It is important to stress that the positions thereby generated are accurate up to fourth order in Δt. The expression for the velocities can be obtained using:

$$\boldsymbol{r}(t+\Delta t) - \boldsymbol{r}(t-\Delta t) = 2\boldsymbol{v}(t)\Delta t + \mathcal{O}(\Delta t^3) \tag{3.17}$$

which gives:

$$\boldsymbol{v}(t) = \frac{\boldsymbol{r}(t+\Delta t) - \boldsymbol{r}(t-\Delta t)}{2\Delta t} + \mathcal{O}(\Delta t^2) \tag{3.18}$$

and is only accurate up to second order.

It is instructive also to look at this algorithm from another point of view: instead of integrating Eq. (3.1) one could attempt to generate set of coordinates that minimise the (discretised) action:

$$\mathcal{S} = \sum_{n=n_{\text{in}}}^{n_{\text{fin}}} \Delta t \left[\frac{m}{2} \left(\frac{\boldsymbol{r}_{n+1} - \boldsymbol{r}_n}{\Delta t} \right)^2 - \mathcal{U}_n(\{\boldsymbol{r}\}) \right] \tag{3.19}$$

where $\boldsymbol{r}_n$ is the position of the atom at time-step $n\Delta t$ and $\mathcal{U}_n(\{\boldsymbol{r}\})$ is the total potential taking into account the position of all the atoms in the system at the same time-step. The action $\mathcal{S}$ is stationary when its derivative with respect to all $\boldsymbol{r}_n$ is zero. This implies:

$$m \left(\frac{2\boldsymbol{r}_n - \boldsymbol{r}_{n+1} - \boldsymbol{r}_{n-1}}{\Delta t} \right) - \Delta t \frac{\partial \mathcal{U}_n(\{\boldsymbol{r}\})}{\partial \boldsymbol{r}_n} = 0$$

or

$$\boldsymbol{r}_{n+1} = 2\boldsymbol{r}_n - \boldsymbol{r}_{n-1} - \frac{\Delta t^2}{m} \frac{\partial \mathcal{U}_n(\{\boldsymbol{r}\})}{\partial \boldsymbol{r}_n} \tag{3.20}$$

which is the Verlet algorithm. This explicitly shows that the trajectory generated by this algorithm "shadows" the true trajectory, i.e. the one that minimises the action in Eq. (3.19), and is exact in the limit $\Delta t \to 0$.

3.2 Modelling

This section describes the main models used to simulate ring polymers and gels in this Thesis. Unless otherwise stated, the parameters used have been defined in the previous Section. Most of the models summarised in this work, focus on polymers whose torsional stiffness is neglected; a good approximation when simulating nicked DNA polymers, i.e. dsDNA segments which have a gap along one of the two strands forming the double-helix. In this case the constraint in the torsion is mechanically released and therefore the torsional stiffness can be neglected.

3.2.1 Modelling (Knotted) Ring Polymers

Ring polymers are, in general, prepared as a string of monomer locations that follow a parametrised curve in $\mathbb{R}^3$ (see Fig. 3.2a). The large majority of knot types investigated in this Thesis can in fact be described in terms of simple functions from S^1 to $\mathbb{R}^3$.

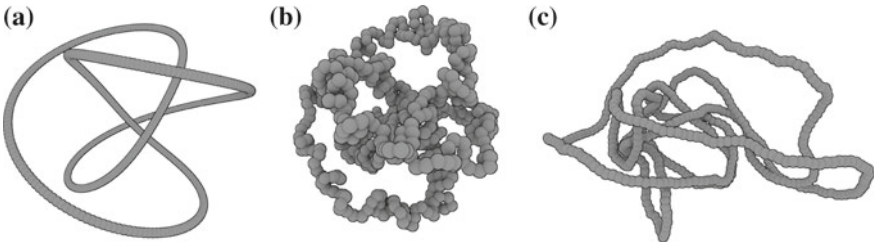

Fig. 3.2 Initialising, pre-equilibrating and equilibrating a trefoil knot

For example the family of (p, q)-torus knots (Adams 1994) can be parametrised as

$$\begin{aligned} x(\phi) &= r(\phi)\cos(p\phi) \\ y(\phi) &= r(\phi)\sin(p\phi) \\ z(\phi) &= -\sin(q\phi) \end{aligned} \tag{3.21}$$

where $r(\phi) = \cos(q\phi) + 2$ and $\phi \in (0, 2\pi)$. This family of knots contains the un-knot (0_1), formed as a $(p, 1)$- or $(p, -1)$-torus knot, the trefoil knot (3_1) formed as a $(2, -3)$-torus knot (left-handed) or as a $(2, 3)$-torus knot (right-handed), the pentafoil (5_1) formed as a $(5, 2)$-torus knot, *et cetera*. The knots belonging to this family are knots that can be drawn on the surface of a torus without self-crossings. In particular, p and q represent the number of turns along the "longitudinal" and the "meridional"[1] direction of a torus, respectively. These have to be relatively prime to form a knot, otherwise one would obtain a link with two or more components.

The figure of eight knot (4_1) is not part of the torus knot family as it cannot be drawn on the surface of a torus (having genus $G = 1$) but it can be embedded on the surface of a genus $G = 2$ surface, i.e. it is a two-embeddable knot (Adams 1994), and has a simple parametrisation:

$$\begin{aligned} x(\phi) &= r(\phi)\cos(3\phi) \\ y(\phi) &= r(\phi)\sin(3\phi) \\ z(\phi) &= \sin(4\phi) \end{aligned} \tag{3.22}$$

where $r(\phi) = 2 + 2\cos(2\phi)$. Other types of knots which are not torus knots, such as the 5_2 or 6_1, can be described as Lissajous knots (Bogle et al. 1994). They can be parametrised as

$$\begin{aligned} x(\phi) &= \cos(n_x\phi + \psi_x) \\ y(\phi) &= \cos(n_y\phi + \psi_y) \\ z(\phi) &= \cos(n_z\phi + \psi_z) \end{aligned} \tag{3.23}$$

[1] The meridian is the circle bounding a disc inside the torus.

where n_x, n_y and n_z are (relatively prime) integers and ψ_x,ψ_y and ψ_z are (real) phases. For instance, the three-half twist knot (5_2) can be obtained by setting $\boldsymbol{n} = (n_x, n_y, n_z) = (3, 2, 7)$ and $\boldsymbol{\psi} = (\psi_x, \psi_y, \psi_z) = (0.7, 0.2, 0)$ while the Stevedore's knot (6_1) is found by setting $\boldsymbol{n} = (3, 2, 5)$ and $\boldsymbol{\psi} = (1.5, 0.2, 0)$.

Knots for which a parametrisation is not known, such as 6_2 and 6_3, are obtained by simulating polymers which are allowed to self-cross, i.e. $\mathcal{U}_{\text{LJ}} = 0$, and selected by computing their Alexander polynomial (Orlandini and Whittington 2007; Micheletti et al. 2011) (see Appendix A for further details on algorithms for identifying knot types). The ones with the desired topology are then considered and used as a template for creating other knotted conformations to be used in other simulations.

Topology-Preserving Equilibration

Each of the polymers is initialised by performing a short run ($\sim$100 τ_{LJ}) in which the atoms forming a chain M beads long repel each-other via a soft potential and consecutive atoms are connected via a harmonic potential (see Fig. 3.2):

$$\mathcal{U}_{\text{pre-eq}} = \sum_{i=1}^{M} \left[\mathcal{U}_{\text{harm}}(\boldsymbol{r}_i, \boldsymbol{r}_{i+1}) + \mathcal{U}_{\text{bend}}(\boldsymbol{r}_i, \boldsymbol{r}_{i+1}, \boldsymbol{r}_{i+2})\right] + \sum_{i=1}^{M-1} \sum_{j=i+1}^{M} \mathcal{U}_{\text{soft}}(\boldsymbol{r}_i, \boldsymbol{r}_j). \tag{3.24}$$

In Eq. (3.24), a modulo-M indexing is taken implicitly, i.e. $M + 1 \equiv 1$, in order to join the chain ends. The persistence length is initially taken small ($\xi_p = 1\sigma$). This allows the system to adjust the length of the bonds and eliminate any unwanted overlapping between atoms at the same time avoiding generating numerical divergences. After the pre-equilibration run, the topology of the knot is generally checked once more, as strand crossings have a non-negligible chance to occur while the soft repulsive potential is on. The equilibration run is then performed using the following intra-chain potential:

$$\mathcal{U}_{eq} = \sum_{i=1}^{M} \left[\mathcal{U}_{\text{FENE}}(\boldsymbol{r}_i, \boldsymbol{r}_{i+1}) + \mathcal{U}_{\text{bend}}(\boldsymbol{r}_i, \boldsymbol{r}_{i+1}, \boldsymbol{r}_{i+2})\right] + \sum_{i=1}^{M-1} \sum_{j=i+1}^{M} \mathcal{U}_{\text{LJ}}(\boldsymbol{r}_i, \boldsymbol{r}_j), \tag{3.25}$$

which strongly suppresses any intra-chain crossings. The length of the equilibration run depends on the system concentration and the ring's length. Typically, this can range between $t_{eq} \simeq 10^4$ to 10^7 τ_{LJ} time-steps. In this Thesis I will consider a system "equilibrated" when each of the rings has travelled a mean square distance of at least its own size, i.e. the mean square displacement of the centre of mass of the rings is at least the radius of gyration squared (see Fig. 3.3).

Throughout pre-equilibration and equilibration runs, the inter-ring interaction can be safely modelled via the Lennard-Jones potential, Eq. (3.3), since different rings are normally prepared distant enough to avoid overlapping during the initial time-steps. The inter-chain potential is therefore:

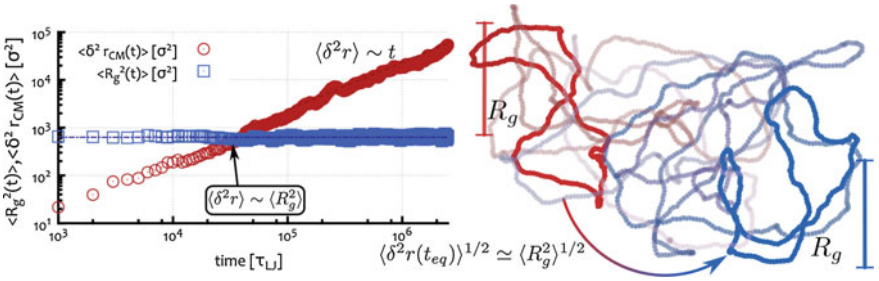

Fig. 3.3 Equilibration of a system rings with $M = 256$ beads in dilute regime. *Red* data-points show the mean square displacement of the centre of mass of the rings $\langle \delta^2 r_{CM}(t) \rangle$ averaged over the rings. *Blue* data-points show the average radius of gyration squared $\langle R_g^2(t) \rangle$. In the long-time limit the mean square displacement follows the law $\langle \delta^2 r_{CM}(t) \rangle = 6Dt$, which is here recovered with $D = 1/M$ (see Sect. 3.1.3). The equilibration is reached once each ring has diffused at least once its own size R_g; in this case $t_{eq} \simeq 3\ 10^4\ \tau_{LJ}$. On the left, a graphical representation of a ring diffusing its own R_g is shown, with *red*→*blue* a proxy for time

$$\mathcal{U}_{inter} = \sum_{\alpha=1}^{N-1} \sum_{\beta=\alpha+1}^{N} \sum_{i=1}^{M} \sum_{j=i}^{M} U_{LJ}(\boldsymbol{r}_{i_\alpha}, \boldsymbol{r}_{j_\beta}), \tag{3.26}$$

where N is the number of chains in the system and the indexes i and j run over the atoms in the chains which are labelled with α and β. In the case there also is a gel in the system (see Sect. 3.2.2), the interaction between beads forming the polymers (of size σ) and the gel structure (of size σ_g) is also modelled as a purely steric interaction via the following potential

$$\mathcal{U}_{mesh} = \sum_{k=1}^{M_{gel}} \sum_{\alpha=1}^{N} \sum_{i=1}^{M} U_{LJ}(\boldsymbol{r}_k, \boldsymbol{r}_{i_\alpha}), \tag{3.27}$$

where k runs over the atoms forming the gel and the minimum distance is $\sigma_c = (\sigma + \sigma_g)/2$.

Characterising Polymer Knots with Their Average Crossing Number

How can we characterise a knot's complexity? This is a very difficult, open problem, which I believe will generate research and scientific discussion for many years to come. Some observables can capture some of the physical properties of knotted polymeric strands. For instance, by parametrising a knot $\mathcal{K}$ as a function $f : S^1 \to \mathbb{R}^3$, one can define the average crossing number (ACN) of $\mathcal{K}$ as its unsigned writhe:

$$ACN(\mathcal{K}) = \frac{1}{4\pi} \int_{\mathcal{K}} \int_{\mathcal{K}} \frac{|(f'(s_1) \times f'(s_2)) \cdot (f(s_1) - f(s_2))|}{|f(s_1) - f(s_2)|^3} ds_1 ds_2. \tag{3.28}$$

In some sense, this formula gives the number of crossings of a certain knot configuration, averaged over the 3D space. This has to be compared with the more common "minimal crossing number" (MCN) which is the minimal number of crossings in any knot diagram of a knot (see Appendix A). The ACN is in general higher than the minimal crossing number of a knot and thanks to the "averaging" property of this quantity, the ACN has been found to be an appropriate quantity to characterise the complexity of knots subject to thermal fluctuations and migrating through a medium. In particular, it is worth stressing that the ACN of knotted polymers possesses two crucial properties: (i) the ACN grows with the length of the polymer and it has been found to increase a little faster than linearly for random walks, i.e. $ACN(M) \simeq M \log(M)$ (Diao et al. 2003; Orlandini et al. 1994) for a M segments-long walk, and (ii) the ACN of knots can be computed from their ideal configuration, for instance generated as energy minimising configurations (Kusner and Sullivan 1994, 1998) or via "tube inflation" procedures (Katritch et al. 1996), and even once these knots are then left to thermalise or their contour length is increased, their thermally averaged (or "mean") ACN is in a one-to-one correspondence to their "ideal" ACN (Katritch et al. 1996). In this respect, the thermally fluctuating knots retain some of their ideal properties and these are well captured by the ACN (Katritch et al. 1996).

This can be observed in Fig. 3.4a where I report the thermally averaged value of the ACN of knots as a function of their "ideal" ACN measured from ideal configurations. In addition, Fig. 3.4b clearly shows that more complex knots with same contour length assume more compact configurations. In particular, it was found (Stasiak et al. 1996) that the square gyration radius is inversely proportional to the ACN, i.e.

$$\langle R_g^2 \rangle^{-1} \sim ACN \tag{3.29}$$

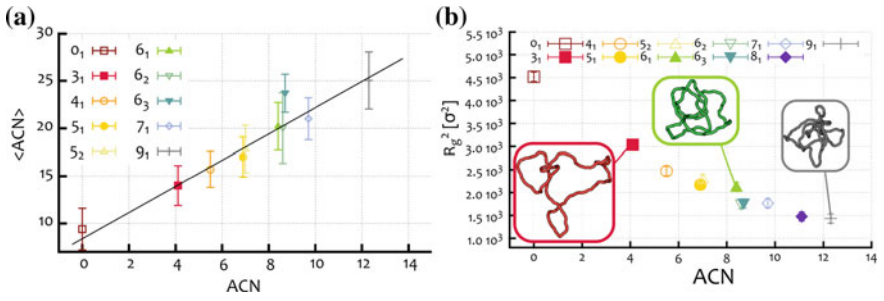

Fig. 3.4 **a** Average crossing number averaged over knotted configuration subject to thermal fluctuations ($\langle ACN \rangle$) as a function of their ACN calculated from energy minimising configurations (Kusner and Sullivan 1994). The one-to-one correspondence allows us to uniquely use the ACN from the ideal configurations. **b** The radius of gyration squared as a function of the ACN clearly shows that more complex knots assume more compact configurations

and that this is related to the faster sedimentation speed (Piili et al. 2013; Weber et al. 2013) and faster electrophoretic migration (Stasiak et al. 1996) of more complex knots. Because of these reasons, the ACN obtained from ideal configurations is a good quantity for identifying the complexity of knots travelling through media and it will be used in Chap. 6 to uniquely distinguish knot types in that context.

3.2.2 Modelling a Physical Gel

Gels are polymer networks formed by cross-linking polymeric strands. Cross-linking is generated by, for instance, the presence of cross-linkers, such as proteins in biological networks (Broedersz and MacKintosh 2014), or a high concentration of polymer bundles, such as in agarose gels (Pernodet et al. 1997), which is one of the most famous and broadly used examples of gels (Ross 1964; Stellwagen 2009; Viovy 2000). Agarose gel is commonly used as a buffer to perform gel electrophoresis experiments in order to separate DNA and other bio-polymers. This technique relies on the fact that charged polymeric strands with different lengths, topology or molecular weight possess different mobilities when moving through porous media (Calladine et al. 1991, 1997; Viovy 2000). The main feature that controls how a gel separates molecules with different sizes is the (typical) mesh size ξ_g (Calladine et al. 1997). The more peaked the distribution of pore sizes is, the more uniformly the gel acts as a barrier for molecules larger than the pore size. In practice, agarose gels present a broad distribution of pore sizes, which becomes narrower and centred around smaller pore sizes as the concentration of agarose increases (Maaloum et al. 1998). In addition, the electrophoretic trapping of circular DNA in agarose gels at strong fields suggests that gels possess dangling fibres which can thread through, and impale, circular DNA and other bio-polymers possessing closed contours (Cole and Åkerman 2003; Stellwagen and Stellwagen 2009).

The Young's modulus of agarose is roughly in the region $E_{\text{agar}} = 0.1 - 1$ MPa and depends on the agarose concentration. In any case, it is around 300 times smaller than the one of DNA: $E_{\text{DNA}} \simeq 300$ MPa (Marko and Cocco 2003; Kolahi et al. 2012). Nonetheless, the persistence length of single agarose fibre of thickness $\sigma_{\text{agar}} \simeq 2$ nm has been found to be $l_p^{\text{agar}} \simeq 10$ nm (Guenet and Rochas 2006). Agarose bundles in the sol/gel phase usually form by aggregating a number $n_f \simeq 10 - 20$ of single fibres into "fibrils", which can then display a thickness $\sigma_{\text{fibril}} \simeq 20 - 40$ nm (Pernodet et al. 1997) and much higher persistence lengths. Even by assuming a simple linear scaling of the persistence length of the bundle as a function of n_f, justified by weak interaction among fibres (Mogilner and Rubinstein 2005), the persistence length of a fibril can still reach values $l_p^{bundle} \simeq 100 - 200$ nm, much higher than than of DNA.

The small Young's modulus of the whole material is often explained as a consequence of the presence of flexible joints in the agarose gel matrix, while the single fibrils and dangling ends (Guenet and Rochas 2006) are generally considered stiff.

Recently developed artificial gels made of solid nano-wires (Rahong et al. 2014) provide a more selective pore size distribution, and possess a very large Young's

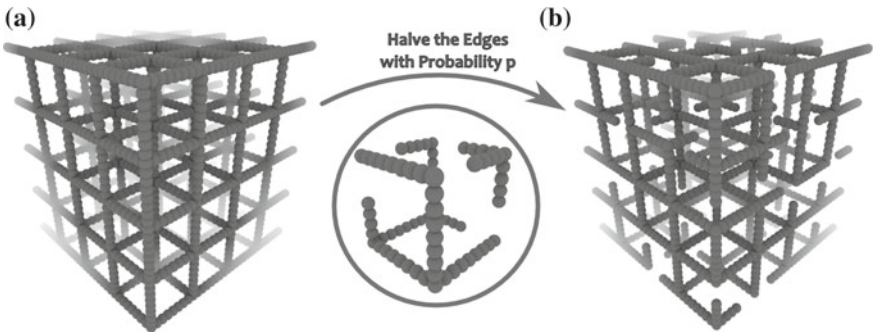

Fig. 3.5 Sketch of the gel structure, modelled as **a** perfect rigid cubic lattice and **b** with dangling ends. Modelling a gel as a rigid mesh is particularly appropriate for artificial gels made of solid nano-wires (Rahong et al. 2014). Including dangling ends in the model can be of paramount importance when investigating gel electrophoresis of ring polymers (see Chap. 6)

modulus ($E_{\text{wires}} \simeq 100$ GPa) which makes the network less susceptible to deformations.

From a theoretical point of view, a gel can be thought of as a collection of strands which create a 3D mesh. For simplicity, this mesh is often approximated as a perfect (cubic) lattice (Weber 2006), with a lattice spacing equal to the average mesh size $\langle \xi_g \rangle$. In this case, the pore size distribution is $p(\xi_g) = \delta(\xi_g - \langle \xi_g \rangle)$. In first approximation, the gel structure can also be considered rigid, i.e. completely static, which is a very good approximation in the case of artificially made gels of solid nano-wires.

In Chap. 4, where I will focus on detecting threadings in systems of rings, I will be modelling the gel as a rigid, perfect, cubic mesh (as in Fig. 3.5a). In this case, the microscopic structure of the gel is not expected to play a crucial role in the diffusion of rings. In addition, the fact that the gel is perfect eases the formulation of an algorithm that can unambiguously detect the threadings.

In other cases, as in Chap. 6, modelling the gel microscopic structure in detail is important. For instance, the electrophoretic mobility of ring polymers in gel has been found to be strongly dependent on the presence of dangling fibres (Mickel et al. 1977; Turmel et al. 1990; Åkerman 2002; Cole and Åkerman 2003; Stellwagen and Stellwagen 2009). Because of this, in Chap. 6, where I will focus on the electrophoretic mobility of knotted ring polymers (Trigueros et al. 2001; Arsuaga et al. 2002), the gel will be modelled as an imperfect mesh, by halving some of the edges forming the cubic lattice with a certain probability p (see Fig. 3.5b).

By tuning the probability p one can directly regulate the average number of dangling ends that can be found in the system, although their length will be fixed to half the lattice spacing, i.e. $l_{de} = \xi_g/2$. Unless otherwise stated, the gel lattice spacing ξ_g has been chosen to reproduce the pore size of an agarose gel at 5 % (Pernodet et al. 1997) or of an artificial gel after 3 growth cycles (Rahong et al. 2014), i.e. $\xi_g = 200\,\text{nm} = 80\sigma$ in MD units. While this value is unusually high for a standard experiment of gel electrophoresis, it is closer to the typical pore size found in high resolution gel

electrophoresis (Stellwagen and Stellwagen 2009). The mesh structure is, unless otherwise stated, made up by static beads of size $\sigma_g = 10\sigma \simeq 25\,\text{nm}$, which is compatible with the diameter of either agarose bundles (30 nm (Pernodet et al. 1997) and the nano-wires (20 nm (Rahong et al. 2014)).

In general, I will be considering gels whose lattice spacing is comparable with the polymer's Kuhn length, this is because, from a physical perspective, lattice spacings much greater than the Kuhn length can leave the gel so sparse that the rings rarely encounter it. Alternatively, for lattice spacings much shorter than the Kuhn length, the simulation includes an increasingly large fraction of passive gel monomers, which tend to increase the volume fraction of the system and hence limit the concentration of rings that can be studied efficiently using numerical schemes.

References

Adams, C.C.: The knot book: an elementary introduction to the mathematical theory of knots. WH Freeman and Company, New York (1994)

Åkerman, B.K.: Electrophoretic capture of circular DNA in gels, Electrophoresis and Cole, pp. 2549–2561. (2002)

Alder, B.J., Wainwright, T.E.: Phase transition for a hard sphere system. J. Chem. Phys. **27**(5), 1208 (1957)

Alder, B.J., Wainwright, T.E.: Studies in molecular dynamics. I. general method. J. Chem. Phys. **31**(2), 459 (1959)

Arsuaga, J., Vázquez, M., Trigueros, S., Sumners, D., Roca, J.: Knotting probability of DNA molecules confined in restricted volumes: DNA knotting in phage capsids. Proc. Natl. Acad. Sci. USA **99**(8), 5373 (2002)

Bogle, M.G.V., Hearst, J.E., Jones, V.F.R., Stoilov, L.: Lissajous knots. J. Knot Theor. Ramif. **3**(2), 121 (1994)

Brackley, C.A., Morozov, A.N., Marenduzzo, D.: Models for twistable elastic polymers in Brownian dynamics, and their implementation for LAMMPS. J. Chem. Phys. **140**(13), 135103 (2014)

Broedersz, C.P., MacKintosh, F.C.: Modeling semiflexible polymer networks. Rev. Mod. Phys. **86**(3), 995 (2014)

Calladine, C.R., Collis, C.M., Drew, H.R., Mott, M.R.: A study of electrophoretic mobility of DNA in agarose and polyacrylamide gels. J. Mol. Biol. **221**(3), 981 (1991)

Calladine, C.R., Drew, H., Luisi, F.B., Travers, A.A.: Understanding DNA: the molecule and how it works. Elsevier Academic Press, Cambridge (1997)

Cole, K.D., Åkerman, B.: The influence of agarose concentration in gels on the electrophoretic trapping of circular DNA. Separ. Sci. Technol. **38**(10), 2121 (2003)

Diao, Y., Dobay, A., Kusner, R.B., Millett, K., Stasiak, A.: The average crossing number of equilateral random polygons. J. Phys. A: Math. Gen. **36**(46), 11561 (2003)

Doi, M., Edwards, S.: The theory of polymer dynamics. Oxford University Press, Oxford (1988)

Frenkel, D., Smit, B.: Understanding molecular simulation: from algorithms to applications. Academic Press, Cambridge (2001)

Guenet, J.M., Rochas, C.: Agarose sols and gels revisited. Macromol. Symp. **242**, 65 (2006)

Karplus, M., Petsko, G.: Molecular dynamics simulations in biology. Nature **347** (1990)

Katritch, V., Bednar, J., Michoud, D., Scharein, R., Dubochet, J., Stasiak, A.: Geometry and physics of knots. Nature **384**, 142 (1996)

Kolahi, K.S., Donjacour, A., Liu, X., Lin, W., Simbulan, R.K., Bloise, E., Maltepe, E., Rinaudo, P.: Effect of substrate stiffness on early mouse embryo development. PloS one **7**(7), e41717 (2012)

Kusner, R., Sullivan, J.: Möbius energies for knots and links, surfaces and submanifolds. Geometric Topology (Proceedings of the 1993 Georgia International Topology Conference) AMS/IP Studies in Adv. Math. pp. 570–604 (1994)
Kusner, R., Sullivan, J.: Möbius-Invariant Knot Energies, In: Kauffman, L., Katritch, V., Stasiak, A. (eds.) Ideal Knots, pp. 315–352. World Scientific Press, London (1998)
Maaloum, M., Pernodet, N., Tinland, B.: Agarose gel structure using atomic force microscopy: gel concentration and ionic strength effects. Electrophoresis **19**, 1606 (1998)
MacKerell, A.D., Bashford, D., Bellott, M., Dunbrack, R.L., Evanseck, J.D., Field, M.J., Fischer, S., Gao, J., Guo, H., Ha, S., Joseph-McCarthy, D., Kuchnir, L., Kuczera, K., Lau, F.T., Mattos, C., Michnick, S., Ngo, T., Nguyen, D.T., Prodhom, B., Reiher, W.E., Roux, B., Schlenkrich, M., Smith, J.C., Stote, R., Straub, J., Watanabe, M., Wiórkiewicz-Kuczera, J., Yin, D., Karplus, M.: All-atom empirical potential for molecular modeling and dynamics studies of proteins. J. Phys. Chem. B **102**(18), 3586 (1998)
Marko, J., Cocco, S.: The micromechanics of DNA. Phys. World. 37–41 (2003)
McCammon, J., Gelin, B., Karplus, M.: Dynamics of folded proteins. Nature **267** (1977)
Micheletti, C., Marenduzzo, D., Orlandini, E.: Polymers with spatial or topological constraints: theoretical and computational results. Phys. Rep. **504**(1), 1 (2011)
Mickel, S., Arena, V., Bauer, W.: Physical properties and gel electrophoresis behavior of R12-derived plasmid DNAs. Nucleic Acids Res. **4**(5), 1465 (1977)
Mogilner, A., Rubinstein, B.: The physics of filopodial protrusion. Biophys. J. **89**(2), 782 (2005)
Orlandini, E., Tesi, M.C., Whittington, S.G., Sumners, D.W., Rensburg, E.J.J.V.: The writhe of a self-avoiding walk. J. Phys. A: Math. Gen. **27**, L333 (1994)
Orlandini, E., Whittington, S.G.: Statistical topology of closed curves: some applications in polymer physics. Rev. Mod. Phys. **79**(2), 611 (2007)
Pernodet, N., Maaloum, M., Tinland, B.: Pore size of agarose gels by atomic force microscopy. Electrophoresis **18**, 55 (1997)
Piili, J., Marenduzzo, D., Kaski, K., Linna, R.P.: Sedimentation of knotted polymers. Phys. Rev. E **87**(1), 012728 (2013)
Rahman, A.: Correlations in the motion of atoms in liquid argon. Phys. Rev. A **136**(2), 405 (1964)
Rahong, S., Yasui, T., Yanagida, T., Nagashima, K., Kanai, M., Klamchuen, A., Meng, G., He, Y., Zhuge, F., Kaji, N., Kawai, T., Baba, Y.: Ultrafast and wide range analysis of DNA molecules using rigid network structure of solid nanowires. Sci. Rep. **4**, 5252 (2014)
Ross, P.: Electrophoresis of DNA. I. On a relationship between electrophoresis and donnan equilibrium experiments on DNA. Biopolymers **2**, 9 (1964)
Rybenkov, V., Cozzarelli, N., Vologodskii, A.: Probability of DNA knotting and the effective diameter of the DNA double helix. Proc. Natl. Acad. Sci. USA **90**(June), 5307 (1993)
Stasiak, A., Katritch, V., Bednar, J., Michoud, D., Dubochet, J.: Electrophoretic mobility of DNA knots. Nature **384**, 122 (1996)
Stellwagen, N.C.: Electrophoresis of DNA in agarose gels, polyacrylamide gels and in free solution. Electrophoresis **30**(1), 1 (2009)
Stellwagen, N.C., Stellwagen, E.: Effect of the matrix on DNA electrophoretic mobility. J. Chromatogr. **1216**(10), 1917 (2009)
Swope, W.C., Andersen, H., Berens, P., Wilson, K.: A computer simulation method for the calculation of equilibrium constants for the formation of physical clusters of molecules: Application to small water clusters. J. Chem. Phys. **76**(1), 637 (1982)
Trigueros, S., Arsuaga, J., Vazquez, M.E., Sumners, D., Roca, J.: Novel display of knotted DNA molecules by two-dimensional gel electrophoresis. Nucleic Acids Res. **29**(13), E67 (2001)
Turmel, C., Brassard, E., Slater, G.W., Noolandi, J.: Molecular detrapping and band narrowing with high frequency modulation of pulsed field electrophoresis. Nucleic Acids Res. **18**(3), 569 (1990)
Viovy, J.: Electrophoresis of DNA and other polyelectrolytes: physical mechanisms. Rev. Mod. Phys. **72**(3), 813 (2000)
Weber, C., Carlen, M., Dietler, G., Rawdon, E.J., Stasiak, A.: Sedimentation of macroscopic rigid knots and its relation to gel electrophoretic mobility of DNA knots. Sci. Rep. **3**, 1091 (2013)

Weber, C.: Stasiak, a., De Los Rios, P., Dietler, G.: Numerical simulation of gel electrophoresis of DNA knots in weak and strong electric fields. Biophys. J. **90**(9), 3100 (2006)
Weeks, J., Chandler, D., Andersen, H.: Role of repulsive forces in determining the equilibrium structure of simple liquids. J. Chem. Phys. **54**(12), 5237 (1971)

Chapter 4
Threading Rings

It looks as if it was a bride, walking down the isle, while her dress is being pulled back by flower girls whose dresses are also being pulled by flower girls whose dresses are pulled by other flower girls …

A.Y. Grosberg

Understanding the dynamical and rheological properties of solutions of long ring polymers is of primary importance in several areas of soft matter, material science and biophysics (Cremer and Cremer 2001; Kapnistos et al. 2008; Halverson et al. 2011b, 2013). As mentioned in Chap. 2, ring polymers do not follow the standard reptation theory and in order to make progress it seems that the scientific community will require innovative and unconventional approaches to analyse their properties.

In this chapter I will address a long-standing problem (Klein 1986; Cates and Deutsch 1986), that of detecting and investigating threadings between rings in solution. In particular, I will first study ring polymers in a particular ensemble: a solution of ring polymers embedded in a rigid gel. Differently from previous works, where "a background of obstacles" was used to mimic the presence of topological obstacles surrounding any specific ring polymer in solution (Rubinstein 1986; Obukhov and Rubinstein 1994; Milner and Newhall 2010), here I intend to introduce a real physical gel, made of a different polymeric units with respect to the ring polymers.

I will focus on this system with the aim of investigating the effect of threadings between rings, i.e. inter-chain threading, on the dynamics of the solution and I will show that these are dominant in the limit of large rings, when a spanning cluster of inter-threading rings emerges.

In the second part of this chapter, I will instead turn my attention to a more conventional system in which ring polymers are forced in a dense solution without the presence of a static gel. In this case, there currently is no algorithm that can unambiguously identify these inter-chain threadings. On the other hand, I will show that these can be detected by appropriately perturbing the system. In particular, this perturbation, borrowed from recent approaches to the glass transition in colloidal and

D. Michieletto, *Topological Interactions in Ring Polymers*, Springer Theses,
DOI 10.1007/978-3-319-41042-5_4

liquid glass formers (Berthier and Biroli 2011), will be shown to trigger a mechanism for which a kinetically trapped state emerges, thereby producing the first in silico evidence of a "topological glass".

4.1 Threading of Rings in a Gel

The polymers are here modelled as N bead-spring chains each formed by M beads and the dynamics is integrated using the MD scheme as described in Chap. 3. The polymers are prepared unlinked and unknotted from either themselves and the gel (see Fig. 4.1a), which is formed by a perfect cubic lattice, *i.e.* without dangling ends, or equivalently by setting $p = 0$ (see Sect. 3.2.2).

The systems under study have $N = 50$ polymers with $M = 64$, $M = 128$, $M = 256$, $M = 512$, $M = 1024$ and $M = 1512$ and the box linear size L is changed in order to keep the monomer density fixed at $\rho = NM/(L^3 - V_{\text{gel}}) \simeq 0.14\sigma^{-3}$. Here the polymers Kuhn length is set to $l_K = 10\sigma$, the gel lattice spacing $l = l_K$ and the mesh structure is formed by beads of size σ equal to that of the polymers (see Chap. 3). The reason for this is twofold: (1) if $l \gg l_K$ the system would map onto the classic "melt" picture, a system in which I am not interested in this chapter; (2) if $l \ll l_K$ the rings would appear rigid on the length scales of the gel structure and, in addition, the system would be overcrowded with atoms forming the gel structure rather than the rings, which would not be efficient in terms of computer

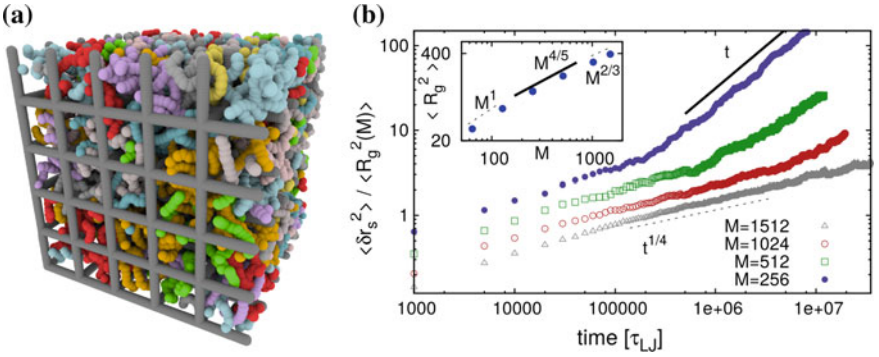

Fig. 4.1 **a** Snapshot of a system with $N = 50$ chains of length $M = 256$. The gel lattice (*grey*) can be seen to be filled with ring polymers each shown in different colour. Periodic boundary conditions are used to ensure the absence of surface effects or dangling ends. **b** Segmental mean squared displacement of the rings $\langle \delta r_s^2 \rangle$ scaled by $\langle R_g^2(M) \rangle$ and plotted against time τ_{LJ}. Notice the difference from the reptation theory prediction for linear polymers in a melt, where $\langle \delta r_s^2 \rangle \sim t^\alpha$, and $\alpha = 1/2, 1/4, 1/2$ before the tube is renewed and the polymer can freely ($\alpha = 1$) diffuse. The inset shows the scaling of the average squared gyration radius $\langle R_g^2 \rangle$ as a function of the chains' length. Notice the crossover from "Gaussian" ($\nu = 1/2$) behaviour to crumpled ($\nu = 1/3$) globule via the Cates–Deutsch exponent $\nu = 2/5$ (see Chap. 2)

resources. The systems are all well into the overlapping regime, i.e. where coils overlap onto each other. The overlapping monomer density for the system with shortest chains is $\rho^* = N^* M/(L^3 - V_{\rm gel}) \simeq 0.05\sigma^{-3}$ where N^* is such that $\phi = 4N^*\pi R_g^3/3(L^3 - V_{\rm gel}) = 1$. In Fig. 4.1a I sketch the system for the case of shortest rings $M = 256$ beads.

Even though these systems are not technically a melt of rings, but a dense solution of rings embedded in a gel whose chemical structure could, in principle, differ from that of the polymers, it is tempting to conjecture that rings may not "feel" the difference between topological interaction caused by neighbouring rings and those caused by the gel structure. In light of this, one could argue that the results I will present in this chapter could, in principle, be translated and applied to the case of a pure melt of rings. In support of this conjecture, in the inset of Fig. 4.1b, I show the three distinct regimes of the squared radius of gyration R_g^2, i.e. $R_g^2 \sim M^{2\nu}$ with $\nu = 1/2 \to 2/5 \to 1/3$, observed in the case of a pure melt of rings (Cates and Deutsch 1986; Grosberg et al. 1993; Grosberg 2014; Halverson et al. 2011a).

As described in Chap. 2, rings in the melt with $M < M_e$, where M_e is the rings' entanglement length, are thought to behave similarly to isolated self-avoiding rings in a gel,[1] for which the Parisi–Sourlas result (Parisi and Sourlas 1981) holds and the rings are found to be in the same universality class of self-avoiding annealed branched polymers, with fractal dimension $d_F = 1/\nu = 2$. For longer rings, the entropy loss due to the conservation of topology, i.e. un-knotted and un-linked from their neighbours, causes the rings to collapse and crossover to a crumpled globule regime, with fractal dimension $d_F = 3$. Although it is far from being a definite proof that the system considered here can be compared to a melt of rings, it is somehow encouraging that the same scaling of R_g is observed here.

In Fig. 4.1b I also report the segmental mean square displacement of the rings, $\langle \delta r_s^2(t) \rangle$, defined as

$$\langle \delta r_s^2(t) \rangle \equiv g_1(t) = \left\langle \frac{1}{M} \sum_i^M [\boldsymbol{r}_i(t + t_0) - \boldsymbol{r}_i(t_0)]^2 \right\rangle. \tag{4.1}$$

This quantity keeps track of the diffusion of single monomers forming the chains and is therefore very susceptible to any kind of entanglement at the level of segmental relaxation. This shows that for the systems with $M \leq 1024$, after an initial sub-diffusive regime where $\langle \delta r_s^2 \rangle \sim t^{1/2}$, the chains freely diffuse only once the polymers have travelled many times their own size, i.e. $\langle \delta r_s^2 \rangle \geq R_g^2$. This is similar to the behaviour observed in a melt of rings (Halverson et al. 2011b) and rather different from the case of a melt of linear polymers (Kremer and Grest 1990) where the free diffusion is reached, via a sequence of distinct sub-diffusive regimes, when the segmental displacement has travelled a shorter distance, of order one R_g^2.

[1] It is interesting to notice that in the ensemble I study in this chapter, the picture of "rings in a gel", or "in a background of obstacles", is more appropriate than in the case of a pure melt.

For the longest chains presented here, $M = 1512$, the freely diffusive regime has not been achieved in the simulation runtime. It is worth stressing that the same number of time-steps had been run for equilibrating the system and it was considered equilibrated based on the following points (Halverson et al. 2011a): (i) the value of $\langle R_g(t) \rangle$ had been observed to settle at a constant value for several decades and (ii) the rings had travelled, on average, at least one R_g. It is also worth noticing that this system displays a slowing down at large times: After an initial Rouse regime, an entangled regime with $\langle \delta r_s^2 \rangle \sim t^{1/4}$ is observed even at times as large as $4\ 10^7\ \tau_{LJ}$ timesteps. All this is, once again, compatible with previous findings in the melt (Halverson et al. 2011b), which suggests that these two systems are, after all, not so different.

Threading between polymers have been thought of as candidates to drive a dynamical slowing down in systems of rings (Lo and Turner 2013), and the severe subdiffusive regime in the segmental displacement (Fig. 4.1) has not yet been investigated in its own right either in a melt or in a gel. In addition, no method to detect topological interactions, such as threadings, exist currently in the melt. This strongly encourages the study of threadings and their effect on the rings dynamics in the system I proposed; as I will show in what follows, the presence of a rigid background structure in fact allows us to unambiguously define and detect the presence of these topological interactions and their persistence in the system.

4.1.1 Detecting Threadings Between Rings

Threadings are not topological invariants, i.e. a threaded configuration such as that in Fig. 1.4b where the shark is threading the other animal, can become un-threaded by smoothly deforming the polymers. For this reason, threadings are very hard to define, let alone identify.

Threadings can be thought of as local properties of the conformation of the rings; the global topology of the rings remains unlinked from both other rings and the gel. The gel architecture provides a natural local volume—a single unit cell—within which a threading of one ring through another can be identified. This is done by exploiting the following property: each polymer enters and exits a given cell through its faces; the unique topological characteristic of ring polymers, unlinked from the cubic lattice, is that each time the contour passes out through a face of any given unit cell, labelled c, this must be accompanied by a returning passage back through the same cell face.

The threading of polymer i by polymer j within cell c can then be defined by performing some operations onto the polymers contour length: First a contraction of ring i is formed by sequentially connecting the points where it passes through any face of cell c by straight lines, as illustrated by the yellow lines in Fig. 4.2b. This procedure creates a closed loop i_c contained entirely within cell c and its bounding faces, and it also takes into account possible re-entrant configurations, where a ring pierces more than once a cell face. This "contraction procedure" in fact joins consecutive intersection points of the polymer with the faces of the box in order to form a closed

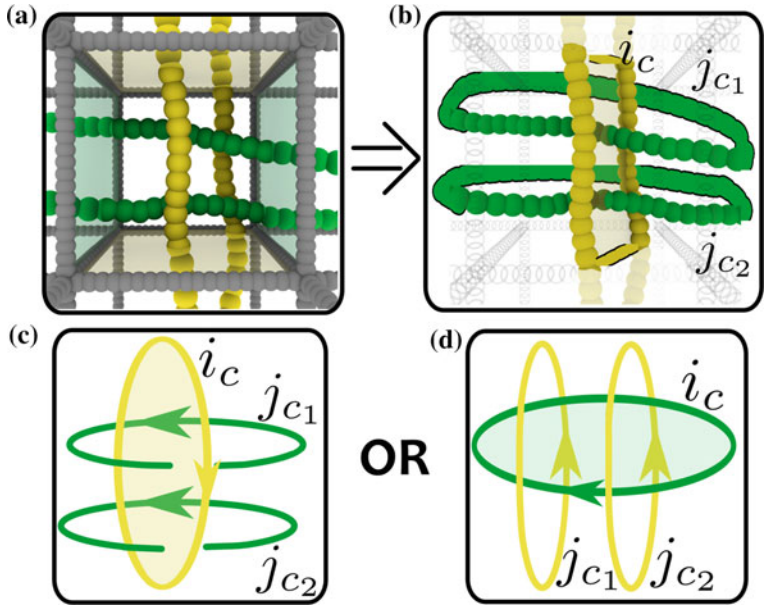

Fig. 4.2 Threading identification procedure. The green strands of chain j passing through a face of the cell are separately closed to form two loops j_{c_1} and j_{c_2}. Each one of them is topologically linked with the yellow contour i_c, a unique contraction of chain i formed by connecting the points that pass through the faces of the unit cell. In contrast, the green ring is not threaded by the yellow, as one can see by reversing the roles of chains i and j (see **d**). This implies that threadings can be sub-divided into "passive" and "active" (see later in the text), differently from other types of topological interactions, such as linking, which is mutual

contour entirely contained within one unit cell. In this way the gel is used to identify threadings as local configurations in which the conformation of the ring outside of the chosen cell is unimportant. Next, each of the other strands occupying cell c and labelled by j_c, belonging to a different polymer j, are considered. These strands connect a single entry and exit point through the faces of c. The ends of each strand can be closed outside the cell to form a closed loop.[2] The next step is then to compute the linking number between each pair of j_c and i_c thereby created. This will be non-zero if, and only if, ring i is threaded by that strand of ring j. There are some cases in which the linking number computation can return zero although the two rings are physically inseparable, as in the case of a Whitehead link (Adams 1994). I expect these exceptions to be rare in our system, as the rings are stiff on the length scale of a gel lattice spacing and therefore such complex configurations are not common.

This procedure is reminiscent of a method used in the literature to measure entanglements in a melt of linear polymers (Orlandini and Whittington 2004), where the authors probed the level of entanglement in the system by ideally carving a box from

[2]These could be closed at infinity, but anywhere away from the cell would suffice.

it and by computing the linking number between pair of curves generated by randomly closing the strands entering and exiting that box. In that case, the procedure was prone to ambiguities in the closing procedure, and, in addition, the size of the box sampled from the system was somehow arbitrary. In the system presented here both these problems are resolved by using the natural entanglement length of the system, i.e. one gel lattice size, this in fact not only gives a natural choice for the size of the probing box but also ensures that every ring entering a face of the box is also exiting the same face, therefore creating a natural choice also for the closing procedure.[3]

To better understand the algorithm, it is perhaps useful to concentrate on a specific example. For instance, consider Fig. 4.2. The two strands of the green ring in Fig. 4.2a are threading the yellow ring. After performing the closing procedure (Fig. 4.2b), the absolute value of the linking numbers between the closed yellow loop and each of the green loops is equal to one (Fig. 4.2c). Inverting the procedure by swapping the roles of i and j would lead to the configuration in Fig. 4.2d, which has linking number of zero between any pair of loops. Note also the emphasis on the fact that I compute the magnitude of the linking number between each pair: the sum of the signed linking numbers would in fact always give zero, as the two original rings are topologically unlinked.

The local threading of ring i by ring j in cell c at time t can therefore be defined by $Th_c(i, j; t) = \frac{1}{2}\sum_{j_c} |Lk(i_c, j_c; t)|$—equal to 1 for the example shown in Fig. 4.2b—and the total threadings between these rings by summing this over all cells

$$Th(i, j; t) = \frac{1}{2}\sum_{c}\sum_{j_c} |Lk_c(i_c, j_c; t)| \,. \tag{4.2}$$

This procedure is perfectly well defined, even when identifying threadings associated with rings that share either the entry and/or the exit faces of the unit cell of the gel, as shown in Fig. 4.3. While the definition of threading used in this chapter is unambiguous, it is helpful to examine what is recorded in the three cases shown: Fig. 4.3a The rings thread through each other in the cell. Both of the yellow/yellow-dashed contours, closed at infinity are linked with the green ring, closed by a straight line connecting the points it leaves the cell. The yellow ring is therefore reported as actively threading the green ring by the algorithm. Figure 4.3b There is no threading in the unit cell since the penetrating ring enters, and then leaves, the green shaded area delimited by the green ring contour. The closed yellow/yellow-dashed contours are both unlinked from the green ring, closed on the edge of the box. In this case the algorithm reports three unlinked rings, hence it detects correctly that there is no threading present, hence no topological constraint. Figure 4.3c shows the case where there are two local threadings which happen in two different unit cells. In this case, one might argue that by summing the contributions of the two cells, the two rings are not threading. On the other hand, in both cells the rings are acting as a constraint

[3] It is fair to say that the similarity between these two methods became apparent, at least to me, only after we finalised the algorithm to detect threadings.

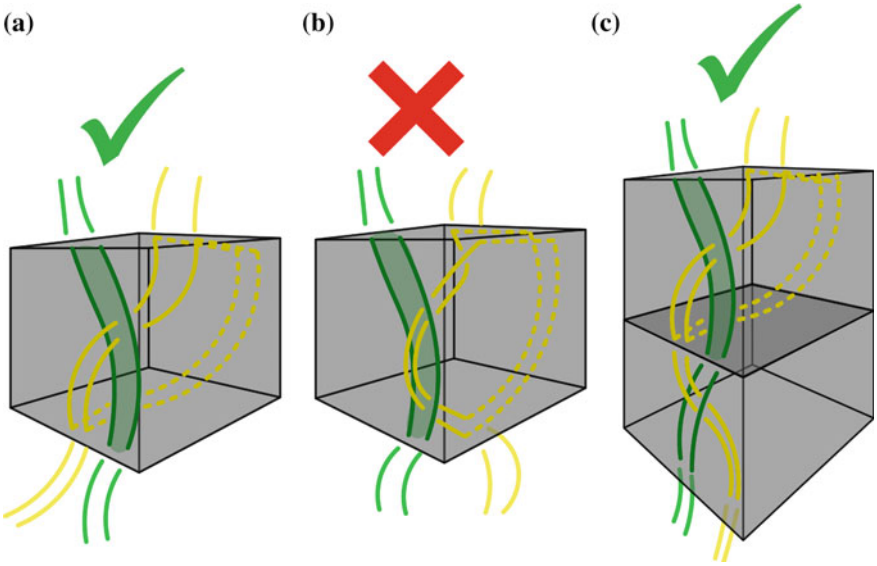

Fig. 4.3 Sketches of "tricky" threadings, where rings share the same entry/exit face and detected by the algorithm described in this chapter. The rings in **a** and **c** would be correctly detected as threading, being the rings configuration locally threaded inside the unit cell. The rings in **b** would also be correctly classified as non-threading being the yellow ring entering and exiting the green contour within the unit cell

for each-other motion within the single cells and therefore the algorithm correctly reports both local threadings. It is finally worth pointing out that pair of threadings like the ones depicted in Fig. 4.3 will usually be short lived, as they can quickly annihilate.

The detection of a threading is necessarily a strictly local measure, on the scale of the cell volume. If the cell volume is increased no threadings will eventually be recorded since rings in the melt are unlinked by construction. A passive threading of ring i by ring j is detected when $Th_c(i, j; t) = 1$ and $Th_c(j, i; t) = 0$ while the ring i actively threads j when $Th_c(i, j; t) = 0$ and $Th_c(j, i; t) = 1$. For example, in Fig. 4.2b, the yellow ring is passively threaded by the green one, and the latter is actively threading the former and not vice versa. This means that threading, unlike linking, is directional and non-mutual.

4.1.2 Extensive Threading Leads to Extensive Correlations

The equilibrium average of threadings over rings and over time can be found by taking $\langle \sum_j Th(i, j; t) \rangle_{i,t} / N \equiv \langle Th \rangle / N$, where $\langle \ldots \rangle_{i,t}$ denotes the average over rings and over time. This represents the number of passive threadings per chain and is reported

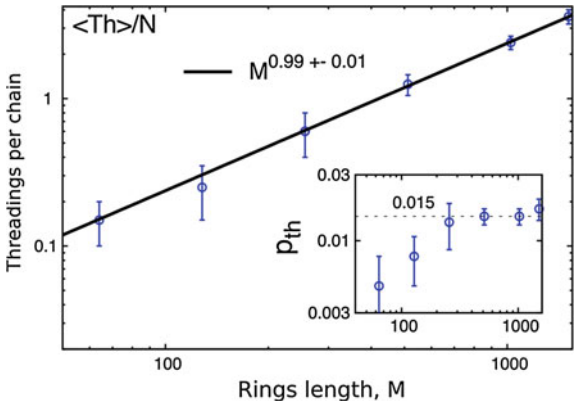

Fig. 4.4 Number of threadings $\langle Th \rangle$ per chain as a function of the length of the chains M. In the inset I plot p_{th}, crudely the probability of threading in a cell containing two different chains, as computed in Eq. (4.4). See text for details

in Fig. 4.4. As one can notice, this quantity is found to scale extensively with M, i.e. it is a critical quantity in the system. Within the lengths used in these simulations, one does not see any deviation from the linear regime. This strongly suggests that longer rings will lead to even more numerous threadings.

One can conjecture that the existence of these penetrations is bound to affect the dynamics of the rings, as they effectively are constraints on the rings diffusion. A measure to quantify the effect of the dynamics is given by the penetrations time-correlation function

$$P_p(t) = \frac{\left\langle \sum_j Th(i,j;t_0)Th(i,j;t_0+t) \right\rangle_i}{\left\langle \sum_j Th(i,j;t_0)Th(i,j;t_0) \right\rangle_i} \tag{4.3}$$

This quantity represents the average fraction of survived passive threadings of ring i after a time interval t, see Fig. 4.5a.

For the longest rings, $P_p(t)$ tends to flatten, resembling a plateau, before relaxing to a constant value $P_p(t \to \infty) \equiv P_p^\infty$, this being the mean probability that two different, randomly chosen chains are penetrating. By using a mean-field argument, one can argue that the probability of threading between two chains in any cell that is occupied by both rings, p_{th}, can be approximated as the large time probability that they are found threading through one another divided by the number of shared cells that they both occupy $N_{\rm sc}$

$$p_{th} = P_p^\infty / N_{\rm sc} \sim P_p^\infty \frac{(L/l)^3}{M^2}, \tag{4.4}$$

or

$$P_p^\infty \sim p_{th} \frac{M^2}{(L/l)^3}, \tag{4.5}$$

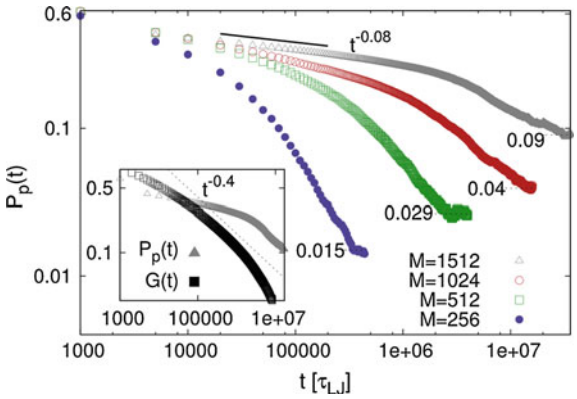

Fig. 4.5 Time-correlation function $P_p(t)$ of the penetrations (or threading persistence) as computed in Eq. (4.3). The *inset* compares the relaxation of the spatial stress carried by the rings, through the modulus $G(t)$ defined in Eq. (4.7), with $P_p(t)$ defined in Eq. (4.3) for the system with $M = 1512$. The spatial stress is clearly relaxed more quickly than the threadings and the *dotted line* indicates a power law decay of $t^{-0.4}$ (Kapnistos et al. 2008)

where $N_{\rm sc}$ is the number of cells c shared between two rings each visiting a fraction $f_c = N_v/(L/l)^3$ of the cells in the system, i.e. $N_{\rm sc} \simeq f_c^2(L/l)^3$. The fraction of cells visited by any one ring was also found to be extensive in the rings length, i.e. $N_v \sim M$. This is compatible with the fact that the rings fractal dimension is $d_F = 3$ in the large M limit, i.e. $R_g^3 \sim M$. Combining this with P_p^∞ (in Fig. 4.5) one can estimate $p_{th} \to 0.015$, reported in the inset of Fig. 4.4. The prediction (dashed line) is particularly well matched by the simulations (data points) at large M, where the scaling $R_g^3 \sim M$ is more appropriate to describe the size of the coils. Crudely, this quantity represents the "background probability" of threading between any two ring segments sharing a gel unit cell, and it is independent of any correlations that may have existed at earlier times. The fact that p_{th} is found to be constant at large M it is very encouraging, as it implies that any two rings sharing a unit cell thread through one another with the same probability p_{th} independently on their length M. As a consequence, by increasing M the system is bound to generate more and more threadings, i.e. constraints on the overall motion of the rings.

In light of this, one could argue that the addition of $\langle Th \rangle$ threadings has the net effect of imposing a number constraints on the system and therefore on the degrees of freedom, $N_{\rm dof}$, of the system. Although it might be non-trivial to quantify the degrees of freedom of a melt of rings, it is safe to assume that, because ring polymers have to preserve their topological state, threadings represent a severe (although temporary), constraint on the translational degrees of freedom, $N_{\rm tr}$, of the chains. As a consequence, one could think that in the case

$$N_{\rm tr}/\langle Th \rangle \sim 1, \tag{4.6}$$

the system has saturated its translational degrees of freedom, and therefore the chains are all correlated to one another via threadings, hindering the fluid motion of the system. This scenario, that could be (loosely) compared to the Maxwell isostaticity condition of frames (Maxwell 1864; Kane and Lubensky 2013), captures the primary motivation of this Thesis, i.e. to find a state in which these topological interactions can drive a dynamically arrested state, or a "topological glass". In this respect, a melt of rings is a more promising candidate than, for instance, a blend of rings contaminated with linear chains (Halverson et al. 2012). Although such a system has showed a surprising rubbery plateau even after small addition of linear contaminants, there are no topological constraints that can be imposed on linear polymers, and for this reason, the largest relaxation time of the system is bound above by the slowest relaxation of the linear polymers, i.e. $\tau_{\text{relax}} \sim M^3$.

In order to better understand the correlation between spatial stress and threading relaxation in the system studied here, one can compare the threading persistence $P_p(t)$ with the stress relaxation modulus, $G(t)$ (Doi and Edwards 1988). Here, the stress carried by the rings can be computed easily, once again making use of the rigid gel structure, as

$$G(t) = \frac{\left\langle \sum_c g(i,c;t_0)g(i,c;t_0+t) \right\rangle_i}{\left\langle \sum_c g(i,c;t_0)g(i,c;t_0) \right\rangle_i} \tag{4.7}$$

where $g(i,c;t) = 1$ if ring i is present in cell c at time t and 0 otherwise. While $G(t)$ is a standard quantity in polymer science and usually measures the rheological response, it is likely that, in practice, this quantity would be difficult to separate from that of the gel structure. Tracking the diffusion of labelled tracer rings is therefore likely to be the most effective experimental probe of their dynamics in the system studied here.

From the inset of Fig. 4.5 it is clear that the stress carried by the rings relaxes more quickly than the threadings, i.e. $G(t)$ decays more quickly than $P_p(t)$. This is consistent with the fact that one ring, penetrated by another in any particular cell, can independently relax the stress it carries in all other cells. A counter-intuitive finding that has been confirmed several times in the literature (Kapnistos et al. 2008; Halverson et al. 2011b, 2013, 2014; Grosberg 2014), is that rings relax their spatial stress much faster than their linear cousins, $G(t) \sim t^{-2/5}$ (Kapnistos et al. 2008), leading to a much lower (zero-shear) viscosity

$$\eta_0 = \int G(t)dt \sim M^{1.4}, \tag{4.8}$$

which is compatible with the one observed here (see dotted line in the inset of Fig. 4.5), they have also been observed to continue their sub-diffusive motion long after the stress has completely relaxed. Long-lived penetrations, such as those leading to the long "fat" tails of $P_p(t)$ in Fig. 4.5, may be responsible for this remarkable and unique finding. In fact, one could argue that a ring can start its free diffusion

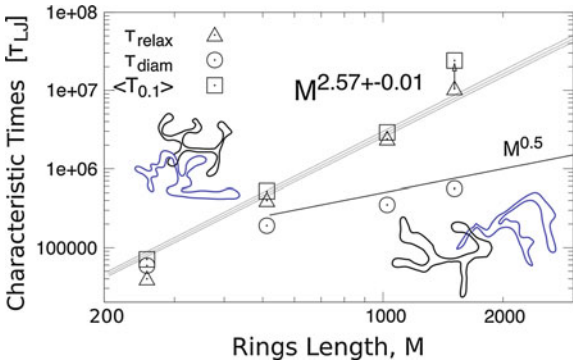

Fig. 4.6 Three dynamic relaxation times for rings in concentrated solution. The time taken for internal re-arrangements (captured by τ_{diam}) is shown to be much shorter than τ_{relax} and $\langle T_{0.1}\rangle$, capturing the self-diffusive and the threading relaxation time-scales, respectively (see text for details). The shadowed region delimits the confidence bounds expected for the final data point for the unthreading time $\langle T_{0.1}\rangle$ at $M = 1512$, were it to continue to follow this power law. This point is approximately 30 standard deviations outside the confidence interval, consistent with a dramatic slowing-down due to the development of a strongly connected network of inter-ring penetrations. The *arrow* on top of the data point showing τ_{relax} for the longest rings $M = 1512$ indicates that this represents a lower bound: the crossover to diffusive motion has not yet occurred at the longest computationally accessible times. A sketch of two rings fully relaxing their configurations while retaining a threading between them is also show

($\langle \delta r_s^2 \rangle \sim t$) only after it has travelled many times its own size $\langle R_g^2 \rangle^{1/2}$ (see Fig. 4.1b), i.e. only once the most persistent penetrations have relaxed, on the time-scales shown in Fig. 4.5.

Figure 4.6 compares three measures for the relaxation of rings:

(i) the re-orientation time τ_{diam}, defined as

$$\tau_{\text{diam}} \equiv \int_0^\infty C_{\text{diam}}(t)dt = \int_0^\infty \frac{\langle \mathbf{d}_i(t_0+t)\cdot \mathbf{d}_i(t_0)\rangle_i}{\langle \mathbf{d}_i(t_0)^2\rangle_i} dt \tag{4.9}$$

where $\mathbf{d}_i(t)$ is the diameter vector of ring i at time t computed by considering fixed pairs of anti-podal beads along the chain (as in Ref. (Halverson et al. 2011a));

(ii) the overall diffusion time τ_{relax} defined as

$$\tau_{\text{relax}} \equiv \langle R_g^2 \rangle / 6D_{CM} \tag{4.10}$$

corresponding to the time taken for a chain to diffuse a distance compared to its radius of gyration;

(iii) the un-threading time-scale $\langle T_{0.1} \rangle$ defined as the solution of the equation

$$P_p(T_{0.1}) \equiv 0.1, \tag{4.11}$$

representing the average time required by a ring to lose 90 % of its original threadings, i.e. the time required to "renew" its neighbours.[4]

Comparing the scaling behaviour of these quantities is exceptionally meaningful: for short rings all these three time-scales are similar to one another, on the other hand, when the size of the rings is increased, one can observed that the internal relaxation decouples from the overall displacement, i.e. $\tau_{\text{diam}} \ll \tau_{\text{relax}}$. This finding is peculiar of ring polymers, since that for linear polymers these two time-scales are related via the tube renewal time-scale. In addition, the un-threading time $\langle T_{0.1} \rangle$ and the diffusion time τ_{relax} seem to instead follow the same scaling, meaning that the time taken to fully diffuse one coil size scales accordingly to the time taken to renew the threadings.

More importantly, these time-scales are observed to deviate from the scaling $\langle T_{0.1} \rangle \sim \tau_{\text{relax}} \sim M^{2.5}$ when the longest chains are simulated. In fact, for the system with $M = 1512$ one finds $\langle T_{0.1} \rangle \simeq 2\ 10^7\ \tau_{LJ}$, that is twice as large as the value expected (see Figs. 4.5 and 4.6), while the value of τ_{relax} represents only a lower bound, having not been able to observe free diffusion of these rings within the simulation run-time (and therefore leading to only an upper bound on the value of D_{CM} for the rings with $M = 1512$). This encourages the conjecture that, at this length, threadings are densely populating the system, thereby creating many long-lived correlations between rings. In particular, one could speculate that the system with $M = 1512$ is approaching the regime in which Eq. (4.6) holds, i.e. the number of translational degrees of freedom are saturated by inter-chain constraints.

In light of the findings reported in Fig. 4.6, it safe to conclude that the un-threading time-scale is strongly related to the time-scale of the overall ring diffusion and it is perhaps the leading contribution to it. In other words, Fig. 4.5 unambiguously proves that threadings impose inter-chain correlations up to times that can be compared with the time taken by the rings to diffuse their centre of mass over many R_g.

4.1.3 The Emergence of a Spanning Network of Inter-Threaded Chains

At this stage it is therefore sensible to ask whether it is also possible to spatially relate such topological constraints. In fact, it is reasonable to imagine that, by increasing the length of the rings, one can generate a situation in which every ring is both, actively threading and passively threaded by, a number of other rings. This clearly

[4] $\langle T_{0.1} \rangle$ can be conceptually compared to the time taken by a linear polymer to renew its confining tube, begin threadings a sort of "tube" (or "cage") for rings.

generates a network of inter-threaded rings. One can therefore ask: are the large-time correlations related to the presence of extended spatial correlations?[5]

In order to quantify the network of penetrations from a "spatial" point of view, it can be useful to make use of the threading matrix $Th(i, j; t)$ introduced earlier. This keeps track of the threading of ring i by ring j at time t and it is, in some sense, the equivalent of an "adjacency matrix" for the threading rings. The graph representation of the network of threaded rings can therefore be described in terms of a directed graph $G = G(\mathcal{E}, \mathcal{V})$ where $\mathcal{V}$ is the set of vertices, a subset of the set of N rings in the system, and $\mathcal{E}$ is the set of directed edges from ring j to ring i, which represent the threadings of ring j through ring i. The time-evolution of the network is given by $Th(i, j; t)$, and from this it is possible to quantify the emergence of extended structures of inter-threading rings by using the size of the largest strongly connected component $|N_{scc}|$ and the first Betti number $b_1(G)$, which naively represents the number of 1-dimensional circular holes in the network, and is therefore a signature of "looped" correlated clusters of rings.

Recalling that a strongly connected component is defined as a sub-graph (G_{scc}) of G for which every vertex has a path to reach every other vertex within that sub-graph, one can notice that every ring in G_{scc} has to have at least one passive (in-coming arrow) and one active (out-going arrow) threading. In other words, all the rings belonging to a strongly connected component are related to one another via a chain of threadings.

In Fig. 4.7 I report the computed values of N_{scc} and $b_1(G)$ averaged over time and show snapshots of some networks as an example. One can notice that while for short rings the components are small, i.e. the network is fragmented, this is no longer true for longer rings. In this case one observes the formation of larger clusters. When the largest connected component contains $\mathcal{O}(N)$ vertices, it signifies that a percolating cluster of inter-penetrating rings has emerged. At this stage, every ring is connected and correlated with some other ring via a sequence of threadings. While such a representation is static, i.e. if one took two snapshots of the network at different times it would look very similar, it is clear that the emergence of system-spanning clusters of threaded rings has to affect the dynamics of the rings. I conjecture that the dynamical effect, or dynamic transition, is actually captured by the significant deviation showed in Fig. 4.6. In other words, the strong increase of relaxation time-scales observed in Fig. 4.6 is related to a corresponding increase of spatial correlations which can be captured by the emergence of a system-spanning connected component of inter-threaded rings.

[5]It is interesting to notice that the same question is also frequently asked when studying more conventional glass-forming materials (Berthier and Biroli 2011).

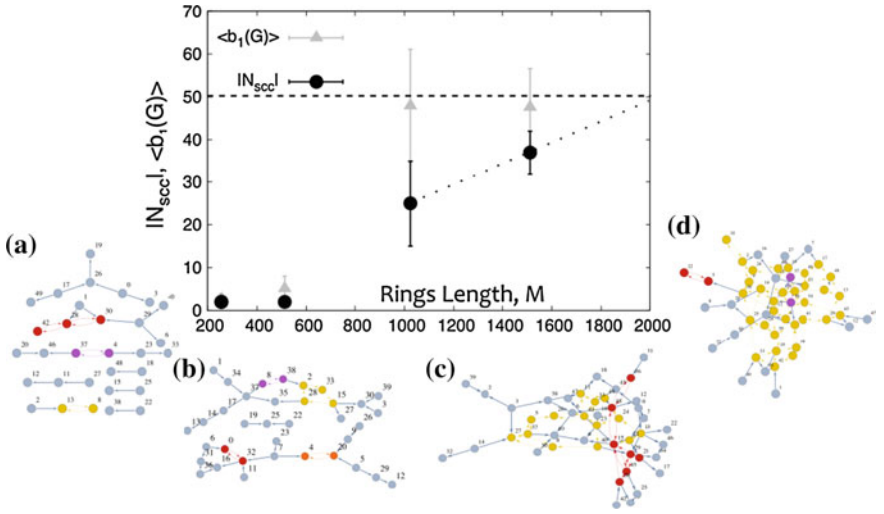

Fig. 4.7 Betti number $b_1(G)$ and size of the largest strongly connected component $|N_{scc}(G)|$ computed by taking the time average of the matrix $Th(i, j; t)$ after equilibration. Snapshots of some graphs $G(\mathcal{E}, \mathcal{V})$ corresponding to $M = 256$ (**a**), 512 (**b**), 1024 (**c**) and 1512 (**d**) beads. The *colors* highlight the strongly connected components in the graphs (see text for details). The numbers near the nodes identify the rings in the simulation. Notice that $N = 50$ (*dashed line*) is the maximum number of rings in the system and the crossover $|N_{scc}(G)| \simeq 50$ appears to be attained at around $M = 2000$ by extrapolating the last two data points (*dotted line*)

4.2 Threading of Rings in Dense Solutions

In the previous section I introduced a method to detect and identify threadings in a solution of rings embedded in a static gel structure. An obvious extension of this work is to try and quantify the effect of threadings in a dense solution. Clearly, the same protocol that I developed in Sect. 4.1.1 will be no longer valid. In this section I will therefore first investigate a solution of rings and then attack the problem of characterising threadings from the kinetic point of view by taking inspiration from recent protocols advanced by some authors in the Condensed Matter community working on glass-transitions (Biroli et al. 2008; Berthier and Biroli 2011; Cammarota and Biroli 2012; Karmakar and Parisi 2013).

In practice, it is computationally straightforward to transform the system investigated in Sect. 4.1 to a pure solution of rings. By taking equilibrated configurations and deleting the beads forming the gel, similar to an in silico etching, one can in fact obtain pure solutions of N rings M beads long. The monomer density of the systems thereby obtained is lower, i.e. $\rho = 0.1\,\sigma^{-3}$, and therefore one expects that the rings will accommodate in order to fill the vacant space. Technically, at these densities, the systems are classified "dense solutions" rather than "melts" being only moderately above the overlap (number) density $\rho^* \simeq 0.03\,\sigma^{-3}$. For computational purposes, I will not increase the density further, hoping that this will not invalidate the extension

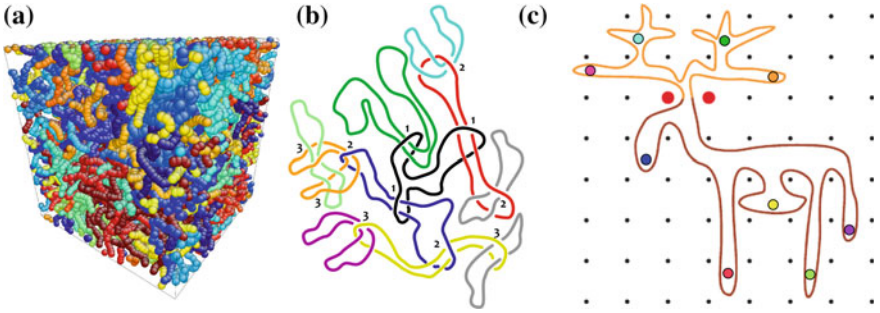

Fig. 4.8 **a** Snapshot from MD simulations of a melt with $N = 50$ and $M = 256$. **b** Schematic representation of inter-threading rings forming hierarchical levels of threadings enumerated from the innermost to the outermost with respect to the black ring. **c** Pierced lattice animal representation of rings in solution (adapted from Ref. (Kapnistos et al. 2008) with permission from Macmillan Publishers Ltd: Nature Materials, copyright 2008)

of the results reported in this section to the case of concentrations that more closely mimic the melt state. After thermalisation, the systems look like the one sketched in Fig. 4.8a where I also report a schematic illustration of a configuration in which many rings thread through one another in a hierarchical fashion starting from the black ring (Fig. 4.8b).

4.2.1 Overlapping Crumpled Globules

As discussed in Chap. 2, the size of a ring polymer in the melt is that of crumpled globule. In reality, this regime is achieved only when rings are large. Shorter rings assume the ideal size with $\nu = 1/2$ which crossovers, via $\nu = 2/5$, to the collapsed regime with $\nu = 1/3$ (see Fig. 4.9). Although this exponent provides us with information regarding the overall size of the polymer coils, it does not inform us of their internal structure. A better way to probe the internal arrangement of the coils is by using the static scattering function, or form factor, $S_1(q)$ defined in Chap. 2 (see Eq. (2.28)). One in fact expects that, in the range $2\pi/R_g < q < 2\pi/\sigma$, this function scales as

$$S_1(q) \sim (q\sigma)^{-d_F} \tag{4.12}$$

where d_F is the fractal dimension of the chain at length scale $2\pi/q$ and it is related to the entropic exponent as $d_F = 1/\nu$ (Rubinstein and Colby 2003). Linear chains in the melt display $d_F = 2$ for a broad range of q's (Halverson et al. 2011a). Ring polymers in the melt have instead a more complex arrangement: because their ideal size differs from the size assumed in the limit of large polymerisation index, one can in principle detect two regimes: at contour lengths below ($s < M_e$) and above ($s > M_e$)

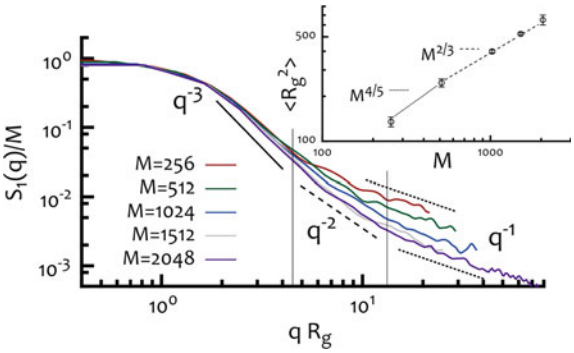

Fig. 4.9 Static scattering function $S_1(q)$ plotted against qR_g and divided by the length M of the rings. The scattering vector q probes length scales $l = 2\pi R_g/(qR_g)$ and shows a more complex behaviour than for systems of linear polymers. *Inset* average radius of gyration squared ($\langle R_g^2 \rangle$) showing the two scaling regimes $R_g^2 \sim M^{2\nu}$ with $\nu = 2/5$ and $\nu = 1/3$ (see Chap. 2)

the entanglement length, or blob size, M_e. In fact, below M_e one expects that the chain simply follows the Gaussian statistics for an open polymer s monomers long; for this reason one expects the size of a blob to scale as $R_b(s < M_e) \sim s^{1/2}$ (being the self-avoidance screened out) (Grosberg 2014). On the other hand, larger contour lengths are more crumpled and follow $R_b(s > M_e) \sim s^{1/3}$. This markedly different behaviour cannot be captured in melt of linear polymers, as both regimes, below the above the entanglement length, follow the Gaussian statistics with $R_b(s) \sim s^{1/2}$.

For the rings the situation is more complicated, as represented in Fig. 4.9. Let us focus on the longest rings $M = 2048$: For $qR_g > 2\pi R_g/l_K \simeq 16$, where $l_K = 10\,\sigma$ is the polymers' Kuhn length, the structure factor probes length scales below the Kuhn length and therefore returns, as expected, a scaling $S_1(q) \sim q^{-1}$, valid for rigid rods. In the regime, $\pi < qR_g < 2\pi R_g/l_K$, the scattering function probes length-scales between $2R_g$ and l_K. In this case, Fig. 4.9 shows that the fractal dimension d_F changes from $d_F = 3$ to $d_F = 2$ at around $qR_g \simeq 4$ corresponding to length scales $l = 2\pi R_g/4 \simeq 40\,\sigma$, i.e. several Kuhn lengths but smaller than the diameter of the chain $2R_g$. In the large length scale limit, $qR_g \ll 1$, the magnitude of wave vector $|\boldsymbol{q}|$ is much smaller than any distance $|\boldsymbol{r}_i - \boldsymbol{r}_j|$ between beads in the chain and therefore the structure factor is simply $S_1(q) = M$.

In Fig. 4.10 I report the scaling of surface monomers m_s computed as the number of monomers of each chain "in contact" with other chains, i.e. having a distance $d \leq \rho^{-1/3}$ from other monomers, and ρ^{-1} being the free volume available to each monomer in units of σ. This quantity has been discussed in Chap. 2 and, in particular, its exponent β has been recognised to be a good measure of the coils "roughness". Contact exponents β close to one indicate highly rough surfaces with a large number of interactions with other chains. In Fig. 4.10 one can observe that $\beta \simeq 1$ within errors for the systems with the longest chains. It is worth stressing that it might seem counter-intuitive that a globule with exponent $\nu = 1/3$ and a contact exponent $\gamma \simeq 1$

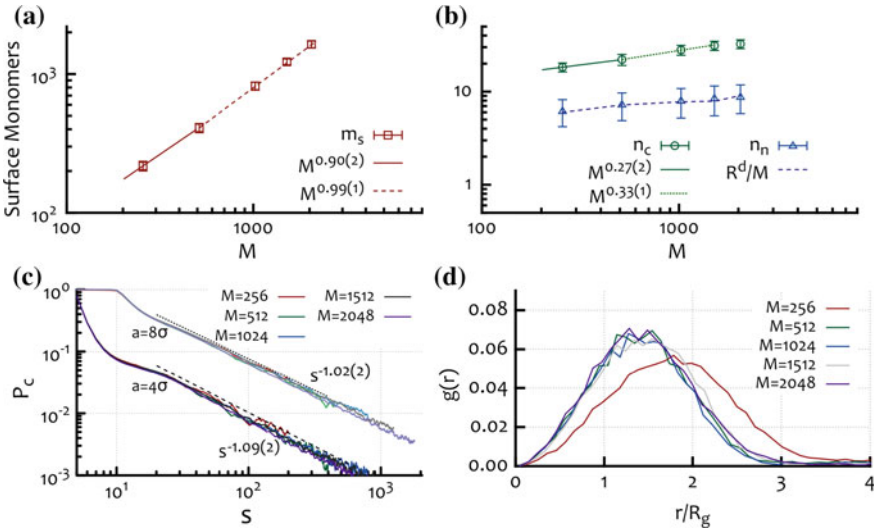

Fig. 4.10 **a** Surface monomers m_s computed as described in the text and the two observed scaling $m_s \sim M^{\beta}$ with $\beta = 0.9$ and $\beta = 0.99$ in agreement with Ref. (Halverson et al. 2011a) and Chap. 2. **b** Number of contiguous chains n_c and neighbouring chains n_n as defined in the text. Notice that the former is quantitatively more numerous than the latter; $N = 50$ is the maximum number of chains in the systems. **c** Contact probability $P_c(s)$ as defined in Chap. 2 and observed to follow a scaling near s^{-1} as predicted in Eq. (2.20) for a crumpled globule (slightly dependent on the chosen cut-off a). **d** Pair correlation function of the coils centre of mass $g(r)$ as defined in Eq. (4.13). The maximum of this function defines the average distance of the chains centre of mass and it is found to be smaller than $2R_g$

(reported in Fig. 4.10c) has a number of contacts that scales nearly linearly with the length of the coil M. The only plausible explanation is that although the coils are collapsed and crumpled, they are also highly inter-penetrating and not segregating. All this strongly suggests that rings in melt might inter-thread, similarly to the rings embedded in the gel studied in the previous section.

The fact that coils are inter-penetrating rather than segregating is also strongly suggested by the pair correlation function of the coils centre of mass:

$$g(r) = \frac{2}{N(N-1)} \sum_{I}^{N} \sum_{J}^{N} \delta \left(|\boldsymbol{r}_{CM,I} - \boldsymbol{r}_{CM,J}| - r \right). \tag{4.13}$$

This function shows a distinct peak at $r < 2r_{\max} \simeq 2.6R_g$, being $R_g = \sqrt{3/5} r_{\max}$ the mean radius of an homogeneous sphere of radius $r_{\max}$, (see Fig. 4.10d), and therefore implies that the coils behave similarly to ultra-soft colloids of size $2r_{\max}$ rather than segregated hard spheres (Likos et al. 2014). In light of this, it is reasonable to study the number of different chains with which each coil can interact with. A very crude approximation of the number of neighbours is $n_n \sim R_g^d / M$, that gives the number

of chains within a d-dimensional volume of linear size R_g centred in any one coil. Equivalently, one can count the number of coils whose centre of mass separation is smaller than sum of their gyration radii, i.e.

$$n_n = \left\langle \sum_J \Theta\left(R_{g,I} + R_{g,J} - |\boldsymbol{r}_{CM,I} - \boldsymbol{r}_{CM,J}|\right) \right\rangle_{I,t}, \tag{4.14}$$

where $\Theta(x)$ is the usual Heaviside function and $\langle \ldots \rangle_{I,t}$ identifies the average over rings and time-steps. One can imagine to define a different measure of "contact" exploiting the measure of the surface monomers. One can define the number of contiguous chains n_c as the number of chains whose monomers are in contact. It is worth noting two features of n_c as reported in Fig. 4.10b: (i) it is larger than n_n, meaning that the contacts between different chains are not restricted to neighbouring chains within a volume R_g^d but go beyond the gyration radius, possibly via long protrusions; (ii) while $n_n \sim R_g^d/M \sim M^{d\nu-1}$ it is roughly constant ($d\nu - 1 = 0$) in the crumpled regime, the number of contiguous chains n_c seems to increase as $M^{1/3}$ before plateauing for the longest chains at around $N \simeq 30$. This means that any given chain is contiguous, in the sense defined earlier, to 30 other chains in the system.

All this is in agreement with previous observations in the melt, where the rings have been found to assume configurations possessing long protrusions and strongly deviating from a compact sphere (Halverson et al. 2011a). This encourages us to probe the dynamics of the rings, and in particular, to design a protocol that allows us to investigate the effects of threadings and their spatial correlations.

4.2.2 The Slow Exchange Dynamics of Rings

At this stage it is reasonable to ask whether one can explicitly measure an inter-chain correlator in order to unambiguously observe the exchange dynamics of rings in solution. Recently, this has been done by tracking neighbouring chains (Lee et al. 2015), i.e. chains whose centres of mass are closer than the sum of their size. Here, we want to exploit the computation of contiguous chains, to define a correlator of contiguity over time. This is done by computing a dynamic $N \times N$ matrix $P(t)$ whose elements are defined as

$$P_{IJ}(t) = \begin{cases} 0 \text{ if } d_{ij} \geq \rho^{-1/3} \\ 1 \text{ if } d_{ij} < \rho^{-1/3} \end{cases} \tag{4.15}$$

where d_{ij} is the distance of any two monomers i and j belonging to chains I and J, respectively. From this it is straightforward to obtain the correlator

$$\varphi_{nc}(t) = \left\langle \frac{1}{N} \sum_{J=1}^{N} P_{IJ}(t) P_{IJ}(t - \Delta t) \dots P_{IJ}(t_0) \right\rangle_{I,t_0} \tag{4.16}$$

where $\langle \dots \rangle_{I,t_0}$ indicates the average over rings and initial times t_0. This function quantifies the exchange dynamics of contiguous chains and, in particular, it is bound to track the quickest time-scale in the exchanging process since it involves the product of P_{IJ} over all the intermediate time-steps between t_0 and t. In other words, if two chains are not contiguous at any time during the simulations, that pair no longer contributes to $\varphi_{nc}(t)$, i.e. $\lim_{t\to\infty} \varphi_{nc}(t) = 0$.

Figure 4.11 shows the behaviour of $\varphi_{nc}(t)$ as a function of the time-lag and for different systems. The exchange dynamics of contiguous pairs can be fitted as a simple exponential for the shortest chains with $M = 256$, while for longer chains the behaviour of $\varphi_{nc}(t)$ is best fitted by stretched exponentials of the form

$$\varphi_{nc}(t) = \exp\left(-\frac{t}{\tau_{\rm nc}(M)}\right)^{\beta_{\rm nc}(M)} \tag{4.17}$$

with $\beta_{\rm nc}$ decaying from $\beta_{\rm nc}(M = 256) = 1$ to $\beta_{\rm nc}(M = 2048) \simeq 0.5$ (see Fig. 4.11). The values of $\tau_{\rm nc}$ instead show a striking exponential increase which suggests the rapid emergence of slow dynamics in the exchange dynamics of the rings. Stretched exponentials with stretching exponents smaller than one and exponentially increasing relaxation times are both strong signatures of the onset of glassy dynamics and dynamical heterogeneities in glass-forming systems (Berthier and Biroli 2011) and it encourages further investigations into the inter-coil correlations in systems of rings.

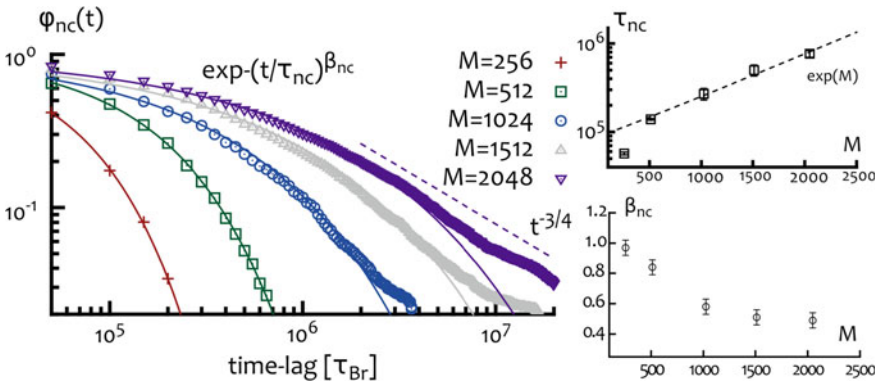

Fig. 4.11 *Left* fraction of persistent contiguous chains $\varphi_{nc}(t)$ is plotted against time for different chains length. It is worth noticing that while the decay for short chains is very well approximated by a simple exponential, for longer chains one observes (i) that the behaviour is well fitted by stretched exponentials (*solid lines*) and also (ii) the presence long-time fat tails. *Right Top* values of τ_{nc} and of *Right Bottom* β_{nc} used to fit the data points $\varphi_{nc}(t)$ with stretched exponentials

It is also worth noticing that the decay time of $\varphi_{\rm nc}(t)$ is conceptually intimately related with the tube renewal time for a system of linear polymers. In fact, one can imagine that very persistent contiguous chains must possess some level of correlation that does not allow them to drift away from each-other, similarly to the chains forming the reptating tube of any one linear polymer. One can therefore argue that the motion of contiguous chains is strongly correlated and one possible cause might be the presence of threadings. Unfortunately, it is not possible to directly check if this is the case in this system, as opposed to the case of rings embedded in a gel.

Finally, it is worth stressing that while linear polymers cannot fully renew their conformation until they decorrelate from the chains forming their tube, there is no explicit constraint for ring polymers to relax the spatial stress stored along their contour by, for instance, renewing their protruding segments (see $G(t)$ in Fig. 4.5 and $\tau_{\rm diam}$ compared with $\tau_{\rm relax}$ in Fig. 4.6), while retaining proximity with contiguous chains. In other words, the type of "entanglement" at which ring and linear polymers are subjected to in dense solutions is rather different and one can speculate it to have a strong "topological" character.

4.2.3 Inducing a Topological Glass by Randomly Pinning Rings

The major problem that one faces when studying threadings in solutions of rings is that this topological interaction is not well defined and virtually impossible to identify and characterise in this condition. As a consequence, the effect of threadings on the dynamics of the rings is even more elusive and for this reason very poorly understood. This is why in this section I will attack this problem from an unconventional perspective. I will in fact make use of techniques adopted by studies on glass-forming systems and in particular I will take inspiration from a number of recent papers that advanced the idea, and investigated the behaviour, of glass-forming systems under an external pinning field (Bouchaud and Biroli 2004; Biroli et al. 2008; Cammarota and Biroli 2012; Karmakar and Parisi 2013; Cammarota 2013; Gokhale et al. 2014; Nagamanasa and Gokhale 2015; Ozawa et al. 2015).

In these systems a fraction c_p of constituents are artificially frozen in time and the response of the system to this perturbation is studied. One of the most striking findings is that the glass transition temperature of prototypical glass formers such as spin-glasses display a dependence on the value of the pinned fraction c_p (Cammarota and Biroli 2012). In the case of spin glasses, this effect has been conjectured to be intimately related with the fact that pinning spins reduces the configurational entropy of the system. This means that the systems are more prone to reach the ideal glass-transition state (at which the systems displays zero configurational entropy) at temperatures higher than the natural T_g (Cammarota and Biroli 2012; Karmakar and Parisi 2013), thereby facilitating their experimental and numerical investigation. Several protocols have been used to probe the response of systems to this

artificial perturbation, and in particular, different geometries have been adopted where the frozen fraction of constituents, spins or particles, are distributed either on a plane (Nagamanasa and Gokhale 2015), randomly (Cammarota and Biroli 2012; Gokhale et al. 2014) or to form cavities (Mézard and Parisi 2001; Cammarota 2009).

The Physics underlying the glass-transition is still very much debated. In particular, whether it can be interpreted as an ideal thermodynamic transition, or solely a kinetic one, is a long debated topic. For sure, systems in which the glass-transition is driven by pinning a fraction of the constituents display a high level of correlations and possibly, complicatedly structured "cooperatively rearranging regions" (CRRs) (Nagamanasa and Gokhale 2015). The existence and growth of these regions when $T \to T_g$ had been suggested 50 years ago by Adam and Gibbs (Adam and Gibbs 1965) in a seminal paper. For instance, in a glass-forming system made of colloidal particles, CRRs are made of particles surrounding any one particle and allow the macroscopic motion of this particle by cooperatively re-arranging their position. As the temperature (or the density) approaches the glass-transition one, these regions grow in size thereby freezing the position of the particle at the centre of the cluster, limiting its motion to local vibrations within a cage. Analogously, if one believes that rings in the melt, or in dense solutions, assume inter-threaded configurations as pictured in Fig. 4.8b then CRRs can be conceptually related to the longest sequence of rings that needs to come undone for the black ring to fully renew its neighbours. When a fraction c_p of constituents in a glass-forming system is frozen, this contributes, in a complex way, to increasing the size of CRRs. In fact, freezing all the neighbours around a probe particle would mean creating an infinitely large CRR around that particle.

In light of this picture it is natural to ask the following question: what happens if one starts to randomly pin a fraction c_p of rings in a solution of rings? or even, what happens if one artificially freezes all the rings apart from one?

If one reasons from a standard reptation theory point of view (Doi and Edwards 1988), then the prediction is that the probe polymer will simply snake or diffuse trough the frozen obstacles. This is in fact what one observes in the case of systems of linear polymers (see lime data points in Fig. 4.12a), where in the limit of large timescales the diffusive behaviour is nearly[6] indistinguishable when compared with the pure melt case ($c_p = 0$). On the contrary, by repeating the same in silico experiment on the corresponding system of equilibrated rings with same contour length, one observes a striking behaviour: the centre of mass of the probe (free) ring is forever trapped in a region smaller than R_g (see red data points in Fig. 4.12a).

This remarkable difference is due to the topology of the constituents, as no other parameter has been changed. One can imagine that if the probe ring assumed conformations such as the moose in Chap. 1 (Fig. 1.4a), i.e. not threaded by other rings, then it would simply diffuse through the frozen background by protruding its contour through the spaces, very much like predicted by the theories of ring polymers motion advanced in the 80's (Rubinstein 1986, 1987; Cates and Deutsch 1986) and more

[6]Since the mobile chain leaves a hole that produces an uniformity in the system density and could, in principle, interfere with a perfectly free diffusion.

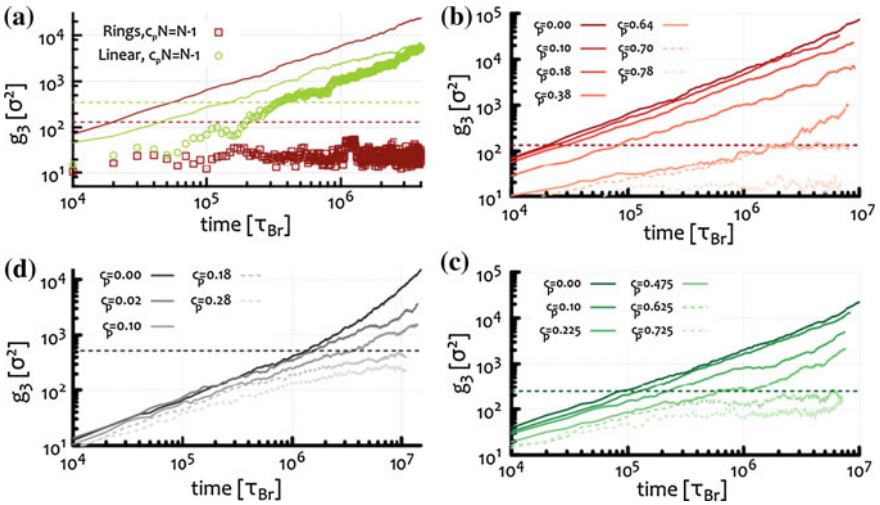

Fig. 4.12 **a** Mean square displacement of the centre of mass $g_3(t)$ of polymer diffusing through $N-1$ frozen polymers. The data points are averaged over many choices of the probe. Lime data points represent linear polymers while red data points represent system of ring polymers both systems are chosen with $M=256$ and $N=50$. The corresponding mean squared displacement for the two systems in the case where no polymer is frozen ($c=0$) is also shown as solid lines. **b–d** Mean square displacement of the centre of mass $g_3(t)$ for different choices of c_p and for different systems: **b** $M=256$, **c** $M=512$ and **d** $M=1512$. The kinetically arrested state $c_p=c_p^{\dagger}$ is reached when the un-frozen polymers cannot diffuse further than R_g and the corresponding g_3 are indicated as dashed lines. Dark horizontal dashed lines represent $\langle R_g^2\rangle$ for the different cases

recently (Milner and Newhall 2010; Smrek and Grosberg 2015). Otherwise, if the probe ring was threaded, such as the modified moose in Fig. 4.8c or the black ring in Fig. 4.8b by its red, green and blue neighbours, then it is reasonable to expect its diffusion to be strongly constrained, or even completely hindered, by the fact that its neighbours become frozen.

A short threading segment is expected to contribute very little, as it can be easily circumvented, but if the threading segment was longer and itself threaded, that would created a much more persistent obstacle for the free ring and perhaps impossible to get rid of (especially if the sequence of rings that needs to be escaped forms a network larger than the ring size or, even, as large as the system size (see Sect. 4.1 and Fig. 4.7)).

Similarly to what has been observed in glass-forming liquids when a region of the system was pinned by, for instance, optical traps (Gokhale et al. 2014; Nagamanasa and Gokhale 2015), here one can argue that it might be possible to exploit the topological interactions occurring within a dense solution of rings to generate a kinetically trapped subset of the system, for instance by adopting the following protocol: Starting from the unperturbed case, i.e. $c_p=0$, one can increase the value of c_p until the mean square displacement of the centre of mass ($g_3(t)$) of the remaining

fraction $f_p \equiv 1 - c_p$ of rings ceases to display free diffusion, i.e. $\lim_{t\to\infty} g_3(t) \sim const$. This value of c_p, to which I will refer to as c^*, is the critical fraction of pinned rings for which all the other non-explicitly pinned rings are trapped by topological interactions, i.e. threadings. An example of this protocol is reported in Fig. 4.12b–d where I show the mean squared displacement of the rings centre of mass for different systems and for a range of c_p.

More formally, one can define $c_p^\dagger$ by introducing the following order parameter:

$$R_c^{-1} \equiv \lim_{t\to\infty} \langle g_3(t)\rangle^{-1/2}, \tag{4.18}$$

which has dimensions of an inverse length and jumps from 0 to finite values only when the un-frozen rings are "caged" by the topological interactions. From this, it is therefore natural to identify $c_p^\dagger$ as the value of c_p at which R_c^{-1} displays the discontinuity. Another way of defining $c_p^\dagger$ that is perhaps more familiar to the common practice in the literature about the glass transition is by measuring the overlap parameter (Karmakar and Parisi 2013) for the coils

$$Q_s^{\rm coil}(t; c_p) = \left\langle \frac{1}{f_p N} {\sum_I}' \Theta(w - |\boldsymbol{r}_{CM,I}(t + t_0) - \boldsymbol{r}_{CM,I}(t_0)|) \right\rangle_{t_0} \tag{4.19}$$

and for the monomers

$$Q_s^{\rm mon}(t; c_p) = \left\langle \frac{1}{f_p N} {\sum_I}' \sum_{i\in I}^{M} \Theta(w - |\boldsymbol{r}_i(t + t_0) - \boldsymbol{r}_i(t_0)|) \right\rangle_{t_0}, \tag{4.20}$$

where $\sum'$ indicates the sum restricted to the un-frozen $fN \equiv (1 - c_p)N$ rings, $\Theta(x)$ is the Heaviside function and the window parameter w is set to $2R_g$ (Karmakar and Parisi 2013) since I am interested in averaging out the jiggling of the coils within cages of linear size $w = 2R_g$.

According to the interpretation of the arrested dynamics that I have given above in terms of cages formed by threadings, one expects that, as c_p approaches $c_p^\dagger$,

$$Q_s^{\rm coil}(t; c_p^\dagger) = 1 \forall t, \tag{4.21}$$

since the center of mass of the un-frozen coils start rattling inside cages of size $2R_g$. At the same time, one also expects that the monomers are instead partially free to decorrelate from their initial state, giving

$$0 < \lim_{t\to\infty} Q_s^{\rm mon}(t; c_p^\dagger) < 1. \tag{4.22}$$

These predictions are nicely recovered from the explicit computation of the overlap parameters whose behaviour is reported in Fig. 4.13.

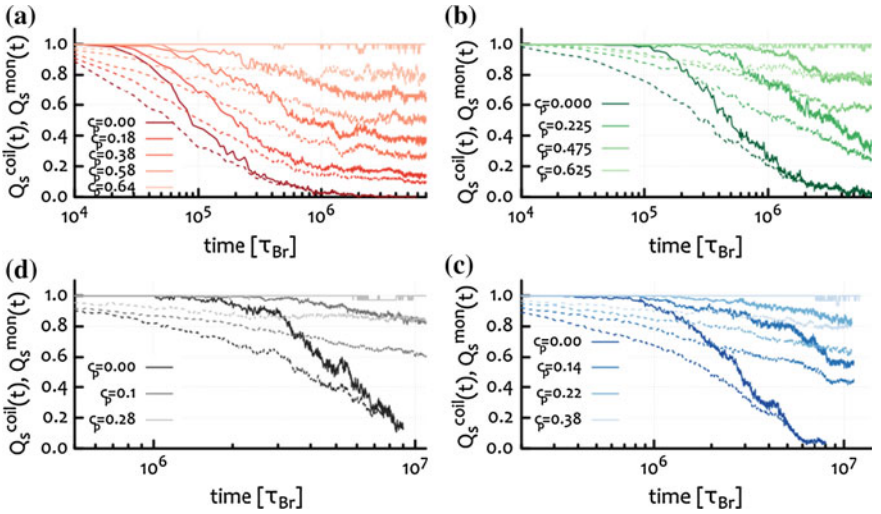

Fig. 4.13 Overlap parameters $Q_s^{\text{coil}}(t; c_p)$ (*solid lines*) and $Q_s^{\text{mon}}(t; c_p)$ (*dashed lines*). It is worth noting that while the large time value of both $Q_s^{\text{coil}}(t; c_p)$ and $Q_s^{\text{mon}}(t; c_p)$ vanish at $c_p = 0$, they display an arrested decay for larger c_p until at $c_p = c_p^{\dagger}$ the overlap parameter $Q_s^{\text{coil}}(t; c_p)$ equals unity at any time

At this stage it is important to stress another message that can be inferred from Figs. 4.12 and 4.13. The value of $c_p^{\dagger}$ is dependent on the length of the polymers M. In fact, this seems to decrease when M is increased, thereby suggesting that fewer and fewer rings need to be artificially frozen in order for the system to display the kinetically arrested state. Before investigating further the M dependence of c^*, I will first discuss the coherent scattering function $S_c(q, t)$, that is often referred to in the glass-transition literature. This is here computed over the $f_p N = (1 - c_p)N$ free rings and can quantify the relaxation, or decorrelation, associated with length scales $l = 2\pi/q$.

It is common practice to tune the scattering vector at values corresponding to $r_{\max}$, where $r_{\max}$ is the position of the peaks of the pair correlation function $g(r)$. In this case, it is more appropriate to tune it to values corresponding to the coils diameter $2R_g$, since this is the length scale above which one is interested to probe the rings' dynamics. For this reason I here choose two values of q: one corresponding to length-scales slightly greater than $2R_g$, i.e. $q_1 = 2/R_g$ and the second corresponding to length scales slightly smaller than $2R_g$, i.e. $q_2 = 4/R_g$. In Fig. 4.14 I report $S_c(q, t)$ for different values of c and compare these choices of q for systems made rings $M = 512$ and $M = 1512$ beads long.

As mentioned in Chap. 2, the scattering function is dominated by pair of beads that have not travelled much further than $2\pi q^{-1}$ after t time-steps, and for this reason it is more sensitive than $g_3(t)$ to the slow elements of the system. In Fig. 4.14 one can observe that when $c_p = 0$, that is the case of an unperturbed system, the

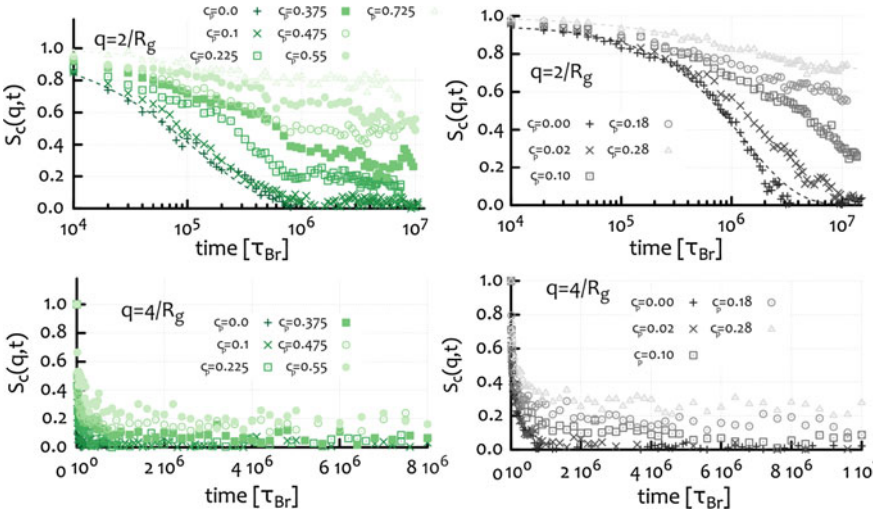

Fig. 4.14 Coherent scattering function $S_c(q,t)$ (normalised by $S_c(q,0)$) for different values of c and for $q = q_1 = 2/R_g$ (*Top Row*) and $q = q_2 = 4/R_g$ (*Bottom Row*) for a system with $M = 512$ (*Left*) and $M = 1512$ (*Right*)

scattering function displays a decay at both values of q. When c_p is increased, the scenario changes dramatically: $S_c(q_1,t)$ shows an arrested decay which is strongly reminiscent of those observed in glass-forming systems approaching T_g (Kob et al. 1997). On the other hand, shorter length-scales, i.e. longer wavelengths, show a much faster de-correlation as showed by $S_c(q_2,t)$. In particular, in this latter case, all the curves seem to differ very little from one another indicating that there is no (or little) effect of the increasing c_p in the relaxation of those length-scales. These findings agree remarkably well with the "pierced lattice animal" representation. As I argued in Chap. 2, threadings that are not dense enough are in fact most likely to slow down the translational degrees of freedom, i.e. long length scales, while leaving shorter length scales free to relax the stress and re-arrange the rings' configuration.

While in the case of vitrifying systems the appearance of a plateau in the intermediate scattering function can have multiple and sometimes not well understood (Berthier and Biroli 2011) origins, in this case it can be explained in terms of threadings: above $c_p^{\dagger}$, length-scales $2\pi q^{-1} \gtrsim \pi R_g$ display no relaxation at all, since the translation of the un-frozen rings at distances greater than $2R_g$ is completely suppressed. On the other hand, length-scales shorter than $2R_g$ can still relax and de-correlate, since rings are free to create new protrusions anywhere along their contour. This means that the two time-scales associate with internal organisation of the ring conformation (equivalent to τ_{diam} of the previous section) and the diffusion of the centre of mass (equivalent to τ_{relax} of the previous section), are decoupled.

In other words, the situation presented here is a clear example of how rings can relax their internal stress without displaying free diffusion, which is temptingly

similar to the phenomenon that has been observed both numerically and experimentally for ring polymers in the melt (Kapnistos et al. 2008; Halverson et al. 2011a; Pasquino et al. 2013) but for which a clear explanation was still lacking.

This scenario is also strongly reminiscent of α and β relaxation modes in Mode Coupling Theory (Aichele and Baschnagel 2001; Berthier and Biroli 2011) of glass transition. Caged polymers spend the majority of their time re-arranging their internal structure without performing macroscopic jumps. In this respect, ring polymers behave like particles in colloidal glass-forming systems as T approaches T_g, for which the macroscopic motion (α relaxation) decorrelates from the local jiggling (β relaxation). In particular, it is common in the glass-transition literature, to define a non-ergodic parameter $f_c(q)$ equal to the value of $S_c(q,t)$ at the plateau (Aichele and Baschnagel 2001). In the case studied here, one can simply take

$$f_c \equiv \lim_{t\to\infty} S_c(q,t), \tag{4.23}$$

computed for $q = 2/R_g$, as the decay of this scattering function is arrested at that value (Fig. 4.14).[7]

Before continuing with the analysis of this system, I would like to stress, once again, that these features are not observed in system of linear polymers, in which an arbitrary fraction c_p of polymers can be artificially frozen while virtually un-affecting the long-time behaviour of the other polymers. The features observed in the systems presented here are solely due to the rings topology, and are the first unambiguous signature of the presence of threadings between rings in solution.

The Phase Diagram of the System Suggests the Emergence of a "Topological Glass" in the Large M Limit

The behaviour of the non-ergodic parameter f_c is reported in Fig. 4.15. It is clear that the transition from $f_c = 0$ for $c_p = 0$ to larger values of the non-ergodic parameter is sharper as the length of the rings increases. This implies that one requires a smaller and smaller perturbation parameter c_p to "force" the system from a liquid-like to a glass-like one. The behaviour of f_c, when plotted against $f_p = 1 - c_p$ (see inset in Fig. 4.15) is well fitted by the functional form

$$f_c = 1 - f_p^{\alpha} = 1 - (1 - c_p)^{\alpha} \simeq \alpha(M) c_p \tag{4.24}$$

in the small c_p limit and where the exponent α seems to increase with the rings length M, indicating a quicker approach to large values of the arrested decay of $S_c(q,t)$.

[7] It is perhaps interesting to think about what would happen if one were to relax the uncrossability condition imposed on the chains and substitute it with a potential barrier of finite height A. In this scenario, one expects the scattering function to re-establish its decay although only after a time $t \sim \langle Th \rangle \exp A$ that corresponds to an activated process where at least some of the threadings must be by-passed. In this picture, the system would probably display a long-time α relaxation which decouples from the local rattling proportionally to the number of threadings in the system.

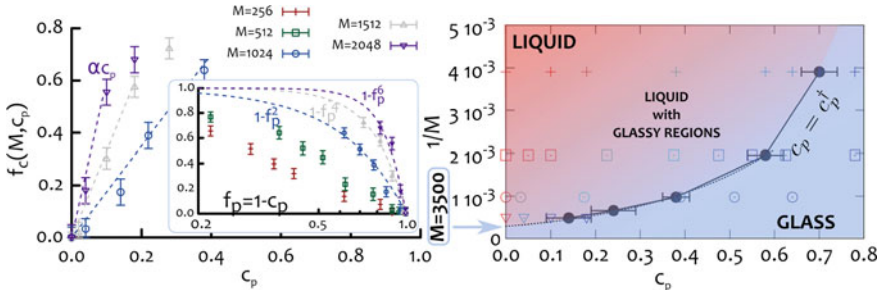

Fig. 4.15 *Left* functional behaviour of f_c plotted against c_p and $f_p = 1 - c_p$ in the inset. The behaviour is well fitted by $f_c = 1 - f_p^\alpha$ with α increasing with the length of the rings. *Right* phase space diagram for a systems with rings M beads long and where a fraction c_p of rings have been artificially frozen in space and time. The coloured data points indicate the value of F_c defined in Eq. (4.25) which goes from $F_s = 0$ (*red*) at $c_p = 0$ to $F_s = 1$ (*blue*) at $c_p \geq c_p^\dagger$. The fit through the last four data points indicates an exponential behaviour of the transition line whose $c_p \to 0$ limit gives $M_g \simeq 3500$ at which a spontaneous glass might emerge

Having defined rigorously defined $c_p^\dagger$ from R_c in Eq. (4.18) or, equivalently, using the overlap parameter Q_s^{coil}, from Eq. (4.21), it is possible to obtain the functional form of $c_p^\dagger(M)$, that is reported in Fig. 4.15.

In addition, one can use the large time value of the coils overlap parameter to define

$$F_s \equiv \lim_{t\to\infty} Q_s^{\text{coil}}(t) \tag{4.25}$$

which is a good estimation of the closeness of the system to $c_p^\dagger$ (recall that $F_s = 1$ at $c_p = c_p^\dagger$). The behaviour of $c_p^\dagger(M)$ and F_s is reported in the phase space $(c, 1/M)$. The straightforward interpretation that comes out from this plot is that the transition line $M^\dagger(c)$, or $c_p^\dagger(M)$, divides the parameter space into a liquid-like and glass-like regions. Furthermore, from this plot it is clear that the limit $c_p \to 0$ is an interesting one. In fact, at $M^\dagger(c_p \to 0) \equiv M_g$, the system is conjectured to display a dramatic response to a tiny perturbation, eventually leading to the emergence of a spontaneously vitrifying system.

The values of $c_p^\dagger$ for the four systems with largest chains follow, remarkably well, an exponential of the form

$$M^\dagger(c_p) = M_g e^{-3.3c_p^\dagger} \tag{4.26}$$

with

$$M_g \equiv \lim_{c\to 0} M^\dagger(c_p) \simeq 3500. \tag{4.27}$$

Although the precise value of M_g might suffer from the finite size of the simulated systems, the general behaviour of the transition line encourage the conjecture that in the limit of large polymerisation index M, a spontaneous glass might occur.

Even though performing simulations with such big M or purifying solutions of very long rings might be too difficult with the current technology, the results that I reported here strongly encourage the experimental realisation of the perturbation protocol employed in this section. The response to this perturbation should in fact become more and more dramatic as the length of the rings increases, eventually requiring only a small fraction of rings to be frozen to cause the whole system to be kinetically trapped.

One can furthermore argue that this perturbation protocol might be experimentally realised by using optical traps as in recent experiments on colloidal glass forming systems (Gokhale et al. 2014). Another option for its experimental realisability could be considering a mixture of polymers having different freezing temperatures. In this scenario, the parameter c could be directly related to the mixture concentration and temperature of the system. Another option could be considering a bi-disperse system or blends, where longer and heavier (and slower) ring polymers are in solutions with lighter ones. By changing the ratio of the concentrations one could in principle control an equivalent c parameter also in this case.

It is finally worth stressing once again that all this is performed at temperatures where the thermal energy equals the LJ interaction energy (the Langevin thermostat is fixed to $T = \epsilon/k_B$) and at fixed monomer density $\rho = 0.1\,\sigma^{-3}$. This implies that the diagram reported in Fig. 4.15 is one of the first instances of vitrification occurring in a system where neither temperature, or density, are the main control parameters used to drive the glass-transition. This is in fact solely driven by topological interactions, and for this reason it cannot be observed in systems of topologically trivial polymers such as linear ones.

One should finally emphasise that the transition observed in these systems is not a thermodynamic one, i.e. there is no divergence of thermodynamic quantities. Although it is clear that at $c_p^\dagger$ the system displays a macroscopically different behaviour, this is only due to the topological interactions present in the system, which cause kinetic traps. In this respect, one can talk of "topological correlations" which, in the case studied here, are the main players controlling the purely kinetic glass transition.[8]

4.3 Conclusions

In this chapter I have tackled the problem of investigating topological interactions in solutions of un-linked and un-knotted ring polymers, i.e. threadings. In the first section of this chapter I showed that these are readily studied when the solution of rings is forced to move inside a static gel structure and I described a novel method to quantify ring-ring penetrations by exploiting its architecture. This method allows one to identify and quantify both, inter-ring threadings and their effect on the rings

[8] and is broadly analogous, although in a much less coarse-grained sense, to what happens in glass-forming systems belonging to the class of "Kinetically Constrained Models" (Palmer et al. 1984).

dynamics. On the other hand, it is worth highlighting that the gel structure can have a non-negligible effect the rings. The presence of the grid, and the consequent topological constraint that acts on the rings (as they have to be unlinked from it at any time), might play an important role on the equilibrium configurations of the rings, which might display more elongated and squeezed shapes, with respect to those assumed in absence of the gel. In addition, the relaxation of the rings might be slowed down by the facts that the rings have additional constraints to respect, on top of those presented by the neighbouring chains. As I will show in the next chapters, the presence of a gel and its detailed microscopic structure, plays a crucial role in the out-of-equilibrium dynamics of ring polymers (see Chap. 6). When an external force is driving the polymers, they can in fact get impaled and permanently entangled. While the effects of the gel on the equilibrium properties of the rings might be less dramatic, quantifying their relevance would nonetheless be important. A more detailed investigation of these effects would be a natural continuation of the work presented in this chapter. This could readily be done by investigating systems in which the gels possess lattice spacings varying from $l \ll l_K$ to $l \gg l_K$. In the former limit, the rings are expected to be in the regime of extreme elongation, while in the latter the system properties could readily be compared to those observed in a pure melt of rings.

The most important and remarkable result of the first section is that threadings are a critical quantity, in that they extensively grow with the length of the rings. It is also worth stressing that I have showed the existence of connected clusters of inter-threaded rings, whose size grows with the number of threadings in the system. A cluster of inter-penetrating rings of size $\mathcal{O}(N)$ has been showed to emerge for the longest chains that I investigated. Correspondingly, the same system displays a dramatic slowing down of its diffusion (see Fig. 4.6).

Although the results presented in the first section of this chapter are formally bound to hold in the case of a dense solution of rings immersed in a static gel structure, it is worth noting that many of the reported findings are in agreement with those for a pure melt of rings. In particular three quantities are worth comparing: (*i*) the scaling of the radius of gyration $R_g^2 \sim M^{2\nu}$ with $\nu = 1/2$ for short rings and $\nu = 1/3$ for long ones, is in perfect agreement with recent MD simulations of a melt of rings (Halverson et al. 2011a; Rosa and Everaers 2014) and theoretical predictions for the melt case (see Chap. 2); (*ii*) the segmental displacement, reported here to reach free diffusion only when rings have travelled many times their own size $\langle \delta r_s^2 \rangle / \langle R_g^2 \rangle > 1$, and to display a slowing down $\langle \delta r_s^2 \rangle \sim t^{1/4}$ for $M = 1512$ is in agreement with (Halverson et al. 2011b); (*iii*) the stress relaxation, found to decay as a power law $G(t) \sim t^{0.4}$ and on time-scales much shorter than the overall relaxation of the chain (free diffusion) is in agreement with experimental and numerical evidence for the melt (Kapnistos et al. 2008; Halverson et al. 2011b). All this strongly encourages the speculation that, after all, the system studied here is not too far from a melt of rings. In particular, the topological constraints to which the chains are subjected to in the case when a gel is present can be thought of as constraints coming from other chains in the melt. This conjecture is in part similar to what was assumed in the literature (Cates and

Deutsch 1986; Rubinstein 1986; Obukhov and Rubinstein 1994) when the authors investigated melt of rings by placing a background of obstacles surrounding the rings (but not threading them!).

In the second section of this chapter I focused on probing threadings in dense solutions of rings. Because no current algorithm is capable of unambiguously identifying threadings in this situation, I have tried to investigate this system from an unconventional point of view, hoping, and to my opinion, managing, to detect signatures directly associated with threadings.

Firstly, I showed that rings in dense solutions display a high level of inter-coil correlations (via measuring the contiguity persistence $\varphi_{\mathrm{nc}}(t)$ reported in Fig. 4.11). These correlations have then been further explored by probing the kinetics of the systems under an external perturbation. This has been implemented by freezing in space and time a fraction c_p of coils in the system. The response of different length-scales to this perturbation has been measured by computing the coherent scattering function $S_c(q,t)$ on the fraction $f_p = 1 - c_p$ of non-frozen rings. This showed that while length scales $l \simeq 2R_g$ are strongly affected by the frozen fraction of rings, shorter length scales are less affected, implying that while the translational degrees of freedom of the rings are suppressed by the frozen rings, internal relaxation modes are largely unhindered. This has been interpreted as a strong signature of the fact that the inter-coil correlations take the form of threadings.

Finally, I showed that the critical fraction of frozen rings $c_p^{\dagger}$ needed to drive a kinetically trapped state for all the remaining $fN = (1 - c_p)N$ rings displays a strong dependence on the length of the rings M. By plotting the transition line $c_p = c_p^{\dagger}$ in the phase space $(c_p, 1/M)$ I then showed that the results from the simulations imply that the limit $c_p \to 0$ gives a critical value for $M(c^{\dagger}) \equiv M_g$ at which a spontaneous glass might emerge.

I hope that these results motivate further investigations into this interesting problem. In particular, I conjecture that novel experimental set-ups that have very recently been used to probe the glass-transition in colloidal and molecular liquid systems (Gokhale et al. 2014; Nagamanasa and Gokhale 2015) might be used to put into practice the perturbation protocol proposed here and finally prove the existence of this long sought "topological glass".

References

Adam, G., Gibbs, J.H.: On the temperature dependence of cooperative relaxation properties in glass-forming liquids. J. Chem. Phys. **43**(1), 139 (1965)

Adams, C.C.: The Knot Book: An Elementary Introduction to the Mathematical Theory of Knots. W H Freeman and Company, New York (1994)

Aichele, M., Baschnagel, J.: Glassy dynamics of simulated polymer melts: coherent scattering and van Hove correlation functions. Eur. Phys. J. E **5**(2), 229 (2001)

Berthier, L., Biroli, G.: Theoretical perspective on the glass transition and amorphous materials. Rev. Mod. Phys. **83**(2), 587 (2011)

Biroli, G., Bouchaud, J.-P., Cavagna, A., Grigera, T.S., Verrocchio, P.: Thermodynamic signature of growing amorphous order in glass-forming liquids. Nat. Phys. **4**(10), 771 (2008)
Bouchaud, J.-P., Biroli, G.: On the Adam-Gibbs-Kirkpatrick-Thirumalai-Wolynes scenario for the viscosity increase in glasses. J. Chem. Phys. **121**(15), 7347 (2004)
Cammarota, C.: Ph.D. thesis, La Sapienza (Roma) (2009)
Cammarota, C.: A general approach to systems with randomly pinned particles: unfolding and clarifying the random pinning glass transition. Europhys. Lett. **101**(5), 56001 (2013)
Cammarota, C., Biroli, G.: Ideal glass transitions by random pinning. Proc. Natl. Acad. Sci. USA **109**(23), 8850 (2012)
Cates, M., Deutsch, J.: Conjectures on the statistics of ring polymers. J. Phys. Paris **47**, 2121 (1986)
Cremer, T., Cremer, C.: Chromosome territories, nuclear architecture and gene regulation in mammalian cells. Nat. Rev. Genet. **2**(4), 292 (2001)
Doi, M., Edwards, S.: The Theory of Polymer Dynamics. Oxford University Press, Oxford (1988)
Gokhale, S., Nagamanasa, K.H., Ganapathy, R., Sood, A.K.: Growing dynamical facilitation on approaching the random pinning colloidal glass transition. Nat. Commun. **5**, 1 (2014)
Grosberg, A.: Annealed lattice animal model and Flory theory for the melt of non-concatenated rings: towards the physics of crumpling. Soft Matter **10**, 560 (2014)
Grosberg, A.Y., Rabin, Y., Havlin, S., Neer, A.: Crumpled globule model of the three-dimensional structure of DNA. Europhys. Lett. **23**(5), 373 (1993)
Halverson, J.D., Lee, W.B., Grest, G.S., Grosberg, A.Y., Kremer, K.: Molecular dynamics simulation study of nonconcatenated ring polymers in a melt. I. Statics. J. Chem. Phys. **134**(20), 204904 (2011a)
Halverson, J.D., Lee, W.B., Grest, G.S., Grosberg, A.Y., Kremer, K.: Molecular dynamics simulation study of nonconcatenated ring polymers in a melt. II. Dynamics. J. Chem. Phys. **134**(20), 204905 (2011b)
Halverson, J.D., Grest, G., Grosberg, A.Y., Kremer, K.: Rheology of ring polymer melts: from linear contaminants to ring-linear blends. Phys. Rev. Lett. **108**(3), 038301 (2012)
Halverson, J.D., Kremer, K., Grosberg, A.Y.: Comparing the results of lattice and off-lattice simulations for the melt of nonconcatenated rings. J. Phys. A **46**(6), 065002 (2013)
Halverson, J.D., Smrek, J., Kremer, K., Grosberg, A.: From a melt of rings to chromosome territories: the role of topological constraints in genome folding. Rep. Prog. Phys. **77**, 022601 (2014)
Kane, C.L., Lubensky, T.C.: Topological boundary modes in isostatic lattices. Nat. Phys. **10**(1), 39 (2013)
Kapnistos, M., Lang, M., Vlassopoulos, D., Pyckhout-Hintzen, W., Richter, D., Cho, D., Chang, T., Rubinstein, M.: Unexpected power-law stress relaxation of entangled ring polymers. Nat. Mater. **7**(12), 997 (2008)
Karmakar, S., Parisi, G.: Random pinning glass model. Proc. Natl. Acad. Sci. USA **110**(8), 1 (2013)
Klein, J.: Dynamics of entangled linear, branched, and cyclic polymers. Macromolecules **118**(33), 105 (1986)
Kob, W., Donati, C., Plimpton, S., Poole, P., Glotzer, S.: Dynamical heterogeneities in a supercooled Lennard-Jones liquid. Phys. Rev. Lett. **79**(15), 2827 (1997)
Kremer, K., Grest, G.S.: Dynamics of entangled linear polymer melts: a molecular-dynamics simulation. J. Chem. Phys. **92**(8), 5057 (1990)
Lee, E., Kim, S., Jung, Y.: Slowing down of ring polymer diffusion caused by inter-ring threading. Macromol. Rapid Commun. **36**, 1115–1121 (2015)
Likos, C.N., Narros, A., Moreno, A., Capone, B.: Multi-blob coarse graining for ring polymer solutions. Soft Matter **10**, 9601 (2014)
Lo, W.-C., Turner, M.S.: The topological glass in ring polymers. Europhys. Lett. **102**(5), 58005 (2013)
Maxwell, J.C.: L. On the calculation of the equilibrium and stiffness of frames. Phil. Mag. **27**, 294 (1864)
Mézard, M., Parisi, G.: The Bethe lattice spin glass revisited. Eur. Phys. J. B **20**, 217 (2001)

Milner, S., Newhall, J.: Stress relaxation in entangled melts of unlinked ring polymers. Phys. Rev. Lett. **105**(20), 208302 (2010)
Nagamanasa, K.H., Gokhale, S., Sood, A.K., Ganapathy, R.: Direct measurements of growing amorphous order and non-monotonic dynamic correlations in a colloidal glass-former. Nat. Phys. **11**(May), 403 (2015)
Obukhov, S., Rubinstein, M.: Dynamics of a ring polymer in a gel. Phys. Rev. Lett. **73**(9), 1263 (1994)
Orlandini, E., Whittington, S.G.: Entangled polymers in condensed phases. J. Chem. Phys. **121**(23), 12094 (2004)
Ozawa, M., Kob, W., Ikeda, A., Miyazaki, K.: Equilibrium phase diagram of a randomly pinned glass-former. Proc. Natl. Acad. Sci. USA **112**(22), 6914 (2015)
Palmer, R.G., Stein, D.L., Abrahams, E., Anderson, P.W.: Models of hierarchically constrained dynamics for glassy relaxation. Phys. Rev. Lett. **53**(10), 958 (1984)
Parisi, G., Sourlas, N.: Critical behavior of branched polymers and the Lee-Yang edge singularity. Phys. Rev. Lett. **46**(14), 871 (1981)
Pasquino, R., Vasilakopoulos, T., Jeong, C., Lee, H., Rogers, S., Sakellariou, G., Allgaier, J., Takano, A., Bras, A., Chang, T., Goossen, S., Pyckhout-Hintzen, W., Wischnewski, A., Hadjichristidis, N., Richter, D., Rubinstein, M., Vlassopoulos, D.: Viscosity of ring polymer melts. ACS Macro Lett. **2**, 874 (2013)
Rosa, A., Everaers, R.: Ring polymers in the melt state: the physics of crumpling. Phys. Rev. Lett. **112**, 118302 (2014)
Rubinstein, M.: Dynamics of ring polymers in the presence of fixed obstacles. Phys. Rev. Lett. **57**(24), 3023 (1986)
Rubinstein, M.: Discretized model of entangled-polymer dynamics. Phys. Rev. Lett. **59**(17), 1946 (1987)
Rubinstein, M., Colby, H.R.: Polymer Physics. Oxford University Press, Oxford (2003)
Smrek, J., Grosberg, A.Y.: Understanding the dynamics of rings in the melt in terms of annealed tree model. J. Phys.: Condens. Matter **27**, 064117 (2015)

Chapter 5
A Bio-Physical Model for the Kinetoplast DNA

Sometimes careful physics-based thinking can illuminate complicated issues in biology

M.E. Cates

The Kinetoplast DNA (or KDNA) (Simpson 1967) is one of the most complex and singular forms of DNA in nature. It is uniquely found in the mitochondrion of a group of unicellular eukaryotic organisms of the class *Kinetoplastida*. Some of these organisms have been studied since the late '60s because they are responsible for several serious diseases such as sleeping sickness and leishmaniasis (Young and Morales 1987), and are among the earliest diverging eukaryotic organisms containing a mitochondrion (Avliyakulov et al. 2004).

The Kinetoplast DNA is made of thousands (∼5000) of short (1–2.5 kbp) DNA loops which are interlinked to form a large network. The short loops, or "mini-circles", are also linked with fewer (∼30) larger loops, or "maxi-circles", consisting of around 30–50 kbp (Shapiro and Englund 1995). The maxi-circles contain standard mitochondrial genetic material, which is made readily translatable only thanks to the guide RNAs (gRNAs) encoded in the mini-circles. These have in fact been found to be mostly made by RNA-editing genes and to be genetically heterogeneous, i.e. few genetic sequences are repeated in every mini-circle (Lukes et al. 2005; Lai et al. 2008; Jensen and Englund 2012). *C. fasciculata* mini-circles assemble in a network whose shape resembles that of a disc. Its dimensions have been found to be around 1 μm in diameter and 0.4 μm in thickness (Pérez-Morga and Englund 1993b; Lukeš et al. 2002; Jensen and Englund 2012). Networks which are removed from the mitochondria, e.g. via cell lysis, expand into an elliptical shape whose minor and major axis are respectively around 10 and 15 μm, i.e. roughly a hundred times bigger than their dimension in vivo (Jensen and Englund 2012), possibly implying that the networks experience a confinement within the mitochondria.

D. Michieletto, *Topological Interactions in Ring Polymers*, Springer Theses,
DOI 10.1007/978-3-319-41042-5_5

A "tripartite attachment complex" (TAC) keeps the Kinetoplast statically in place near the basal body, from which it is physically separated by the mitochondrial envelope (Ogbadoyi et al. 2003). Electron microscopy images of Kinetoplast networks in vivo (Renger and Wolstenholme 1971, 1972; Lukeš et al. 2002; Ogbadoyi et al. 2003; Gluenz et al. 2007; Lai et al. 2008; Souza et al. 2009; Docampo et al. 2010) show the mitochondrion as an elongated organelle connected to a bulge containing the Kinetoplast via a narrow neck. This strongly suggests that the network experiences a geometric confinement within a specific region of the mitochondrion. The mitochondrial envelope can therefore be thought of as acting a physical constraint on the outer structure of the network, while it is likely that histone-like proteins, such as p16, p17 and p18, or "KAP proteins" encoded in genes KAP2, KAP3 and KAP4, act as chemical constraint on the inner structure (Xu and Ray 1993; Xu et al. 1996; Hines and Ray 1998; Silver 1986; Lukeš et al. 2001; Avliyakulov et al. 2004).

The concentration of DNA in the Kinetoplast has been found to be around 50 mg/ml (Shapiro and Englund 1995), similar to that measured in bacteria (20 mg/ml) but far smaller than the one inside the head of a T4 bacteriophage (800 mg/ml or more) (Kellenberger et al. 1986). This suggests that the mini-circles are overlapping but there is considerable space between DNA strands (Shapiro and Englund 1995). Previous findings showed that the loops are linked only once with their neighbours (Chen et al. 1995b). In addition, the valence of each ring, i.e. the number of linked neighbours, has been found to be around 3 in a pre-replicating network and approaching 6 at the end of duplication and before the network is split into the two daughter cells (Chen et al. 1995a, b; Liu et al. 2005). This has been thought of as a consequence of the fact that during replication the Kinetoplast doubles the number of mini-circles, while retaining roughly the same volume. Only after that the network has been fully duplicated, the cell increases its volume and separates into two progeny cells. In light of this, the density of mini-circles is expected to play a major role in the network topology (Diao et al. 2012). In addition, the mini-circles have been observed to be in a non-supercoiled state (Rauch et al. 1993). This has been conjectured to be a consequence of evolutionary pressure: because relaxed loops are more likely to form linked structures than supercoiled ones (Rybenkov et al. 1997), some of these organisms seems to have traded supercoiling in order to preserve the network linkedness (Rauch et al. 1993).

During replication, catenation between the loops represents a non-trivial topological problem, which is solved as follows: First Topoisomerase II disentangles one loop at a time from the network (Shlomai 1994; Liu et al. 2005), the loop then diffuses through a region called the Kinetoflagellar Zone (KFZ), where the duplication process begins. The latter is then always completed at the "anti-podal sites" (Drew and Englund 2001), specific regions that flank the Kinetoplast where a higher concentration of ligase, polymerase and topoisomerase enzymes has been observed (Melendy et al. 1988; Morris et al. 2001). Finally, the two progeny mini-circles are re-attached to the periphery of the network (Pérez-Morga and Englund 1993b). The Kinetoplast in *C. fasciculata* has been found to spin relatively to the anti-podal sites (Pérez-Morga and Englund 1993b; Liu et al. 2005), and the newly

duplicated mini-circle become re-attached with some lag-time with respect to the original mini-circle, most likely to allow specific enzymes to fill the gaps between DNA sequences (Shlomai 1994). This process has the side-effect to ensure an uniform distribution of the genetic material contained in the mini-circles throughout the network (Liu et al. 2005). Both mini-circles are catenated to the network in a nicked state. The nicks along one of the two DNA strands have been conjectured to act as "bookkeepers" (Englund 1978, 1979; Kitchin et al. 1984). Thanks to this mechanism, it is in fact very likely that mini-circles can be safely duplicated only once during the replication of the network (Shlomai and Linial 1986).

During this process, the physical size of the network has been observed to remain constant, while the number of mini-circles contained and the valence of each mini-circle to double (Chen et al. 1995a). At the end of duplication, around the stage of cell division, the volume of the Kinetoplast doubles and the valence of the network is brought back to 3, thanks to topoisomerase enzymes, the nicks and gaps in the mini-circles are repaired (Englund 1978) and two copies of the network are produced by slicing the network through the middle, once again, most likely mediated by topo II (Pérez-Morga and Englund 1993b; Liu et al. 2005).

The organisation and duplication of the KDNA has the unique feature that it must undergo complex topological changes in a precise and consistent order. This could not be done without the action of topoisomerases, which is crucial for this machinery to work correctly, not only for decatenation of mini-circles from the network, but also for the re-attachment at the end of duplication (Shlomai and Zadok 1983; Chen et al. 1995b). RNA interference (RNAi) experiments showed that by suppressing the production of topoisomerase enzymes, the Kinetoplast is unable to form and most of the mini-circles remain in a free (unlinked) state (Wang et al. 2000). As a consequence, the progeny cells are typically malfunctioning and likely to die. Type II topoisomerase is well-known for playing a crucial role in simplifying knots and catenanes which occur in DNA (White et al. 1987); On the other hand, it has also been shown that the same enzyme is also capable of creating complex, linked structures (Hsieh and Brutlag 1980; Kreuzer and Cozzarelli 1980; Brown and Cozzarelli 1981), and its action to be tuned by a number of factors, such as DNA concentration or condensation mediated by the presence of polyamines, e.g. spermidine (Krasnow and Cozzarelli 1982).

All this strongly suggests that, on one hand, the KDNA is a complicated biological structure regulated by many subtle biological processes. On the other hand, seen from a purely physical perspective, the KDNA is represented by a state in which loops are linked to each other to form a connected component that spans the entire genetic repertoire. In particular, the presence of topoisomerase enzymes regulates the ability of loops to link to, or unlink from, one another thereby tuning the ability of the network to form.

In this chapter I will describe a effective 1D model for the replication of the Kinetoplast DNA. One of the most puzzling and interesting aspects of its replication is that it generates the same network structure at each replication cycle with very few, or none, mistakes (Jensen and Englund 2012). The cell viability requires a key

feature: the genetic information contained in the Kinetoplast has to be passed on to the progeny. This means that either quantity and quality of the genetic material have to be conserved.

In this chapter I have shown that it can be argued that the percolating network structure of the Kinetoplast could have been evolved in order to meet the need to conserve the quantity of genetic material. The percolating nature of the network can in fact be though of as a natural mechanism through which these organisms ensure that most of the mini-circles belong to a unique component and therefore are not free to diffuse away from the Kinetoplast. On the other hand, the linkedness of the network might not be beneficial to the cell during replication as in fact it could hinder the duplication process. How the Kinetoplast is duplicated and divided into the progeny is, in fact, far from being well understood (Chen et al. 1995a; Jensen and Englund 2012), and this is mainly due to its complexity. In spite of this, from a bio-physical perspective, the duplication of the Kinetoplast can be thought of as made of three major stages which correspond to three topological changes in the network structure. As a consequence, in what follows I will introduce a minimal analytical model that focuses on these three steps and attempt to get some insight into this complicated issue by aggressively simplify the problem, in the same spirit of this chapter.

5.1 Modelling the Network Replication

As mentioned before, the replication of the Kinetoplast involves three major stages:

(*i*) the removal of mini-circles from the network via the action of Topoisomerase II (Shlomai 1994),

(*ii*) the free diffusion of the un-linked mini-circles away from the Kinetoplast core and toward the anti-podal regions where they are duplicated (Jensen and Englund 2012)

(*iii*) the re-attachment of the progeny mini-circles to the periphery of the network (Pérez-Morga and Englund 1993b).

These three conditions are necessary for the network replication and the organism viability. These stages can be translated in three pseudo-equations as follows:

(*i*) Each mini-circle is unlinked from its linked neighbours at a rate that is proportional to the *local* concentration of Topoisomerase II (ϕ_T) (see Fig. 5.1a):

$$(N)Linked \xrightarrow{R\phi_T} Unlinked + (N-1)Linked. \tag{5.1}$$

(ii) While diffusing, each mini-circle begins its duplication thanks to polymerase enzymes present in the kinetoflagellar zone around the Kinetoplast (Morris et al. 2001; Drew and Englund 2001). This process occurs at a rate α which is regulated by the speed at which polymerases duplicate the genetic sequence. Mini-circles can only be transcribed at this stage alongside to their duplication, i.e. while their are unlinked from the network. This is supported by the fact that transcription enzymes cannot

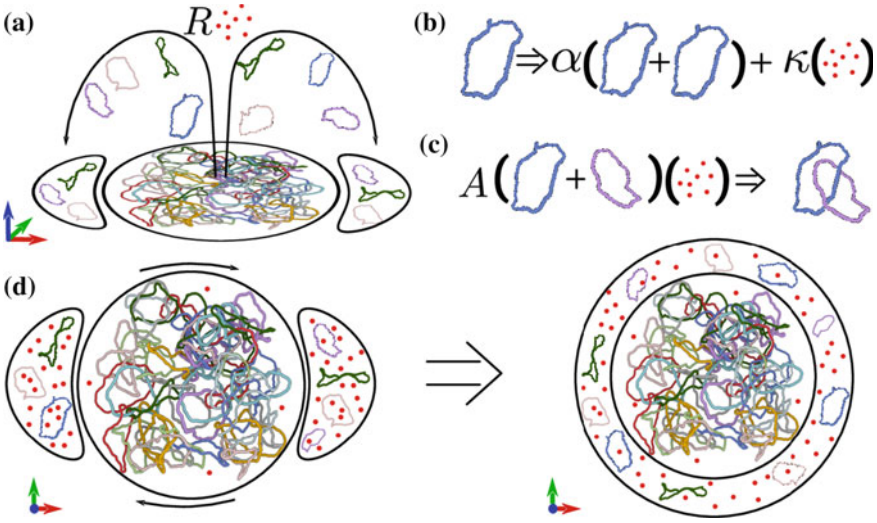

Fig. 5.1 **a** Graphical representation of the reaction in Eq. (5.1). Topoisomerase (*red dots*) unlinks mini-circles (*coloured loops*) from the central connected network. **b** Graphical representation of the reaction in Eq. (5.2). Each mini-circle duplicates at rate α and indirectly triggers the downstream production of Topoisomerase (*red dots*) at rate κ. **c** Graphical representation of the reaction in Eq. (5.3). Each mini-circle forms a catenane with another mini-circle (either free or linked) at a rate proportional to the local concentration of Topoisomerase. **d** The model is further simplified by substituting the two anti-podal sites where re-attachment occurs with a shell; this can be thought of as an average over the relative position of the (rotating) Kinetoplast core with respect to the anti-podal sites within the replication time-window

easily enter the depths of the compact network structure, and even in the case they would, the entanglement caused by the density of material would strongly suppress any transcriptional activity. In other words, I assume that the genetic information contained in the mini-circles is more easily and readily accessible at the stage when they are free from the network.

Relying on the well established fact that mini-circles contain RNA-editing genes (Jensen and Englund 2012), I further assume that mini-circles transcription triggers, among other things, the downstream production of topoisomerase II at a rate κ via transcription and RNA-editing factors encoded in the mini-circles genetic material (see Fig. 5.1b). This assumption is supported by RNA interference (RNAi) experiments (Wang et al. 2000), in which the expression of genes encoding for topoisomerase II and mitochondrial mRNA synthesis are inhibited, causing loss of Kinetoplast and cell death. In pseudo-equations this stage reads:

$$\begin{aligned} &\mathit{Unlinked} \xrightarrow{\alpha} \mathit{Unlinked} + \mathit{Unlinked} \\ &\text{and} \\ &\mathit{Unlinked} \xrightarrow{\kappa} \mathit{Topoisomerase}. \end{aligned} \tag{5.2}$$

(iii) Once the progeny mini-circles diffuse to the anti-podal sites, they are re-ligated by gap-filling enzymes (Pérez-Morga and Englund 1993a) and re-attached at the periphery of the network. The re-attachment rate can be thought again proportional to the *local* concentration of topo II (ϕ_T) (Wang and Englund 2001) (see Fig. 5.1c):

$$\textit{Unlinked} + \textit{Unlinked} \xrightarrow{A\phi_T} \textit{Linked}$$

or

$$\textit{Unlinked} + \textit{Linked} \xrightarrow{A\phi_T} \textit{Linked} \tag{5.3}$$

where the pseudo-equations represent the cases in which the free mini-circle is re-linked to an other un-linked or an already linked mini-circle, respectively. Finally, the rates R and A are key parameters in this model and represent the rates of removal (R) and re-attachment (A) of mini-circles from and to the network.

A final comment on the model is in order: During the replicating phase of *C. fasciculata*, the Kinetoplast core has been observed to rotate relatively to the anti-podal sites where re-attachment occurs (Pérez-Morga and Englund 1993b). In light of this, and of the inherent rotational symmetry of the final replicated network (Pérez-Morga and Englund 1993b; Jensen and Englund 2012), one could argue that effectively, the two anti-podal complexes can be replaced with a shell that surrounds the Kinetoplast core (see Fig. 5.1d). This substitution is equivalent to perform a time-average of the relative position of the complexes with respect to the core over the whole replicating phase. The entire system can be visualised as a rotationally symmetric 2-dimensional disk divided into a core $r \leq R_k$ filled by the Kinetoplast at the beginning of the replication ($t = 0$) and a shell $R_k < r < R_{max}$ (initially empty of genetic material) which plays the role of region where re-attachment occurs.

Modelling Topological Changes

The three stages are therefore related to three topological operations: (*i*) un-linking of mini-circles from the network, (*ii*) duplication of single mini-circles and (*iii*) linking of the progeny mini-circles back to the network. These are captured by the pseudo-equations (5.1)–(5.3).

One can now argue that the system could be also described in terms of the relative density of linked $\rho_l(\boldsymbol{x}, t)$ and unlinked $\rho_u(\boldsymbol{x}, t)$ mini-circles and of topoisomerase II enzyme $\phi_T(\boldsymbol{x}, t)$. At the beginning of replication, the (normalised) density of linked mini-circles is 1 within the Kinetoplast core ($\rho_l(\boldsymbol{x}, 0) = 1$ for $|\boldsymbol{x}| \leq R_k$ and 0 otherwise), and there are no unlinked mini-circles ($\rho_u(\boldsymbol{x}, 0) = 0 \ \forall \ \boldsymbol{x}$). During the replicating phase, the total number of mini-circles grows and at the end of the replication the total number of mini-circles is twice the initial number, i.e. $\rho_l^* + \rho_u^* = 2$, where ρ_l^* and ρ_u^* are the final (uniform) values of ρ_l and ρ_u, respectively.

By describing the system in terms of these local densities, or "fields", one can translate Eqs. (5.1)–(5.3) into three coupled equations:

$$\frac{d\rho_l}{dt} = -R\rho_l\phi_T + A\phi_T\rho_u\,(\rho_l + \rho_u) + D_l\nabla^2\rho_l \tag{5.4}$$

$$\frac{d\rho_u}{dt} = +R\rho_l\phi_T - A\phi_T\rho_u\,(\rho_l + \rho_u) + D_u\nabla^2\rho_u + \alpha\rho_u\,[2 - (\rho_u + \rho_l)] \tag{5.5}$$

$$\frac{d\phi_T}{dt} = +\kappa\rho_u - \frac{\phi_T}{\tau} + D_T\nabla^2\phi_T, \tag{5.6}$$

where the first and second terms in Eqs. (5.4)–(5.6) capture the reactions represented by Eqs. (5.1)–(5.3) and the last term in Eq. (5.5) ensures that the un-linked mini-circles duplicate at rate α until the sum $\rho_u + \rho_l$ reaches 2, at which point the growth is stopped, while the third terms describe the usual diffusion of mini-circles and topo II with their respective diffusion constants.

The value of α at which mini-circles are duplicated can be estimated by noting that polymerase replicates DNA at a speed between 20 bp/s (in bacteria) and 500 bp/s (in eukaryotes) (Dignam et al. 1983; Wickiser et al. 2005; Schwartz and Quake 2009). Therefore the typical duplication time results to be of about $\alpha^{-1} \simeq 2000\,\text{bp}/(100\,\text{bp/s}) = 20\,\text{s}$.

In addition, the rate of (indirect) production of topo II is set as $\kappa = \alpha = 0.05\,\text{s}^{-1}$. This choice is justified by the fact that the transcription of mini-circles is expected to take a time comparable to their duplication. Finally, the decay time τ associated to topoisomerase enzymes can be set to $\tau = 600\,\text{s}$, being this its typical half-life in bacteria (Taniguchi et al. 2010).

Since unlinked mini-circles are freed from the network, they are expected to diffuse away from the Kinetoplast core. Previous studies have reported that mini-circle duplication begins in the Kinetoflagellar Zone (KFZ), a dense matrix of filaments which attaches the Kinetoplast to the flagellar basal body (Ogbadoyi et al. 2003), surrounding the Kinetoplast and filled with Polymerase enzymes, and it is always completed inside the anti-podal regions, where a high concentration of gap-filling enzymes has been found (Jensen and Englund 2012). The diffusion coefficients, D_l, D_u and D_T regulate the diffusive behaviour of, linked and unlinked mini-circles and of topo II enzymes, respectively.

In other words, the values of all the parameters (a part from A and R) in Eqs. (5.4)–(5.6) can be directly informed by biological evidence. The rate of attachment A and of removal R are therefore the only true free parameters of this model and possibly the most difficult to study experimentally.

5.2 The Stable Point Is a Marginally Linked Network

Equations (5.4)–(5.6) are most readily studied numerically, also thanks to the rotational symmetry of the problem. Here I will instead study these equations analytically. Equations (5.4)–(5.6) correctly describe an unstable fixed point of the system when topo II is depleted from the system. In other words, the state

$$S(t=0) = \begin{cases} \rho_l(\boldsymbol{x}, 0) = 1 \; \forall \, \boldsymbol{x} \text{ s.t. } |\boldsymbol{x}| \leq R_k \\ \rho_u(\boldsymbol{x}, 0) = 0, \, \phi_T(\boldsymbol{x}, 0) = 0 \; \forall \, \boldsymbol{x} \end{cases} \tag{5.7}$$

satisfies Eqs. (5.4)–(5.6) and is a fixed point of the system. I would like to stress that this state can be truly thought of as the biological initial state of the Kinetoplast as the replication cannot take place without the presence of a topological enzyme in solution. As soon as some molecules of topo II are added to the system,[1] Eqs. (5.4)–(5.6) quickly drive the system away from this state and toward full replication, i.e. $\rho_u + \rho_l = 2$, which is the true stable fixed point of the system.

This can be easily found by setting the left hand side of Eqs. (5.4)–(5.6) to zero and by assuming that, thanks to diffusion, at the end of the replication time T_R the densities of linked and unlinked mini-circles and of topo II are uniform across the Kinetoplast, i.e. $\rho_{u,l}(\boldsymbol{x}, T_R) = \rho_{u,l}(T_R)$ and $\phi_T(\boldsymbol{x}, T_R) = \phi_T(T_R)$, one obtains

$$\rho_l^* = \frac{4}{R/A + 2} = 2 - \rho_u^*. \tag{5.8}$$

This shows that the final state of replication $S(t = T_R)$ corresponds to a system in which $\rho_u(\tau_R) + \rho_l(\tau_R) = \rho_u^* + \rho_l^* = 2$ and that the relative abundance of linked and un-linked mini-circles

$$\frac{\rho_u^*}{\rho_l^*} = \frac{1}{2}\frac{R}{A} \tag{5.9}$$

is directly dependent on the ratio $R/A \equiv \beta$. In the case $\beta \simeq 0$ one can expand the stable fixed point in Eq. (5.8) and obtain

$$\rho_l^* \sim 2 - \beta + \mathcal{O}(\beta^2) \tag{5.10}$$

and

$$\rho_u^* \sim \beta + \mathcal{O}(\beta^2). \tag{5.11}$$

In this case the final state corresponds to a system in which a small fraction ρ_u^* of mini-circles is un-linked from the network and almost all the other mini-circles in the system belong to the Kinetoplast network.

Because the aim is to generate a fully linked network, one can naïvely imagine to simply set $R = 0$ so that $\beta = 0$; by doing so one instead forbids the network replication, as the initial removal is of paramount importance for the mini-circles to fully duplicate in the anti-podal complexes. The other option to minimise β is to have a large attachment rate, i.e. the time taken by topo II to catalyse a single-strand passage τ_{cross} has to be short. On the other hand, τ_{cross} should be itself related to the

[1] This could be argued to be too sensitive to the presence of topo II, and some threshold could be added to regulate the sensitivity of $S(t = 0)$ to the value ϕ_T. In order to keep things simple I decided to neglect this correction.

inverse of the activity (or the "turnover number") k_{cat} of topo II (Duplantier et al. 1995), which has been studied in the past by measuring the ATPase activity of DNA gyrase in presence of DNA substrates (Maxwell and Gellert 1984). In light of this, it is possible to relate the attachment rate A to the experimentally measured turnover (ATPase activity) number as

$$A \sim k_{\text{cat}} \sim 1s^{-1}, \tag{5.12}$$

which provides a bound on the values assumed by this parameter. In other words, the value of the attachment rate A cannot be arbitrarily changed, but depends on the bio-chemical structure of topo II and its efficiency. In addition, it has to be stressed that the removal of a mini-circle from the network requires, at least, three strand-crossing operations in order to free the ring from the average number of neighbours (which is three, see Ref. (Chen et al. 1995b) and this chapter). This implies that R is necessarily smaller A, and taking into account the condition $R > 0$, one arrives at

$$0 < \beta < 1. \tag{5.13}$$

The expression in Eq. (5.13) is a strong statement on the topology of the network. In fact, any state in which $R/A \equiv \beta$ is strictly greater than zero corresponds to a marginally linked network, i.e. a network that does not include all the mini-circles in the system. In particular, Eqs. (5.8) and (5.13) imply $2/3 < \rho_l^*/(\rho_l^* + \rho_u^*) < 1$ and $0 < \rho_u^*/(\rho_l^* + \rho_u^*) < 1/3$ or (using Eq. (5.9))

$$0 < \rho_u^*/\rho_l^* < 1/2. \tag{5.14}$$

This means that in any case (even in the very unlikely case that $R = A$) the final fraction of mini-circles linked to the Kinetoplast core is the largest majority, i.e. the Kinetoplast will always form a unique spanning component. This is rather encouraging as this implies that the Kinetoplast will never fail to form a percolating core and it is therefore, in this respect, foolproof. Obviously, the best result is achieved at small β, for which the final state is the closest to a fully linked network. On the other hand, Eqs. (5.12) and (5.13) imply that β can be tuned only by acting on R in the range $0 < R < A$.

At this stage it is also worth pointing out that acting on R is likely to not only affect the final topology of the network but also the time required to replicate the network in full (T_R). By looking at Eqs. (5.5) and (5.6) one can in fact notice that unlinked mini-circles are produced at rate R from the linked structure proportionally to the local concentration of topo II, ϕ_T, which is itself (indirectly) produced by the presence of unlinked mini-circles. In other words, decreasing R is likely to have a double negative feedback effect on the network replication. It is therefore likely that T_R is strongly dependent on β, and in particular, small removal rates R might lead to very long replication times T_R.

5.3 Redundancy in the Genetic Material Allows for Faster Replication Times

Being the evolutionary pressure very high for these organisms, the replication time T_R is a crucial parameter for their survival. Having a long replication time is in fact far from being an evolutionary advantage. On the other hand, their survival is also strongly related to their ability to pass on their vital genetic information, i.e. their ability to preserve the genetic material, which is itself strongly dependent on the linkedness of the network (this chapter). In light of this it is therefore tempting to speculate that the value of β had been tuned by evolution to balance the need of a well-linked network, i.e. $\rho_l^* \simeq 2$, and that of a reasonably short time to complete replication.

The competition between these two effects can be summarised in one equation that describes the growth of a population of N organisms as a function of two parameters: β and γ. The latter can be interpreted as the critical lethal fraction of mini-circles unlinked from the Kinetoplast at the end of replication, beyond which the progeny cells are no longer viable. The equation reads:

$$\frac{1}{N}\frac{dN}{dt} = T_R^{-1}(\beta)\left[1 - \gamma\left(2 - \rho_l^*(\beta)\right)\right] = f(\beta). \tag{5.15}$$

Equation (5.15) simply states that a population of N organisms grows at a rate proportional to the speed of replication,[2] i.e. proportionally to $T_r^{-1}(\beta)$ and to the likeliness of possessing a number $\rho_u^* = 2 - \rho_l^*$ of un-linked mini-circles smaller the critical lethal fraction γ. In other words, if β and γ are such that

$$\gamma\rho_u^*(\beta) = \gamma(2 - \rho_l^*(\beta)) \geq 1, \tag{5.16}$$

the population cannot grow, as the Kinetoplasts generated are not retaining enough genetic material to ensure the viability of the progeny.

All this strongly relies on the crucial assumption that mini-circles which are not linked to the Kinetoplast at the end of the replication are most likely lost during cell division and are, therefore, not passed onto the progeny cells. This means that γ sets a necessary fraction of mini-circles that need to be linked below which not enough genetic material is retained for the progeny to be viable.

Since f measures the total growth rate of a population of Kinetoplasts, it gives a measure of the species evolutionary fitness. Maximising such fitness means finding the most "fit" pair $\{\beta, \gamma\}$. By setting $df/d\beta = 0$, one finds:

$$\frac{df}{d\beta} = -\frac{1}{T_R^2(\beta)}\frac{dT_R(\beta)}{d\beta}\left(1 - \gamma\rho_u^*(\beta)\right) - \frac{1}{T_R(\beta)}\gamma\frac{d\rho_u^*}{d\beta} = 0. \tag{5.17}$$

[2] In a time T, N_0 initial cells duplicate $T/T_R = m$ times, i.e. $N_m = N_0 \exp(m \log(2))$.

As I showed before, in the limit $\beta \ll 1$ one can approximate $\rho_u^* \sim \beta + \mathcal{O}(\beta^2)$, which gives:

$$-\frac{1}{T_R^2(\beta)}\frac{dT_R(\beta)}{d\beta}(1-\gamma\beta) - \frac{1}{T_R(\beta)}\gamma\left(1-\frac{\beta}{4}\right) + \mathcal{O}(\beta^2) = 0. \tag{5.18}$$

By assuming that in the range $0 < \beta < 1$ the replication time $T_R(\beta)$ cannot be zero or infinitely large, one can write:

$$\frac{1}{T_R(\beta)}\frac{dT_R(\beta)}{d\beta} = -\gamma\frac{1-\beta/4}{1-\gamma\beta} \tag{5.19}$$

which, once again approximating for small β, leads to

$$\frac{d}{d\beta}\log T_R(\beta) \simeq -\gamma\left[1+\beta\left(\gamma-1/4\right)\right]. \tag{5.20}$$

This implies that in the lowest approximation, the functional form of the replication time $T_R(\beta)$ can be estimated as

$$T_R(\beta) \sim e^{-\gamma\beta+\mathcal{O}(\beta^2)}. \tag{5.21}$$

Although this functional form of the replication time should be, in principle, be recovered from Eqs. (5.4)–(5.6), it is rather appealing (or fortunate) that it is obtained from maximising the fitness function in Eq. (5.15). On the other hand, this restricts the validity of Eq. (5.21) to the case in which the fitness is maximum, i.e. a precise combination of γ and β, rather than to the whole space and also to the case in which β is small. In light of this, one can assume that T_R takes the form in Eq. (5.21) and go back to Eq. (5.17) to write

$$\gamma e^{\gamma\beta}\left(\frac{\beta+2-2\gamma\beta}{\beta+2}\right) - \gamma e^{\gamma\beta}\frac{4}{(\beta+2)^2} = 0 \tag{5.22}$$

and finally obtain

$$\gamma = \frac{1}{2}\frac{\beta+4}{\beta+2}. \tag{5.23}$$

In Fig. 5.2 I show the curve given by Eq. (5.23) which identifies the maximum fitness line in the space (γ, β). As mentioned before, γ describes the critical lethal fraction of mini-circles unlinked from the Kinetoplast at the end of the replication, i.e. $\rho_u^* = 2 - \rho_l^*$. Because each mini-circle carries genetic material, the parameter γ can also be interpreted as "redundancy" in the genetic material carried by the mini-circles. It is worth noting that in the limit $\gamma \to 1$, the system requires $\beta \to 0$ in order to satisfy Eq. (5.23). This means that every mini-circle needs to be linked to the network at the end of the replication, i.e. every mini-circle is crucial for the

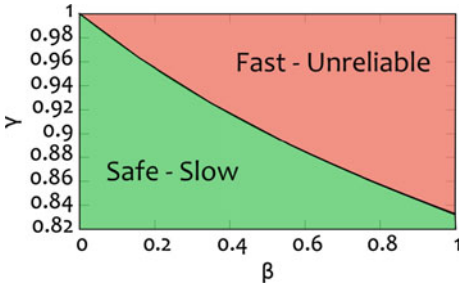

Fig. 5.2 Relation between the parameters γ and $\beta = R/A$ as obtained in Eq. (5.23). For a given value of γ, Eq. (5.23) gives a threshold for β^* above which the replicated network (although built faster) is too poorly linked to retain the necessary fraction of genetic material γ, and the progeny is therefore not viable. On the other hand below β^* the replicated network is safely generated as the linkedness of the network ensures that enough genetic material is passed on, although T_R^{-1} is much slower. The balance is given by the *thick line* for which the replication rate is the fastest given that a fraction γ of genetic material needs to be linked to the Kinetoplast and it identifies, therefore, the "maximum fitness" line

survival of the organism (see Eq. (5.15)). This can be interpreted with the fact that, in this case, each mini-circle carries unique genetic information, and any loss of mini-circles would cause the reduction of evolutionary fitness. In other words, setting the parameter $\gamma = 1$, signifies that there is no redundancy in the genetic material carried by the mini-circles, and each one of them has to be passed on to the progeny in order for the organism to survive.

On the other hand, the mini-circles in the Kinetoplast have been observed to possess a slightly redundant genetic information, meaning that they encode largely heterogeneous genetic material but display some highly conserved genes (Jensen and Englund 2012). This is in agreement with Eq. (5.23) and Fig. 5.2 and, in particular, sets a rough estimation of γ below unity. This implies that β is not so close to zero and therefore the final network is most likely to be marginally linked and the replication process to be faster than it would be if γ was set to one.

All this also implies that the initial assumption that $\beta \sim 0$ is not crude at all, in particular because (i) the Kinetoplast is notably well linked, i.e. $\rho_u^* \simeq 0$ and $\rho_l^* \simeq 2$ and (ii) the redundancy of the genetic material is strictly greater than zero, although very small, i.e. $\gamma \simeq 1$.

It is important to bear in mind that all this is dependent on the assumption that any mini-circle which is not linked to the Kinetoplast at the end of the replication is lost during the separation into progeny cells. While this assumption might at first sound too crude, it is worth stressing that it is supported by experimental evidence, which assessed the viability of the progeny cells when topo II is inhibited from the Kinetoplast, i.e. κ in Eq. (5.6) set to zero. This means that the Kinetoplasts were not able to topologically regulate their formation, and as a consequence, the resulting networks appeared fragmented, not forming a spanning component and ultimately led to progeny cells death (Wang et al. 2000; Wang and Englund 2001). All this

implies that the formation of a nearly perfect spanning component is crucial for the organism survival and this could have been evolutionarily adapted, by introducing some genetic redundancy, to allow a faster replication.

5.4 Conclusions

In conclusion, in this chapter I introduced an analytical model for the replication of the Kinetoplast DNA. Although this model aggressively simplifies this complex biological system, some of its crucial assumptions are supported by experimental evidence and a careful analysis of the results can give some insight into the Kinetoplast unique structure.

In particular, the replication of this biological network can be described as a self-regulated process, requiring only the input of a small initial level of topoisomerase to fully replicate the Kinetoplast. The final topological state of the network is found to be crucially controlled by the ratio between the removal rate R and the re-linking rate A, i.e. $\beta = R/A$, with the degree of linkage decreasing with increasing β. I also showed that taking into account precision and speed of the replication, it is possible to explicitly write a fitness function whose maximisation leads to a maximum fitness line in the parameter space (γ, β), γ being a "redundancy factor" or the critical fraction of unlinked mini-circles at the end of the replication. This finally allowed me to argue that it may be possible that the Kinetoplast is poised at a critical point where the redundancy of its genetic material allows for a faster replication without compromising its fitness, although this intriguing conjecture ought to be supported by future experiments. It is in fact my hope that further biological experiments on this genome will shed new light onto its complicated and beautiful organisation.

From the work I presented here and somewhere else (Michieletto et al. 2015) I drew a key message: the available experimental findings on the Kinetoplast can be understood in terms of simpler systems, boiled down to few crucial elements.

First of all, the mini-rings form linked structures by passing through one another and a good quantitative agreement with the available experimental observations can be retrieved simply by assuming that the network is formed by a random strand-crossings and that its level of linkage can be regulated by the concentration of mini-circles within the mitochondrion. The network is found to be neither too poorly, nor too heavily, connected, but near what is seems to be the percolation threshold (Michieletto et al. 2015). Being close to the percolation transition may well provide an evolutionary advantage for the Kinetoplast DNA network, as this structure may be favoured over a more heavily connected network, as it facilitates the decatenation during replication, but at the same time ensures that mini-circles are not released by mistake, conferring robustness and increasing the conservation of genetic material across generations. In other words, too heavily linked network would be very good at preserving the genetic material, but would severely slow down the replication stage of the network, where the Kinetoplast has to be taken apart. On

the other hand, networks that are too poorly linked might result in the loss of genetic material during cell mitosis and therefore put the cell viability at risk.

I have also shown that by considering a simple mathematical model for the network replication, one is able to argue two crucial aspects of the Kinetoplast: first, that the network replicates efficiently if it is marginally linked, which supports the findings reported in Ref. (Michieletto et al. 2015) which showed that the Kinetoplast is neither too poorly nor too heavily linked, and second that the genetic composition of the mini-circles may be tuned in order to display some redundancy with the goal of speeding up replication without losing fitness or viability.

A final remark is in order: these organisms have had a very unusual evolutionary path. They show a uniquely structured mitochondrial genome, very distant from anything else in Nature. On the other hand, they seem to have found an (unstable) equilibrium, since small changes in the Kinetoplast structure usually lead to the evolution of novel species which rapidly diverge from their common ancestor (Lai et al. 2008) (in some cases, the network structure seem to have been traded for super-coiling, e.g. in the Pan-KDNA structure of *Cryptobia helicis* (Lukeš et al. 2002)). I here speculate that this equilibrium must have been reached via successive "attempts", i.e. mutations, which slightly modified the topological structure until a balance between several key elements, such as speed of replication, accuracy and resistance against mistakes had been reached, leading to the to-date KDNA structure.

Finally, I would like to stress again that the survival of these organisms depends on the regulation of the Kinetoplast topology; Nonetheless, their genome is consistently duplicated with very few, or no, mistakes at every duplication cycle. Such reliable topology regulation is far from being trivial to achieve. During the '70s de Gennes advanced the idea of an "Olympic gel" (de Gennes 1979) and 40 years later, the scientific community has not made much progress toward its realisation. Perhaps the answer lies within these organisms, as they have made an Olympic gel out of their own mitochondrial genome (it is fair although to say that they had some millions of years to try and make it!).

A better understanding of how they manage this incredible feat would surely improve the current understanding and ability to realise similar topological materials, perhaps using techniques drawn from modern synthetic biology.

References

Avliyakulov, N.K., Lukes, J., Ray, D.S.: Mitochondrial histone-like DNA-binding proteins are essential for normal cell growth and mitochondrial function in crithidia fasciculata. Eukaryot. Cell **3**(2), 518 (2004)

Brown, P.O., Cozzarelli, N.R.: Catenation and knotting of duplex DNA by type 1 topoisomerases: a mechanistic parallel with type 2 topoisomerases. Proc. Natl. Acad. Sci. USA **78**(2), 843 (1981)

Chen, J., Englund, P.T., Cozzarelli, N.R.: Changes in network topology during the replication of kinetoplast DNA. EMBO J. **14**(24), 6339 (1995a)

Chen, J., Rauch, C.A., White, J.H., Englund, P.T., Cozzarelli, N.R.: The topology of the kinetoplast DNA network. Cell **80**(1), 61 (1995b)

de Gennes, P.G.: Scaling Concepts in Polymer Physics. Cornell University Press, Ithaca (1979)
de Souza, W., Attias, M., Rodrigues, J.C.F.: Particularities of mitochondrial structure in parasitic protists (Apicomplexa and Kinetoplastida). Int. J. Biochem. Cell. B. **41**(10), 2069 (2009)
Diao, Y., Hinson, K., Kaplan, R., Vazquez, M., Arsuaga, J.: The effects of density on the topological structure of the mitochondrial DNA from trypanosomes. J. Math. Biol. **64**, 1087 (2012)
Dignam, J., Lebovitz, R., Roeder, R.: Accurate transcription initiation by RNA polymerase II in a soluble extract from isolated mammalian nuclei. Nucleic Acids Res. **1**(5), 1475 (1983)
Docampo, R., Ulrich, P., Moreno, S.N.J.: Evolution of acidocalcisomes and their role in polyphosphate storage and osmoregulation in eukaryotic microbes. Phil. Trans. R. Soc. B **365**(February), 775 (2010)
Drew, M.E., Englund, P.T.: Intramitochondrial location and dynamics of Crithidia fasciculata kinetoplast minicircle replication intermediates. J. Cell Biol. **153**(4), 735 (2001)
Duplantier, B., Jannink, G., Sikorav, J.L.: Anaphase chromatid motion: involvement of type II DNA topoisomerases. Biophys. J. **69**(4), 1596 (1995)
Englund, P.: The replication of kinetoplast DNA networks in Crithidia fasciculata. Cell **14**, 157 (1978)
Englund, P.: Free minicircles of kinetoplast DNA in Crithidia fasciculata. J. Biol. Chem. **254**, 4895–4900 (1979)
Gluenz, E., Shaw, M.K., Gull, K.: Structural asymmetry and discrete nucleic acid subdomains in the Trypanosoma brucei kinetoplast. Mol. Microbiol. **64**, 1529 (2007)
Hines, J.C., Ray, D.S.: The Crithidia fasciculata KAP 1 gene encodes a highly basic protein associated with kinetoplast DNA 1. Mol. Biochem. Parasit. **94**, 41 (1998)
Hsieh, T., Brutlag, D.: ATP-dependent DNA topoisomerase from D. melanogaster reversibly catenates duplex DNA rings. Cell **21**, 115 (1980)
Jensen, R.E., Englund, P.T.: Network news: the replication of kinetoplast DNA. Annu. Rev. Microbiol. **66**, 473 (2012)
Kellenberger, E., Carlemalm, E., Sechaud, J., Ryter, A., Haller, G.: Considerations on the condensation and the degree of compactness in non-eukaryotic dna-containing plasmas. In: Gualerzi, C.O., Pon, C.L. (eds.) Bacterial Chromatin, pp. 11–25. Springer, Berlin (1986)
Kitchin, P., Klein, V., Fein, B., Englund, P.: Gapped Minicircles. A novel replication intermediate of kinetoplast DNA. J. Biol. Chem. **259**(24), 15532 (1984)
Krasnow, M., Cozzarelli, N.: Catenation of DNA rings by topoisomerases. J. Biol. Chem. **257**, 2687 (1982)
Kreuzer, K., Cozzarelli, N.: Formation and resolution of DNA catenanes by DNA gyrase. Cell **20**(May), 245 (1980)
Lai, D.-H., Hashimi, H., Lun, Z.-R., Ayala, F.J., Lukes, J.: Adaptations of Trypanosoma brucei to gradual loss of kinetoplast DNA : Trypanosoma equiperdum and Trypanosoma evansi are petite mutants of T. brucei. Proc. Natl. Acad. Sci. USA **105**(6), 1999 (2008)
Liu, B., Liu, Y., Motyka, S.A., Agbo, E.E.C., Englund, P.T.: Fellowship of the rings: the replication of kinetoplast DNA. Trends Parasitol. **21**(8), 363 (2005)
Lukes, J., Hashimi, H., Zíková, A.: Unexplained complexity of the mitochondrial genome and transcriptome in kinetoplastid flagellates. Curr. Genet. **48**(5), 277 (2005)
Lukeš, J., Hines, J., Evans, C., Avliyakulov, N.K., Prabhu, V.P., Chen, J., Ray, D.S.: Disruption of the Crithidia fasciculata KAP1 gene results in structural rearrangement of the kinetoplast disc. Mol. Biochem. Parasitol. **117**, 179 (2001)
Lukeš, J., Guilbride, D., Votýpka, J.: Kinetoplast DNA network: evolution of an improbable structure. Eukaryot. Cell **1**(4), 495 (2002)
Maxwell, A., Gellert, M.: The DNA dependence of the ATPase activity of DNA gyrase. J. Biol. Chem. **259**(23), 14472 (1984)
Melendy, T., Sheline, C., Ray, D.S.: Localization of a type II DNA topoisomerase to two sites at the periphery of the kinetoplast DNA of Crithidia fasciculata. Cell **55**, 1083 (1988)
Michieletto, D., Marenduzzo, D., Orlandini, E.: Is the kinetoplast DNA a percolating network of linked rings at its critical point? Phys. Biol. **12**, 036001 (2015)

Morris, J.C., Drew, M.E., Klingbeil, M.M., Motyka, S.A., Saxowsky, T.T., Wang, Z., Englund, P.T.: Replication of kinetoplast DNA: an update for the new millennium. Int. J. Parasitol. **31**(5–6), 453 (2001)

Ogbadoyi, E., Robinson, D., Gull, K.: A high-order trans-membrane structural linkage is responsible for mitochondrial genome positioning and segregation by flagellar basal bodies in trypanosomes. Mol. Biol. Cell **14**(May), 1769 (2003)

Pérez-Morga, D., Englund, P.: The structure of replicating kinetoplast DNA network. J. Cell. Biol. **123**(5), 4 (1993a)

Pérez-Morga, D.L., Englund, P.T.: The attachment of minicircles to kinetoplast DNA networks during replication. Cell **74**(4), 703 (1993b)

Rauch, C.A., Pérez-Morga, D., Cozzarelli, N.R., Englund, P.T.: The absence of supercoiling in kinetoplast DNA minicircles. EMBO J. **12**(2), 403 (1993)

Renger, H., Wolstenholme, D.: Kinetoplast and other satellite DNAs of kinetoplastic and dyskinetoplastic strains of Trypanosoma. J. Cell. Biol. **50**, 533 (1971)

Renger, H., Wolstenholme, D.: The form and structure of kinetoplast DNA of Crithidia. J. Cell. Biol. **5**, 346 (1972)

Rybenkov, V.V., Vologodskii, A.V., Cozzarelli, N.R.: The effect of ionic conditions on the conformations of supercoiled DNA. II. Equilibrium catenation. J. Mol. Biol. **267**(2), 312 (1997)

Schwartz, J.J., Quake, S.R.: Single molecule measurement of the 'speed limit' of DNA polymerase. Proc. Natl. Acad. Sci. USA **107**(3), 1254 (2009)

Shapiro, T., Englund, P.: The structure and replication of kinetoplast DNA. Annu. Rev. Microbiol. **49**, 117 (1995)

Shlomai, J.: The assembly of kinetoplast DNA. Parasitol. Today **10**(9), 341 (1994)

Shlomai, J., Linial, M.: A nicking enzyme from Trypanosomatids which specifically affects the topological linking of duplex DNA circles. J. Biol. Chem. **261**(34), 16219 (1986)

Shlomai, J., Zadok, A.: Reversible decatenation of kinetoplast DNA by a DNA topoisomerase from trypanosomatids. Nucleic Acids Res. **11**(12), 4019 (1983)

Silver, L.E., Torri, A.F., Hajduk, S.L.: Organized packaging of kinetoplast DNA networks. Cell **47**(4), 537 (1986)

Simpson, L.P.: Morphogenesis and the function of the kinetoplast in "Leishmania". Atlas de Symposia sobre a Biota Amazonica (Pathologia), **6**, 231 (1967)

Taniguchi, Y., Choi, P.J., Li, G.-W., Chen, H., Babu, M., Hearn, J., Emili, A., Xie, X.S.: Quantifying E. coli proteome and transcriptome with single-molecule sensitivity in single cells. Science **329**(5991), 533 (2010)

Wang, Z., Englund, P.: RNA interference of a trypanosome topoisomerase II causes progressive loss of mitochondrial DNA. EMBO J. **20**(17) (2001)

Wang, Z., Morris, J.C., Drew, M.E., Englund, P.T.: Inhibition of Trypanosoma brucei gene expression by RNA interference using an integratable vector with opposing T7 promoters. J. Biol. Chem. **275**(51), 40174 (2000)

White, J.H., Millett, K.C., Cozzarelli, N.R.: Description of the topological entanglement of DNA catenanes and knots by a powerful method involving strand passage and recombination. J. Mol. Biol. **197**(3), 585 (1987)

Wickiser, J.K., Winkler, W.C., Breaker, R.R., Crothers, D.M.: The speed of RNA transcription and metabolite binding kinetics operate an FMN riboswitch. Mol. Cell **18**(1), 49 (2005)

Xu, C.W., Ray, D.S.: Isolation of proteins associated with kinetoplast DNA networks in vivo. Proc. Natl. Acad. Sci. USA **90**, 1786 (1993)

Xu, C.W., Hines, J.C., Engel, M.L., Russell, D.G., Ray, D.S.: Nucleus-encoded histone H1-like proteins are associated with kinetoplast DNA in the trypanosomatid Crithidia fasciculata. Mol. Cell. Biol. **16**(2), 564 (1996)

Young, D., Morales, A.: Isolations of Leishmania braziliensis (Kinetoplastida: Trypanosomatidae) from cryopreserved colombian sand flies (Diptera: Psychodidae). J. Med. Entomol. **24**, 587 (1987)

Chapter 6
The Role of Topology in DNA Gel Electrophoresis

The Red Queen said: "Now, here, you see, it takes all the running you can do, to keep in the same place"

L. Carroll

Topology plays a key role in the biophysics of DNA, and is intimately related to its functioning. For instance, transcription of a gene redistributes twist locally to create what is known as supercoiling, while catenanes or knots can prevent cell division, hence they need to be quickly and accurately removed by specialised enzymes known as topoisomerases. But how can one establish experimentally the topological state of a given DNA molecule? By far the most successful and widely used technique for this is gel electrophoresis (Calladine et al. 1997; Bates and Maxwell 2005). This method exploits the empirical observation that the mobility of a charged DNA molecule under an electric field and moving through a gel depends on its size, shape and topology (Bates and Maxwell 2005; Stasiak et al. 1996). Nowadays, gel electrophoresis is a ubiquitous technique (Calladine et al. 1997; Viovy 2000; Dorfman 2010), since it readily allows the separation of polymers with different physical properties and it is systematically used for DNA identification and purification (Calladine et al. 1997).

Gel electrophoresis is so empirically reliable that it can be used, for instance, to map replication origins and stalled replication forks (Olavarrieta et al. 2002), to separate plasmids with different amount of supercoiling (Olavarrieta et al. 2002; Cebrián et al. 2014), and to identify DNA knots (Stasiak et al. 1996; Arsuaga et al. 2005). The most widely employed variant of this technique nowadays is two-dimensional gel electrophoresis, where a DNA molecule is subjected to a sequence of two fields, applied along orthogonal directions (Bates and Maxwell 2005). The two runs are characterised by different field strengths, and sometimes also gel concentrations (Cebrián et al. 2014); with suitable choices, the joint responses leads to increased sensitivity.

Even though widely employed, gel electrophoresis of topologically non-trivial polymers present some difficult theoretical challenges and remain largely theoretically unexplained. Some other aspects are reasonably well established. For instance,

D. Michieletto, *Topological Interactions in Ring Polymers*, Springer Theses,
DOI 10.1007/978-3-319-41042-5_6

it is now widely accepted that the physics of the size-dependent migration of linear polymers can be explained by the theory of biased polymer reptation (Rubinstein 1987; Duke 1989; Viovy and Duke 1993; Barkema et al. 1994; Viovy 2000). Likewise, the behaviour of, for example, nicked, torsionally relaxed, DNA knots in a sparse gel and under a weak field is analogous to that of molecules sedimenting under gravity (Weber et al. 2013; Piili et al. 2013). The terminal velocity can be estimated via a balance between the applied force and the frictional opposing force, which is proportional to the average size of the molecule: as a result, more complex knots, which are smaller, move faster under the field. However, the mechanisms regulating the electrophoretic mobility of DNA knots at intermediate fields, and in more concentrated agar gels, are much less well understood (Viovy 2000; Weber et al. 2006a; Cebrián et al. 2014).

In these cases, experiments suggest that the mobility of DNA knots is usually a non-monotonic function of the knot complexity, or, more precisely, of their average crossing number (Katritch et al. 1996; Stasiak et al. 1996) (ACN): initially knots move more slowly as their ACN increases, while, past a critical ACN, more complex knots move faster. The combination of the responses to external fields directed along two perpendicular directions leads to a characteristic electrophoretic arc which allows one to separate the first simple knots more clearly in a 2D slab (Trigueros et al. 2001; Arsuaga et al. 2002, 2005; Cebrián et al. 2014). There is currently no theoretical framework that quantitatively explains the non-monotonic behaviour at intermediate or large fields and the consequent formation of arc patterns.

In this Chapter I will show that much of the difficulty in capturing their behaviour may be due to an incorrect model for the gel structure. In the past, the standard way to tackle this problem was to treat the gels as perfect meshes of obstacles (Calladine et al. 1991; Alon and Mukamel 1997; Viovy 2000). On the other hand, it is well known that physical gels have irregularities, such as dangling ends (Whytock and Finch 1991; Cole and Åkerman 2003; Rahong et al. 2014). These are common in agarose gels formed at low agarose concentrations because many of the agarose bundles fail to cross-link with other fibers, thereby generating partially cross-linked open strands (Whytock and Finch 1991). More recently, dangling ends have also been directly observed in artificial gels made of solid nano-wires using transmission electron microscopy (Rahong et al. 2014) (see also Chap. 3 for details on gels and their modelling).

The presence of these dangling ends plays a very weak role when linear polymers are undergoing gel electrophoresis. Conversely, gel electrophoresis experiments involving polymers with looped structures are expected to depend rather strongly on the topological interactions between the polymers and the gel structure (see for instance Fig. 6.1). When a dangling end threads through the ring polymer, the latter becomes “impaled” and its free motion is re-established only when the threading is removed. This makes the presence of dangling ends in the gel a key element for a realistic model of gel electrophoresis experiments and to study the dynamics of topologically looped polymers.

Inspired by these observations, in this Chapter I will focus on the dynamical properties of rings subject to an external force that move within a mesh of obstacles

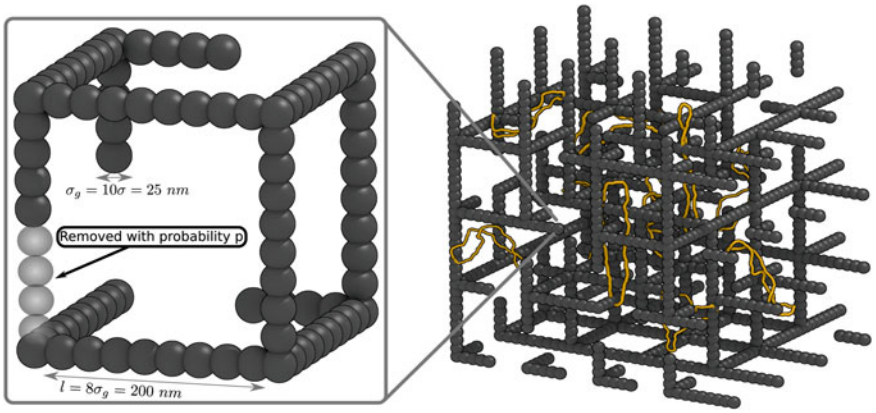

Fig. 6.1 Assembling a random environment: A probability p is assigned to each edge so that half of it can be knocked out at a random end. By assembling multiple cells it is possible to construct a random environment which resembles the disordered structure of a gel, where dangling ends populate the medium. To the right a typical snapshot of the system is shown. The external force in this case is directed upward. Periodic boundary conditions are applied to the simulation box and the gel structure is here thinned for clarity

modelled as a 3D irregular cubic lattice. The "irregularities" are represented by randomly positioned dangling ends (see Fig. 3.1 in Chap. 3 or Fig. 6.1 in the next section). I expect that these defects interacting with the rings and may result in interesting behaviours that may have been overlooked in the past.

In particular, in Sect. 6.1 I will show that, in the regime of strong electric field and sufficiently high concentration of dangling ends, un-knotted ring polymers migrate slower as the external bias (force) is further increased. This means that the system displays a "negative differential mobility" (Zia et al. 2002; Baerts et al. 2013; Ghosh et al. 2014), which has been beautifully captured by the phrase "getting more from pushing less" in the literature. In other words: the flux generated by large external fields is smaller than the one produced by weaker ones and in the system studied in this chapter, this phenomenon is entirely due to the topology of the polymers.

I will also show that the topological interactions between ring polymers and the gel architecture can provide information on the microscopic structure of the gel. The results presented in fact suggest that a gel electrophoresis experiment can establish the level of disorder in the medium by comparing the results obtained by running linear and ring polymers. This represents a novel way to exploit topology to "sense" the disorder in the microscopic structure of a material in a non-invasive way.

Finally, in Sect. 6.2 I will investigate the gel electrophoresis of knotted ring polymers and, in particular, I will describe a model that captures the electrophoretic arc (i.e. non monotonic mobility) in 2D gel electrophoresis techniques. This will be explained in terms of competition between shrinking size and increasing complexity of DNA knots.

6.1 Gel Electrophoresis of DNA Rings and Strands

The model I am introducing here is that of a random gel through which the rings are forced to move. The gel is constructed starting from a regular cubic lattice from which a random fraction p of dangling ends is created. These are made by halving some edges of the cubic lattice with probability p[1] and directed toward a random direction (see Chap. 3). A typical configuration of this random mesh is shown in Fig. 6.1. Different values of p produce various levels of disorder which I can accurately tune. The mesh size is set at 200 nm which is comparable to that of agarose gels at concentrations around 5 % (Pernodet et al. 1997). The strands are made of static beads of diameter $\sigma_g = 10\sigma = 25$ nm.

The choice of modelling the gel as completely static might seem very crude approximation but several experiments reported values for the persistence length of single agarose fibers in the range of 2–10 nm; in particular, Guenet and Rochas (2006) reports a persistence length of about 9 nm (the same work also presents evidence of the presence of dangling ends in the gel). Furthermore, each agarose bundle is formed by a number n_f of fibers, with n_f ranging between 10 and 20 (Guenet and Rochas 2006), and has a diameter of 10–20 nm (Sugiyama et al. 1994). The persistence length of a full fibril might depend linearly or quadratically on n_f (depending on the structure of the bundle and strength of inter-fiber interactions) (Mogilner and Rubinstein 2005). In light of this, a conservative estimate of the persistence length for an agarose bundle is about that of DNA, i.e. 50 nm. This implies that agarose is quite rigid on the scale of a dangling end. This approximation also allows one to save computer time and simulate longer DNA rings for longer times, which is important to monitor the speed of the polymers.

Rings moving through the gel are modelled by a set of N circular semiflexible chains each of M beads of diameter $\sigma = 2.5$ nm (see Chap. 3 for details). Here I consider either systems of $N = 10$ rings with $M = 512$ beads each or systems of $N = 20$ rings and $M = 256$ beads. These two cases correspond to circular DNA of about 3.7 kbp (contour length $L_c \simeq 1.3\,\mu$m) and 1.9 kbp ($L_c \simeq 0.65\,\mu$m) respectively. The simulation box has linear dimension $L = 320\sigma$ and periodic boundary conditions in all three directions. In both cases considered, the systems are in the dilute limit and interactions between rings are therefore neglected in the analytic calculations, although they might rarely occur in the simulations.

The external electric field is modelled as a constant force applied on each monomer. Assuming that the electric charge is uniformly distributed along the rings, the total force $\boldsymbol{F}$ can be distributed uniformly on each monomer, which is subjected to a force $\boldsymbol{F}/M$. The force acting on each ring can be thought of as resulting from an electric field as $\boldsymbol{F} = q_r \boldsymbol{E}$, where $q_r = Mq$ and q is the representative charge of a single bead. The force acting on each bead can be expressed in units of $\epsilon/\sigma \simeq 1.6$ pN, the total force acting on the rings being a multiple of $F = 1.6\,M$ pN. Since each

[1] The halving probability p is always taken smaller than the critical (inverse) percolation probability $1 - p_c \simeq 0.75$ (p_c being the bond percolation probability on a cubic lattice) to avoid the presence of sparse un-connected clusters of un-physically rigid parts of the gel.

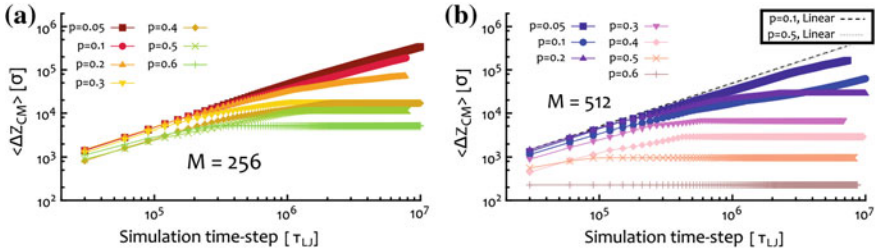

Fig. 6.2 Average centre of mass displacement along the field direction, $\langle \Delta Z_{CM} \rangle$. The field strength in this case is $E = 0.05\ \epsilon/q\sigma$ and the two sets of rings considered have (**a**) $M = 256$ and (**b**) $M = 512$ beads. The curves refer to different values of p. Linear polymers are here observed to be insensitive to the gel disorder as they show (*dashed black* and *dotted grey lines*) no variation in speed when p is varied **(b)**. To ease comparison with real units one can bear in mind that is possible to map simulation units in real units, and it turns out that $10^6\ \sigma \simeq 2.5$ mm and $10^7\ \tau_{LJ} \simeq 0.37$ s (see Sect. 3)

bead corresponds to $\sigma = 2.5$ nm $\simeq 7$ bp, and each base-pair contains two phosphate groups which account for a negative charge each, one can approximate the charge in each bead as $14q_e$, where q_e is the electron charge.[2]

The force exerted to the beads can therefore be thought of as a result of the action of an external electric field pointed towards $-\hat{z}$ and re-scaled by the charge of a bead. In this case, the field strength felt by each bead can be expressed in units of V/cm as $\tilde{E} = 1.6/22.43\ 10^{19} pN/C \simeq 7$ kV/cm. In this chapter, the fields used range from 10^{-3} to $10^{-1}\tilde{E}$, i.e. between 7 and 700 V/cm, which are roughly compatible to the values used in standard DNA gel electrophoresis (Mickel et al. 1977; Levene and Zimm 1987; Viovy 2000).

6.1.1 *Linear Polymers Are Insensitive to Microscopic Disorder*

In order to investigate the effect of the dangling ends on the dynamics of the DNA rings, I am going to monitor the average centre of mass displacement along the direction $\hat{z}$ of the field, $\langle \Delta Z_{CM} \rangle$ for different values of the parameter p (see Fig. 6.2). It is evident from the figure that the polymers severely slow down their motion as the fraction p of dangling ends increases. In order to show that this is due to the ring topology, I repeated an identical simulation where the rings were swapped with linear polymers of same contour length. Their displacement is reported as black dashed and grey dotted lines in Fig. 6.2 and clearly show that the variation of fraction of dangling ends does not interfere with the motion of the linear chains. I therefore argue that, as

[2]Here, I neglect the screening due to ions in solution (Maffeo et al. 2010; Stefano et al. 2014). These will be considered in the next section. In any case, the correction due to the presence of ions account only for a pre-factor on the corresponding real-life values of the fields used in the simulations.

expected, linear polymers are insensitive to changes in the microscopic structure of the gel whereas the motion of ring polymers is crucially related to the disorderedness of the gel.

The mobility of the rings $\mu(M, p)$ is readily recovered from Fig. 6.2. This can be found using the relation

$$\mu(M, p) = \frac{\langle v \rangle}{|\boldsymbol{F}|} \tag{6.1}$$

where the average velocity $\langle v \rangle$ is computed using the average displacement of the centre of mass at the longest simulation time step, namely

$$\langle v \rangle = \frac{\langle \Delta Z_{CM}(t = 10^7 \tau_{LJ}) \rangle}{10^7 \tau_{LJ}}. \tag{6.2}$$

It is worth stressing that even though the total simulation time is arbitrary, if this is long enough, it gives the right relative speed between the rings moving through gels at different p. The same principle is used to obtain the mobility of DNA molecules gel electrophoresis experiments.

In the main panel of Fig. 6.3 the mobility $\mu(M, p)$ is reported for rings of $M = 256$ beads driven by two different external fields strengths $|\boldsymbol{E}| = E$, as a function of the average fraction of dangling ends p. For fixed E and M, the mobility decreases as p increases since rings are more likely to become threaded, and hence immobilised, by the gel's dangling ends. This behaviour seems to be well captured by an exponential law of the form $\mu \sim e^{-Bp}$, where B is shown to scale extensively with MqE (inset of Fig. 6.3). This result can be interpreted within the assumption that the rings move with mobility μ_0 only when not impaled and otherwise are essentially immobile. Hence one can write

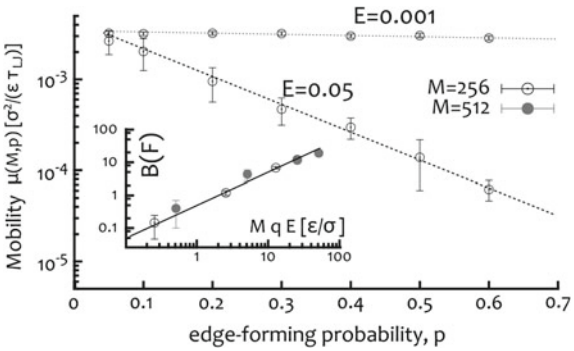

Fig. 6.3 The mobility μ is reported as a function of p. The data points report the two choices for M and to two values of the field strength E, as labelled. One can notice that the data points can be fitted by exponentials of the form $\mu \sim e^{-Bp}$ (*dotted* and *dashed lines*). In the *inset*, I show that the pre-factor B seems to scale extensively (*solid line*) with $F = MqE$. This supports the conjecture that impaled rings can be thought of as particles trapped in potential wells whose height is proportional to the field strength (see text)

$$\mu = (1 - s)\mu_0 \tag{6.3}$$

with s the fraction of time in which a ring is stuck. This may be approximated by

$$s = \frac{\alpha p v}{\alpha p v + e^{-\Delta G/k_B T}}. \tag{6.4}$$

Here, the rate of hitting a dangling end when a ring is moving through the gel is assumed to be proportional to both the velocity v and the density of ends p. Furthermore, the disentanglement rate is assumed Arrhenius-like and proportional to $e^{-\Delta G/k_B T}$ with ΔG the free energy barrier needed to disentangle a ring from a dangling end. The energy barrier ΔG may be thought of as begin itself proportional to the force exerted on the ring times the length of the dangling end, i.e. $\Delta G = MqEl/2$, since a ring must move the length of the penetrating segment $l/2$ against a force $F = MqE$. As one can notice from the picture, this conjecture very well captures the exponential variation with $B \sim MqE$. On the other hand, it does not explain the exponential dependence in p. I have yet to find an analytical explanation for this, but one can imagine being related to more complicated forms of entanglements, where more than one dangling end is involved in the impalement. If this was the case, the energy barrier needed to be overcome for a ring in order to free itself would be somewhat proportional to the density of dangling ends, and therefore the presence of p in the exponent somewhat justified.

6.1.2 *Getting More from Pushing Less*

Another very interesting feature that one can observe in this system is shown in Fig. 6.4. The figure reveals a very intriguing non-equilibrium property of the system:

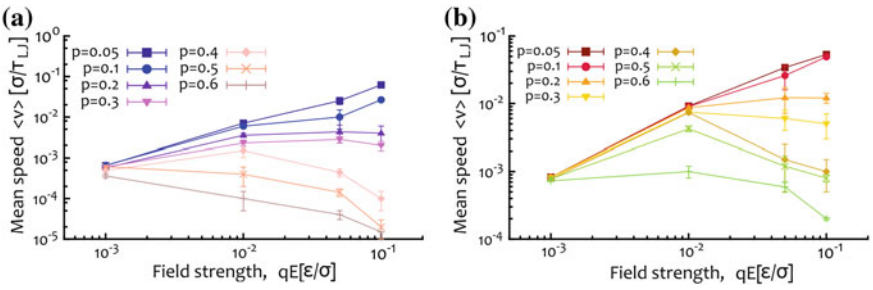

Fig. 6.4 The average speed $\langle v \rangle$ of the rings is here shown as a function of the force exerted on a single bead qE. The two panels show the two choices of rings' length: (**a**) $M = 512$ and (**b**) $M = 256$ beads. One can readily notice that for $p \gtrsim 0.4$ the functional form of the average speed versus field strength shows a non-monotonic behaviour. This is quite unique and defines a negative differential mobility $\partial\langle v \rangle/\partial E < 0$ for fields $E > 0.01\ \epsilon/q\sigma$ and $p > 0.3$. In order to ease the comparison with read units one can bear in mind that it is possible to map $0.1\ \sigma/\tau_{LJ} \simeq 6.7$ mm/s and $0.01\ \epsilon/q\sigma \simeq 70$ V/cm (see Chap. 3)

the average centre of mass speed $\langle v \rangle$ decreases as the strength of the field E increases for sufficiently high density of dangling ends p.

This behaviour can be related to the definition of the mobility in Eq. (6.1) combined with the result expressed in Eq. 6.3. In particular:

$$\langle v \rangle = \mu F \sim F e^{-Fpl/2k_BT} \mu_0, \tag{6.5}$$

which clearly shows that the average velocity is expected to display a non-monotonic behaviour in F.

One can better capture this behaviour by measuring the differential mobility (Baiesi et al. 2009, 2011; Baerts et al. 2013) of the rings. Numerically this can be readily obtained as:

$$\mu_D^N = \frac{\partial}{\partial F} \langle v(F) \rangle. \tag{6.6}$$

This quantity is reported in Fig. 6.5 and it clearly shows the field strength at which the rings start to decrease their mobility. By mapping the simulation units in real units (see Chap. 3) one finds that

$$\mu_D^N(F) = 0 \tag{6.7}$$

at $F \simeq 0.01\ \epsilon/q\sigma \simeq 70$ V/cm.

Although this value is around one order of magnitude larger than the values used to observe "exclusion" from the gel of rings with similar length than the ones studied here, i.e. some rings would not travel through the gel when pushed with a field of around 4–8 V/cm, in Mickel et al. (1977), there is to say that there are viscosity of the solution, salt concentration, screening of electric charges and other factors are

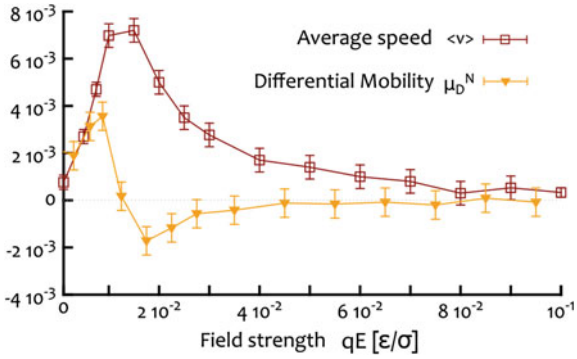

Fig. 6.5 The average speed of the centre of mass of rings, $\langle v \rangle$ in units of σ/τ_{LJ} is shown for a system of $N = 20$ rings with $M = 256$ beads and with $p = 0.4$ (diamonds in Fig. 6.4). The numerical differential mobility can be computed as reported in the text and is here expressed in units of $\sigma^2/\epsilon\tau_{LJ}$, as a function of the force acting on single beads qE. One can readily notice the change from positive to negative mobility as $qE \simeq 0.01\epsilon/\sigma \simeq 70$ V/cm

only crudely taken into account in the model presented in this chapter. The addition of these details in fact would have made the model more complete but also more complicated and would have perhaps hidden some of the effects that I have reported in this chapter.

In agreement with the results presented here, the findings in Mickel et al. (1977), Cole and Åkerman (2003) report that usually, closed circular samples migrated faster than linear DNA, and this could be explained in terms of the average size of rings which is smaller than the one for linear DNA, for equally long molecules. Under some conditions, the same literature instead reports an inversion of this trend, which can be explained by the fact that either field strength or dangling ends have started to trap the rings.

Another finding reported in Cole and Åkerman (2003) and supporting the conjecture explored in this chapter is that rings travelling through more concentrated agarose gels, although having overall lower mobility, they show a negative differential mobility turning point at higher field strengths. This can be explained with the fact more concentrated agarose gels are known to possess less dangling ends (Sugiyama et al. 1994), since the fibres are more likely to fuse together rather than remain non cross-linked. In light of this, a smaller p in fact might lead to a larger critical field at which $\mu_D^N = 0$, although I have not explored this case in the chapter.

Finally, Mickel et al. (1977) reports that for fields around 4–8 V/cm, the closed circular DNA roughly 2 kbp long, would not even travel through the gel and would display a broad electrophoretic band. This is a clear indication suggesting a strong entanglement effect, which causes the broadening, or "smearing" of bands.

It is also worth stressing that a behaviour in which objects pushed by an external force are observed to travel slower when the force is increased has recently attracted much scientific interest. On the one hand, the reason for this is that new theories are starting to well describe non-equilibrium physics for the first time (Baerts et al. 2013). Formulating generalised relations for fluctuation-dissipation theorems and diffusion coefficients in systems where energy is absorbed and consumed is of primary importance in order to achieve a better understanding of the physics of life. On the other hand, experiments (Galajda et al. 2007) and simulations (Ghosh et al. 2014) are probing new designs where "active", i.e. out-of-equilibrium, elements and non-trivial environments are made interact in order to tune arbitrarily desired responses. In light of this, the present system can be thought of as an excellent example of system where one can obtain more by pushing less (Zia et al. 2002). The rings are in fact shown to show a larger mobility at low external fields rather than high ones. In other words, this would be like getting more current in your circuit by applying less voltage...a rather strange system!

6.1.3 Topology Can Sense Disorder

In this Section I investigated the role played by topology in the motion of un-knotted ring polymers through a gel modelled as a disordered environment. It is remark-

able that by comparing the behaviour of linear and circular polymers one can infer the degree of microscopic disorder in the medium (Fig. 6.2). On one hand the findings presented here provide us with an explanation for irregular migration speeds detected in experiments comparing linearised and circular plasmids (Mickel et al. 1977; Levene and Zimm 1987; Trigueros et al. 2001); on the other, they also strongly encourage the speculation that with a proper choice of a "topological" polymeric probe, there is the possibility to explore the properties of complex disordered environments from a novel perspective. Polymers with specific topologies may in fact be exploited to design novel ways of sensing the changes in the microscopic structure of porous environments in a new and non-invasive way, e.g. by looking at their mobilities.

Novel techniques nowadays allow the construction of gels with arbitrary topologies. One way to measure the level of order/disorder in such materials would be to compare the mobilities of linear and ring charged polymers moving though them. Because such procedure would also be non invasive, the same sample could be probed by means of, for example, atomic force microscopy in order to have several ways of assessing the structure.

In the previous Sections I also showed that the trapping of ring polymers by the environment is an effect that can be quantified by a simple reasoning leading to Eqs. (6.3)–(6.4). These equations state that the entanglement effect, represented by the fraction of time spent in the immobile state, s, is analogous to an Arrhenius process. In other words, this means that in order to re-establish the free motion, the rings have to retrace their steps and overcome an energy barrier that I shown to be proportional to the force exerted on each ring $F = MqE$ times the length of the obstacle, which is here simply taken as half the length of the lattice spacing. This in tunr implies that the entanglement barrier is as strong as the force drifting the rings through the gel. Stronger external fields not only mean that they travel faster when free, but also that they have to overcome an exponentially larger barrier when immobile. In simplified models (Baiesi et al. 2015) this effect is often modelled as particles pushed by an external force and falling into wells whose height is proportional to the external force itself, leading to the same negative differential mobility reported here.

The phrase "getting more from pushing less" has recently been used to describe situations in which a higher current can be obtained by lowering the field strength (Zia et al. 2002; Baerts et al. 2013). This phenomenon has been shown to well describe the behaviour of ellipsoidal Janus particles in corrugated channels (Ghosh et al. 2014). Here, another important realisation of this phenomenon, which is intimately related to the broadly used gel electrophoresis technique, has been illustrated. This is an instance of "negative response" and can be interpreted with recent advances in the field of non-equilibrium statistical mechanics. The covariance between displacement and average experienced force, which is zero in equilibrium conditions, may become the dominant contribution to non-equilibrium susceptibilities (as the mobility) and overtake the diffusion term to render the response negative.

6.2 Gel Electrophoresis of DNA Knots

In the previous Section I studied the behaviour of un-knotted DNA rings and linear strands. In this Section I will instead focus on knotted DNA rings and their behaviour in (2D) gel electrophoresis experiments. This topic presents some outstanding questions which require a satisfactory answer in order for experiments to exploit the separation properties of gels at their best. In particular, the formation of an arc-shaped pattern in 2D gel electrophoresis experiments of DNA knots is largely mysterious (Trigueros et al. 2001; Olavarrieta et al. 2002; Trigueros and Roca 2007; Cebrián et al. 2014). Although this finding is nowadays a broadly accepted empirical fact, there is no accurate theoretical explanation of this phenomenon from first principles. The aim of this Section is to shed some light into the physics governing this topological pattern.

In analogy to the previous Section I start with a system of 10 nicked, i.e. torsionally relaxed, DNA loops of $M = 512\sigma \simeq 3.7$ kilo-base pairs (kbp) knotted DNA chains migrating through a gel with lattice spacing $l = 80\sigma = 200$ nm. In order to simulate a 2D gel electrophoresis experiment (see for instance Cebrián 2014) I perform a simulation in which a weak external field is directed toward z and afterwards, once the first field has been switched off, a second one, stronger in intensity, is applied in a perpendicular (y) direction. The simulations are performed using a Brownian Dynamics scheme (see Chap. 3 for details) and the gel is constructed as in the previous Sections: a cubic mesh to which some (half) edges are removed at random (see also Chap. 3) and in what follows the probability of generating a dangling end p is fixed at $p = 0.4$ (see Fig. 6.6. The DNA rings are prepared either un-knotted, or form one of the first few simple knots (with up to 9 crossing in their minimal projection (Adams 1994)). Most of the knots are prepared simply by using the parametrisations given in Chap. 3. If a simple curve to form a knot was not known, I had simulated polymers which could randomly perform strand crossings until the knot detection algorithm (see Appendix A) would indicate the occurring of the wanted knot.

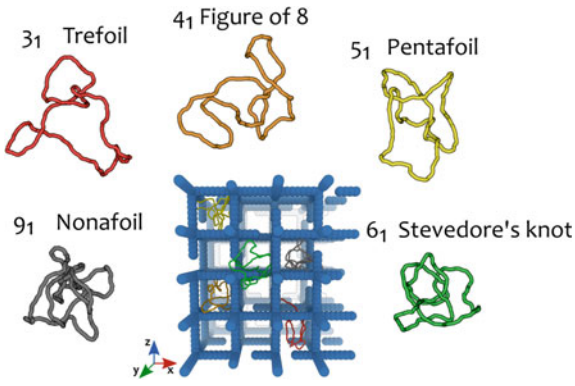

Fig. 6.6 Snapshot of the system to scale together with some examples of DNA knots. The gel is generated as in the previous section, with $p = 0.4$, and knots are made travel through it. Also shown some equilibrium configurations knotted polymers; being the figure to scale one can readily appreciate that the size of the knots tends to decrease with the knot complexity

The average crossing numbers (ACN) for the knots is a good measure for their complexity. The ACN used in this Section have been obtained from Kusner and Sullivan (1994), where the authors computed the ACN corresponding to Möbius energy minimising knotted configurations. The thermally averaged ACN of the samples used in this work has been computed from equilibrated configurations and has been found to be in a one-to-one correspondence to the values in Kusner and Sullivan (1994) (see Chap. 3 Fig. 3.4), confirming the known linear relationship between the ACN of ideal and thermally equilibrated configurations (Katritch et al. 1996).

The rings were equilibrated by running a simulation at zero external field of 5×10^6 τ_{Br} time steps, which are disregarded before the external force is switched on. The rings were then subjected to an in silico gel electrophoresis process where a weak electric field is first applied ($\lesssim$50 V/cm) along the vertical (z) direction, followed by a stronger field ($\gtrsim$150 V/cm) along a transversal, say y, direction. I will refer to these two fields as "weak" and "stronger", or "moderate", in what follows. The mean and standard error of various properties, as the mean displacement along $\hat{z}$, are understood in the usual non-equilibrium meaning, i.e. they are calculated by averaging over the rings in the system and over different runs starting from different (equilibrated) initial conditions, and not over time.

As in the previous Section, the external field is modelled as a force $\boldsymbol{f}$ acting on each bead forming the polymers. Differently to before, here I assume that in physiological conditions half of the charges from the phosphate groups are screened by counter-ions (Maffeo et al. 2010; Stefano et al. 2014).[3] In line with this choice, each bead ($\sigma = 2.5$ nm $\simeq$ 8 bp) contains a total charge of $q_b = 16 q_e/2$, where q_e is the electron charge. It is therefore possible to map the external force applied onto each bead to an effective electric field $\boldsymbol{E} = -\boldsymbol{f}/q_b$. Although this mapping is a crude approximation of the Coulomb interaction between the charged DNA, the ions in solution and the applied electric field, I find that one can recover a "weak field" behaviour of the knotted samples, i.e. linear increase of the speed as a function of their ACN, up to ~50 V/cm, which is roughly comparable with the field intensity used in experiments. The fields used in this section range from $E = 1.25$ V/cm to $E = 625$ V/cm. This range also corresponds to a range of forces acting on each bead from $f = 1.6\ 10^{-4}$ pN to $f = 0.08$ pN or total forces $F = Mf$ from 0.08 pN to 20 pN, which are compatible with forces used in both gel electrophoresis and single-molecule experiments.

6.2.1 Non-monotonic Speed of DNA Knots in Gel

By monitoring the trajectories of the knots through the gel (Fig. 6.7 shows also the cases for $p = 0$ for completeness) I computed the average speed of their centre of

[3] Differently to the previous Section, the parameters used here are closer to the ones used recently in the literature (Stefano et al. 2014).

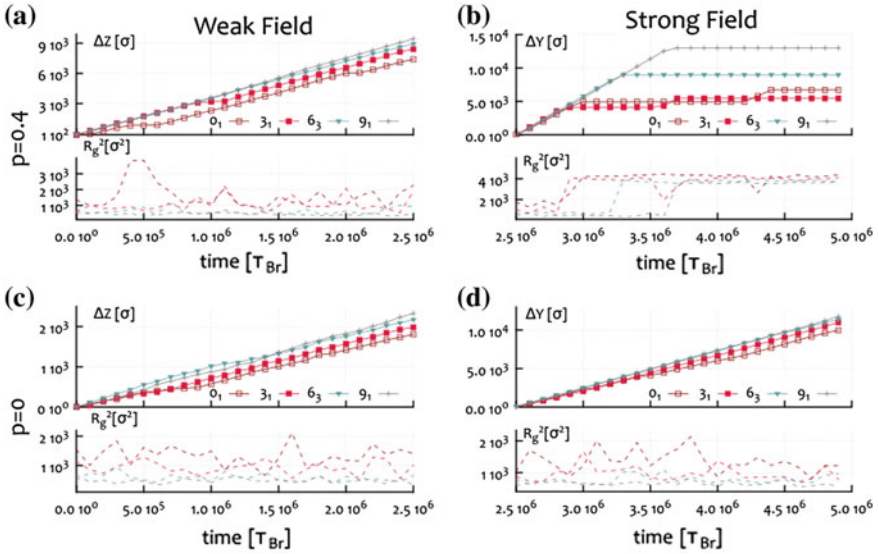

Fig. 6.7 In this figure I show the trajectories of some of the knots together with their instantaneous radius of gyration for different cases. **a** and **b** refer to the case of a gel with dangling ends while for reference, I also show in **c** and **d** the case of a gel without dangling ends. From top-bottom, figures **a**–**c** show te response of the knots under weak fields (∼50 V/cm) while figures **b**–**d** show the response under strong fields (∼150 V/cm). From these figures it is important to notice that while the weak field response of the knots is similar in the case with or without dangling ends, the response under strong field is radically different. When dangling ends are present the knots become entangled for long times, as one can see from the long stalls in displacement and the large values of their R_g. This intermittent motion is unique to this case and it can be directly observed in experiments done by fluorescent tagging the DNA samples. For a clip in which fluorescent plasmids are travelling through a network of nanowires (Rahong et al. 2014), see http://www2.ph.ed.ac.uk/~dmichiel/Rings_GelEP.mp4

mass along each of the field directions (Fig. 6.8). As expected, the mobility along the direction of the weak field increases with the topological complexity of the configurations. Along the direction of the moderate field, however, the mobility of the knots displays a non-monotonic behaviour. In particular, the un-knot now moves faster than either the trefoil or the 4_1 twist knot, and has an average speed similar to the 5_1 knot. This non monotonic behaviour of the knot mobility, as a function of the ACN, was previously observed in typical experiments with torsionally relaxed DNA knots (Trigueros et al. 2001; Arsuaga et al. 2002, 2005; Trigueros and Roca 2007; Cebrián et al. 2014).

It is interesting to notice that one cannot observe the electrophoretic arc in simulations where the gel is a regular cubic mesh, i.e. a mesh with no dangling ends and $p = 0$. While this has been so far the typical way to model an agarose gel (Weber et al. 2006a, b), it does not lead to a non-monotonic behaviour of the knot mobility. This result is in agreement with previous simulations based on lattice knots in regular gels (Weber et al. 2006a).

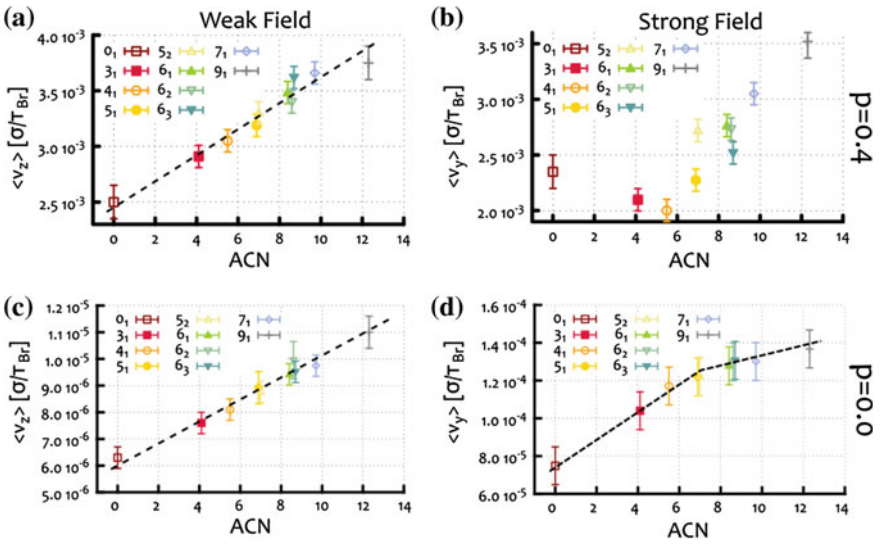

Fig. 6.8 The average velocity of different knot types along the direction of the weak (**a**–**c**, ∼50 V/cm) and the moderate (**b**–**d** ∼150 V/cm) field. From *left-right* **a**–**b** represent the case in which the gel has dangling ends, while **c**–**d** the case in which $p = 0$. One can notice that while the weak field case displays a linear increase in speed with knot type, the strong field case shows a non-monotonic behaviour. The combination of a monotonic behaviour along the weak field direction with a non-monotonic one along the stronger field, gives rise to the arc shape in agreement with the ones observed in experiments (Trigueros et al. 2001; Trigueros and Roca 2007; Cebrián et al. 2014). It is worth stressing that the $p = 0$ case instead shows a monotonic increase also at strong fields. The *dashed lines* are not fitted functions but guides for the eye

These findings therefore strongly suggest that the causes for the non-monotonic behaviour, observed in the case of irregular gels, are to be found in the interaction between the knots and the gel dangling ends. It is worth highlighting that in Weber et al. (2006a, b) the authors already investigated the behaviour of knots under weak and strong fields. In their work, they reported a monotonic behaviour between knot complexity and its speed even at very high fields. Although they observed that for electric fields stronger than a certain critical value more complex knots migrated slower than simpler ones, their findings would not lead to the arc pattern observed in experiments of 2D gel electrophoresis but to a straight line where simpler knots would travel further than more complex ones. In light of this, the results presented here, that the presence of dangling ends in the gel is crucial for retrieving the non-monotonic speed of the knots, while regular gels always lead to monotonic separations, do not contradict previous results (and in particular the ones in Weber et al. (2006a, b)) but instead suggests a different explanation for the experimentally observed, and yet unexplained, arc pattern.

The conjecture that I pursue here, that the interaction with the dangling ends is crucial in the mobility of the knots, is also supported by the fact that linear (open) DNA

samples, are frequently observed to migrate faster than covalently closed (unknotted) ones, in gel electrophoresis experiments performed in both strong and weak fields (Trigueros et al. 2001; Arsuaga et al. 2005; Trigueros and Roca 2007; Cebrián et al. 2014). As I shown in the previous Section, this can be simply explained by the fact that rings become impaled and entangled with the gel's dangling ends therefore supporting the conjecture that a complete model for gel electrophoresis has to take into account topological polymer-gel interactions.

6.2.2 Entanglement with Dangling Ends

Having established that the presence of dangling ends in gels severely affect the transport properties of the knotted DNA loops under moderate electric fields, it is natural to look at the possible mechanisms ruling this phenomenon.

The typical trajectories and average extension of some knotted loops, as they move through a regular model gel and a gel with dangling ends are markedly different at moderate fields (see Fig. 6.7. In a regular gel, knots respond to the field, by shrinking their size so as to channel through the pores of the gel more efficiently. This mechanism, also known as "channelling", for which polymers squeeze through the gel pores, has already been observed in previous works (Mohan and Doyle 2007a, b), and it was previously conjectured to play a role in the non-monotonic separation of DNA knots in gels, as more complex knots could deforming differently when squeezing through the pores (Cebrián et al. 2014). On the other hand, as discussed previously, I find that this behaviour is not sufficient to explain the electrophoretic arc, as for regular gels I always observe a monotonic, although not linear, increase in speed with the knots' complexity (Fig. 6.8).

On the contrary, in the case of irregular gels, knotted loops entangle with the dangling ends. These entangled states (or "impalements") require some time to be unravelled and this is the reason of the anomalously long pauses observed in the knot trajectories (see Fig. 6.7). Clearly, as the DNA gets longer, "impalements", which can either be parallel or perpendicular with respect the direction of the field, become progressively more likely. As a matter of fact this could be one of the reasons why it is in practice infeasible to perform efficient gel electrophoresis experiments with circular DNA longer than 10 kbp (Dorfman 2010): at these sizes impalements are so frequent that they may cause DNA breakage.

In analogy with the phenomenon of threading, which slows down the dynamics of un-knotted loops either in a melt or in a gel (as discussed in detail in Chap. 4), and that of "crawling" of knots around obstacles (Weber et al. 2006b), it is reasonable to expect that more complex knots will take longer to disentangle themselves from an impalement. One can argue that this mechanism, when competing with the reduced Stokes drag of more complex knots in gels, is ultimately responsible for producing a non-monotonic dependence as a function of their complexity, i.e. their ACN.

6.2.2.1 Competition Between Size and Knottedness

Given that "impalement" events are key factors in determining the mobility of DNA knots within gels with dangling ends, it is important to find a way to define and measure this entanglement. Impalement may occur with dangling ends oriented along several directions but it is reasonable to expect that all these events involve a similar mechanism in which, i.e. one dangling end "pierces through" the knot.

To quantify the degree of knot-gel entanglement, I consider an equilibrated knot configuration in the gel, and project it on the plane Π perpendicular to the field direction. I then choose randomly a base point P, at a distance from the projection plane that is much bigger than the radius of gyration of the projected configuration, R_g^{proj}. Starting from P it is possible to draw an arc which pierces only once the projection plane Π at a point, Q, chosen randomly, within a disk D defined as

$$D \equiv \left\{ \boldsymbol{r} \in \Pi \middle| \, |\boldsymbol{r} - \boldsymbol{R}_{CM}| < R_g^{proj} \right\} \tag{6.8}$$

and with uniform probability so that the whole D is un uniformly sampled. The arc and the plane define a semi-space and one can close the path with a second arc connecting Q and P and living in the other semi-space (see Fig. 6.9a. To measure the topological interaction of the arbitrary curve with the knotted configuration, I compute the absolute value of the linking number, $|Lk|$, between the circular path and the knot. Figures 6.9b, c show the result of this procedure when applied to two different knots, the un-knot and the 9_1.I finally define the "average entanglement number", $\langle \pi \rangle$ (AEN) by averaging the value of $|Lk|$ obtained using many closed paths with different Q, and over different knot configurations. This is taken as a measure of the degree of (possible) entanglement between a knotted molecule and the surrounding gel.

In some sense, this procedure is reminiscent of the one used to assess the "group" of a knot (Adams 1994), or one might think of this as "piercing" the Seifert surface of the knot and taking the average over many "piercings" ($\langle \pi \rangle$) (see Chap. 3 and Appendix A).

It is perhaps important to highlight at this stage that the linking number measures how much two closed curves are homologically linked but it cannot tell whether two loops are topologically linked. For instance the Whitehead link (Rolfsen 2003) is a topological link but has linking number zero. Consequently, the definition of entanglement number may make use of configurations which can having linking number 0 although topologically inseparable. This means that some regions within a projected knot might give rise to a locally null entanglement number $\pi(x, y) = 0$ for $(x, y) \in W$. W being a region of the knot projection through which a loop, if drawn, would lead to a topological link between the loop and the knot, with linking number 0. This means that this measure is not perfect, but in absence of something better, it will be used in what follows to quantify DNA-gel entanglements.

From Fig. 6.9d one can notice that $\langle \pi \rangle$ increases roughly linearly with ACN: it is reasonable that more complex knots in fact can, on average, become more entangled

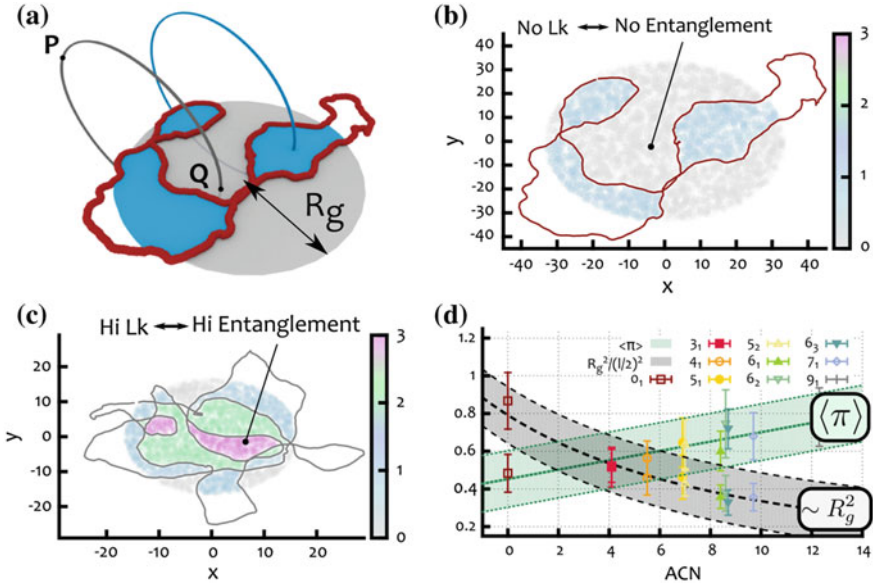

Fig. 6.9 **a** The "piercing", or "entanglement", number is defined by averaging over many projections of an equilibrated knotted configuration on the plane Π and by computing the linking number between random loops passing through the disk D as defined in Eq. (6.8). **b** and **c** show the results of the procedure described in panel **a** for an un-knotted configuration in (**b**) and a 9_1 knot in (**c**). The regions of D are coloured according to the computed absolute value of the linking number (see colour map at the *right*). Note that for the 9_1 case there are regions of high linking number $|Lk| = 3$, which are completely absent from the unknotted case. These are clearly more prone to become severely entangled with the dangling ends of the gel since once that region is threaded, more than one winding of the chain is needed to free the whole polymer. **d** shows the final average entanglement number $\langle\pi\rangle$ directly compared with the mean squared radius of gyration divided by $(l/2)^2$ (remember that l is the gel pore size) for different knot types classified in terms of ACN

with the gel. On the other hand, I do not have an explanation about why $\langle\pi\rangle$ should grow linearly with ACN. Nonetheless, it is interesting to compare this behaviour with that of the mean squared radius of gyration normalised by the size of (half) the gel lattice spacing (see Fig. 6.9d). As I shown in Chap. 3, the average extension of a knot is inversely proportional to its ACN (Stasiak et al. 1996; Piili et al. 2013).

Furthermore, the curves in Fig. 6.9d indicate a possible interpretation of the non-monotonic mobility of the knots in disordered gels based on the interplay between the size of a knot and its knottedness,leading to a well defined "entanglement complexity" with the gel dangling ends. On the one hand more complex knots experience less frequent collision with the gel structure, and hence should travel more easily through the pores. On the other hand, once a knot-gel collision takes place, more complex knots experience a more intricate entanglement with the gel (higher values of AEN are more probable) and in turn, this will take longer to be unravelled (Stasiak et al. 1996; Weber et al. 2006a, b, 2013).

6.2.2.2 Hitting and Waiting Times

The above argument suggests the existence of two time scales in the process: one is the time τ_f between two successive knot-gel collisions yielding a local entanglement; the other, τ_{dis}, is the time needed by the knotted loop to fully disentangle from the impalement. The time scale τ_f increases as the knot average size decreases and hence increases with knot complexity (ACN). In other words more complex knots experience, on average, less collisions with the gel than their simpler counterparts. The second time-scale, τ_{dis}, is instead an increasing function of $\langle \pi \rangle$ (see Fig. 6.9d) and hence of the knot complexity (measured in terms of ACN). According to this conjecture, the slowest topoisomer in an irregular gel with a given lattice spacing will be the one with the "worst" compromise between a high rate of collisions, and a sufficiently high value $\langle \pi \rangle$.

To investigate more quantitatively the dependence of τ_f and τ_{dis} on the knot type (ACN), one can analyse the trajectories of the knotted loops in the gel by computing: (i) the average number of times a knot arrests its motion in the gel (entanglement event), $\langle n_e \rangle$, and (ii) the distribution of the duration of these entanglement events. The duration of the entanglement events can be identified as the time intervals during which the spatial position of the centre of mass of the configuration deviates significantly from the expected collision-free field-driven linear motion with speed $v_{free} = F_{z,y}/M\zeta = f_{z,y}/\zeta$.

In Fig. 6.10a I also show that the average number of entanglement events $\langle n_e \rangle$ decreases with the knot complexity (i.e. ACN). On the other hand, the distribution of the duration of these events displays an intriguing bimodal shape, with two peaks occurring respectively at short and very long times (see Fig. 6.10c). Furthermore, as reported in Fig. 6.10d, the average fraction of time in which the knot is trapped, τ_w/τ_{tot} (τ_{tot} is the time of the full trajectory), is a non-monotonic function of the ACN, in line with the result on the mobility under moderate field (Fig. 6.8).

The peak at long times in the waiting time distribution can be interpreted as the signature of "head-on" collisions of the knots with the gel. In these cases the dangling ends involved are opposite to the direction of the knot motion and result in very strong entanglements and very difficult to unravel. Nonetheless, either if this long-time peak is excluded or not from the statistics, the characteristic disentanglement time τ_{dis} turns out to increase (linearly) with the knot complexity, i.e. with ACN (see Fig. 6.10b).

One can assume that this bi-modal shape is due to a shift in the energy barrier that the knots have to overcome in order to disentangle from the dangling ends. In analogy to the previous Section, one can think to this process as an Arrhenius process, where the energy barrier is a function of the length of the dangling end and of the magnitude of the external field, as seen in the case of unknotted rings travelling through a disordered gel. In addition, and differently from before, one should also take into account the fact that the energy barrier should have a dependence on the knot complexity.

When the external field is too strong, disentanglement events are very rare, for any knot type. All knots end up being permanently entangled; on the other hand, when the field is too weak, the typical disentanglement time is very short, and the

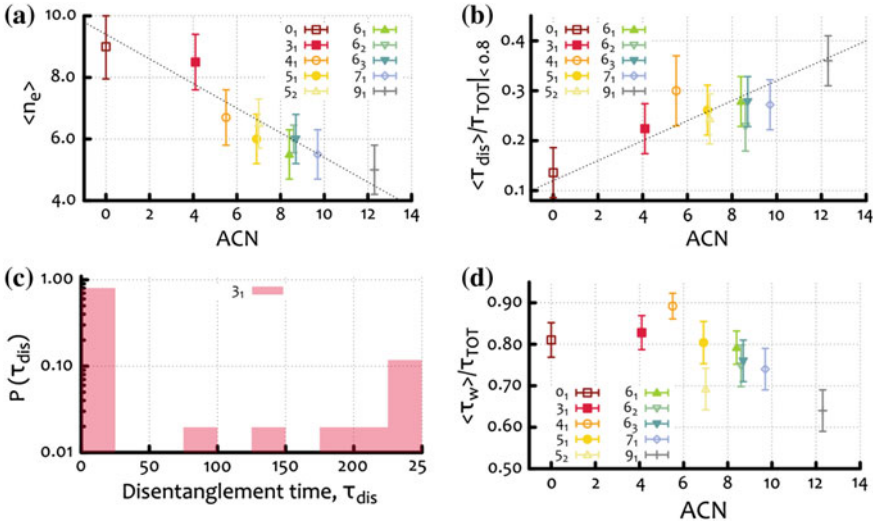

Fig. 6.10 **a** Average number of events in which the knot is entangled with the surrounding gel (entanglement events) as a function of ACN. **b** Average disentanglement time as a function of ACN. In these estimates only entanglement events with duration shorter than 200 τ_{Br} are considered. This is done in order to remove the "head on" impalements. **c** Typical distribution of waiting times. The examples reported is that of a trefoil knot 3_1, showing the bimodal shape discussed in the text. **d** Average fraction of "waiting" (immobile) time as a function of ACN shows a non-monotonic behaviour that complements the one seen for the speed of the knots. It in fact shows that the slower knots are the ones, unsurprisingly, that are the more "waiting"

dependence of τ_f as a function of the ACN dominates the motion of the polymers, re-establishing the usual linearly increasing speed.

6.2.3 An Equivalent Random Walk Description

As shown in previous sections, 2D electrophoresis experiments and Brownian Dynamics simulations of knotted loops in irregular gels are in qualitative agreement under many aspects.

In this section I propose a simple model to understand more deeply the findings reported in the previous Sections. In this model, I consider a knotted DNA molecule moving within the irregular gel as a biased as a 1-dimensional Biased Random Walker (BRW). The BRW can move to the right (arbitrary direction of the external force) by one step (broadly this corresponds to one unit cell of the gel) unless it is trapped into an entangled state (due to impalement) with a probability $\lambda_e(\mathcal{K}) = \tau_f^{-1}(\mathcal{K})$, obtained from the MD simulations.

In the weak field regime one can consider the disentanglement time very small and therefore simply assume that any knot will only stop for one time step with

probability λ_e. In other words, there is no dependence on topology for the waiting part of the BRW. This is equivalent to a Poisson process whose probability of getting entangled after t time-steps is given by:

$$P_{ent}(x(ACN), t) = 1 - [1 - \lambda_e(R_g(\mathcal{K}))]^t \simeq 1 - \exp[-\lambda_e(\mathcal{K})t], \tag{6.9}$$

where we stress the dependence of λ_e on the knot type via its size R_g. The average time between interactions is given by $\langle \tau_f \rangle \simeq \lambda_e^{-1}$ and the average number of stops on a time t is $\langle n_e \rangle = \lambda_e t$. The relative separation between two knots can be expressed as

$$\begin{aligned} \Delta x(\mathcal{K}_1, \mathcal{K}_2) &= v_{free}(t_{free}(\mathcal{K}_1) - t_{free}(\mathcal{K}_2)) \\ &= v_{free} t (\lambda_e(\mathcal{K}_2) - \lambda_e(\mathcal{K}_1)) \end{aligned} \tag{6.10}$$

where v_{free} is the velocity of the knots when no interactions occur (when hydrodynamics is negligible this is the same for all knots), t is the observation time and $t_{free} = t - \lambda_e t$. From this is clear that the separation between knots $\mathcal{K}_2$ and $\mathcal{K}_1$ is proportional to the difference of their entanglement rates, as expected.

Now, I will introduce a topology dependent disentanglement time: every time that the BRW undergoes a "stop", I require that it has to wait an amount of time that increases proportionally to its average entanglement number (see $\langle \pi \rangle$ in Fig. 6.9). The disentanglement time is picked from an exponential distribution with characteristic time given by the empirical one observed in the MD simulations (see Fig. 6.10), i.e.

$$t_w = -\ln x / \lambda_{\text{dis}} \tag{6.11}$$

where x is a random number between 0 and 1 and $\lambda_{\text{dis}}^{-1} = \tau_{\text{dis}}$. As discussed before, the disentanglement time τ_{dis} is expected to be a function of $\langle \pi \rangle$, i.e. to increase linearly with the ACN. One can therefore use:

$$\tau_{\text{dis}}(ACN) = A\langle \pi \rangle + \tau_{\text{dis}}(0_1) \tag{6.12}$$

where $A = 5\,\tau_{Br}$ is an empirical parameter fitted from the simulations and $\tau_{dis}(0_1) = 30\tau_{Br}$ is the empirical average disentanglement time of the unknot. In addition, long waiting times which are typical of head-on impalements are taken into account by adding a small probability ($q \simeq 0.05$, compatible with the bimodal distribution in Fig. 6.10) and conditioned to the fact that an entanglement event happened. For this one can set $\tau_{long} = A\langle \pi \rangle + 250$. So the average disentanglement time from a head-on impalement is still knot-dependent but is much longer than any characteristic disentanglement time for other types of entanglements.

As one can see from Fig. 6.11 this crudely simplified model strikingly recovers the non-monotonic mobility of the knots as a function of their ACN and can predict the shape of the arcs for many other values of the ratio $R_g(0_1)/l$ which controls the hitting probability.

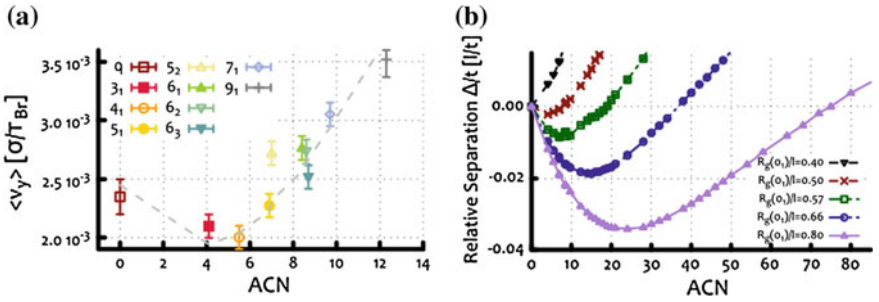

Fig. 6.11 **a** Average speed along the direction of the moderate field from Fig. 6.8b. The *dashed line* is obtained from the biased continuous random walk model, and corresponds to the (shifted and rescaled) *red curve* in (**b**). **b** Average relative separation (in units of lattice spacing over time) of the knots as a function of the ACN for different parameters, as predicted by the continuous random walk model. The *grey dashed line* in (**a**) is obtained by shifting the *red curve* in (**b**) by the value of $\langle v_y \rangle(0_1)$ and rescaling it by the free velocity v_{free}

It is worth stressing that in this simple description the only relevant parameters are the hitting rate, or τ_f, for the unknot and the parameters characterising the bimodal distribution of waiting (i.e. disentanglement) times, i.e. τ_{dis}. The values of these parameters are set in order to reproduce the data reported in Fig. 6.10. Once calibrated on the MD simulations, this model can be used to predict the shape of the electrophoretic arc for any arbitrarily large ACN without explicitly performing the MD simulation. In particular, it can predict the electrophoretic arc also for molecules with different length with respect to the size of the gel pores l. This enters as a parameter in the hitting probability λ_e, as longer molecules have larger size and hence larger λ_e.

Because simple, I argue that this model is able to show that the key physical mechanisms leading to the non-monotonic mobility at moderate field are the hitting and waiting times, which are both depending on the knot's topology, but in diametrically opposite ways (Fig. 6.10). Note that, as the random walker solely moves to the right, the field strength does not enter explicitly into the model, but rather, it is considered to be neither too weak to allow backward moves or too strong to completely suppress disentanglement of the knots. Both these cases in fact would not deliver an electrophoretic arc.

One can finally simplified model to predict the moderate field mobility and the shape of the electrophoretic arcs of DNA knots in gels of variable pore size, e.g. tuned via agarose concentration (Pernodet et al. 1997) or nano-wire growth cycle (Rahong et al. 2014). The plots presented in Fig. 6.11b suggest that tighter gels give rise to more curved (or deeper) arcs where the slowest knot has a higher ACN with respect to sparser gels. Moreover, since the entanglement rate λ_e and the disentanglement time τ_{dis} (both of these relative to the same quantities for the un-knot) should depend only on the ratio between the knot extension and the gel pore size l, a similar trend should be observed also by increasing the DNA loop contour length by keeping fixed l. This is in qualitative agreement with experiments, as electrophoretic arcs are straighter for

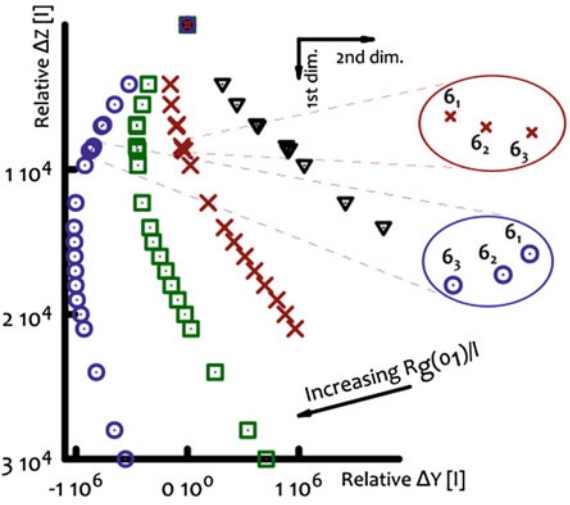

Fig. 6.12 Reconstruction of a 2D gel electrophoresis experiment from the data in Fig. 6.11b and zoom over the relative position of the family of 6-crossings knots for two cases in which the minimum of the arc is at their *left* and their *right*

shorter DNA molecules (Trigueros and Roca 2007). A further quantitative prediction can be drawn from these findings is that the relative position of the three 6-crossing knots can be controlled by tuning the pore size (Fig. 6.12) of the gel. Indeed the size of the pores determines whether the 6_1 Stevedore's knot is to the left or to the right of the minimum of the mobility curve: in the former case 6_1 will moves faster in the gel than the 6_2 and 6_3 knots (which, having higher ACN have also higher AEN), while in the latter case it will move more slowly. This detailed prediction could be tested in future electrophoresis experiments with knotted DNA loops moving within different gels.

6.3 Conclusions

In this Chapter I have studied the behaviour of linear, un-knotted circular and knotted polymers drifting in a disordered gel. There are several open questions in this field, which are all pertinent to the theoretical understanding of gel electrophoresis techniques, such as the anomalous mobility of ring polymers in gels, and the non-monotonic speed of knotted DNA samples.

In Sect. 6.1 I showed that the mobility of ring polymers moving through a physical gel is strongly affected by their interaction with the surrounding environment. Ring polymers can be slowed down by several order of magnitude by becoming entangled with the gel structure. This is strongly correlated with the fact that the topology of the rings is closed, and has to remain closed at all times. Linear polymers can disentangle from the gel structure with virtually no slowing down (or at least much more quickly than rings).

Because the entanglement of ring polymers becomes stronger as the field driving the polymers is increased, there exists a critical field E^* above which ring polymers will travel slower than their linear counterparts. In the limit of very large external fields, ring polymers show very low gel mobilities, as experimentally observed (Mickel et al. 1977; Cole and Åkerman 2003; Stellwagen and Stellwagen 2009).

It is also worth pointing out that this peculiar behaviour of rings in gels can be used to probe the microscopic disorder of porous materials. Ring polymers could in fact be adopted as "topological probes" and their mobility compared with that of linear samples, thereby providing us with information regarding the microscopic disorder of materials.

In Sect. 6.2 I studied a system of knotted polymers moving through a gel possessing rigid dangling ends. At weak fields one can recover the well-known linear relationship between migrating speed and knot-type while at stronger fields, one can instead observe a non-monotonic behaviour. This puzzling feature, has been tackled in the literature but never fully explained. In particular, in Weber et al. (2006a, b) the authors studied the effect of crawling of knots around gel obstacles and dragged by weak and strong fields. Although they reported a very interesting field inversion effect (where more complex knots were observed to travel slower than less complex ones) their findings would nonetheless lead to a monotonic response of the knots' speed as a function of their complexity, i.e. the knots would from a straight line in a 2D gel electrophoresis experiment. On the other hand, the findings presented in this chapter show that in order to obtain a non-monotonic response of the knots speed, the presence of dangling ends is key. Only by accounting for dangling ends, the non-monotonic speed, and therefore, the re-entrant envelope displayed by the knotted DNA strands, can be retrieved. This pattern can, in fact, be better understood by taking into account the topological interactions, or impalements, of the knots with the irregularities of the surrounding gel. While more complex knots assume more compact configurations, and hence smaller Stokes friction than simpler knots, they also experience more complex impalements with the gel and hence longer disentanglement times. These two competing effects give rise to the non-monotonic speed of the knots observed in the experiments, a feature that, remarkably, is absent for knotted loops moving in a regular gel (i.e. no dangling ends). It is also remarkable that the patterns observed in the experiments can be reproduced via a simple Biased Random Walk model, with "topology-dependent" hitting and disentangling times, where the depth of the arc pattern can be finely tuned via few key parameters. Even though it is clear that the findings reported in this chapter can reproduce the arc pattern thanks to the addition of dangling strands in the gel, it is still unclear what is the microscopic disentanglement mechanism undergone by the knots once they interact with the gel. While the results show that more complex knots take longer time to disentangle, the reason why this is the case is still an open question. This might be due to complex tightening around the dangling ends, which would be knot dependent, or due to some correlations between the strands that need to overcome the obstacle in order for the knot to re-establish its motion. Yet unexplained, this complex disentanglement mechanics is surely worth exploring in the future.

It is my hope that the results presented here will inform and stimulate further experimental and numerical investigations of the role of topology in the anomalous electrophoretic mobility of circular and knotted polymers. I aimed to provide models as simple as possible while retaining the essential physics, and to provide sound and testable outcomes that can inform more accurate experimental set-ups to separate bio-polymers of different topology.

It is also worth stressing that this chapter is a clear example of how topology not only affects the intrinsic properties of a polymer, such as its size (gyration radius), but also how it interacts with the surrounding environment. The "topological interaction" of a knotted DNA with the irregular environment of a physical gel, for instance, has been here shown to play a key role in driving the non-monotonic electrophoretic mobility of DNA topoisomers.

References

Adams, C.C.: The Knot Book: An Elementary Introduction to the Mathematical Theory of Knots W. H. Freeman and Company, New York (1994)

Alon, U., Mukamel, D.: Gel electrophoresis and diffusion of ring-shaped DNA. Phys. Rev. E **55**(2), 1783 (1997)

Arsuaga, J., Vazquez, M., McGuirk, P., Trigueros, S., Sumners, D.W., Roca, J.: DNA knots reveal a chiral organization of DNA in phage capsids. Proc. Natl. Acad. Sci. USA **102**(26), 9165 (2005)

Arsuaga, J., Vázquez, M., Trigueros, S., Sumners, D., Roca, J.: Knotting probability of DNA molecules confined in restricted volumes: DNA knotting in phage capsids. Proc. Natl. Acad. Sci. USA **99**(8), 5373 (2002)

Baerts, P., Basu, U., Maes, C., Safaverdi, S.: Frenetic origin of negative differential response. Phys. Rev. E **88**(5), 052109 (2013)

Baiesi, M., Maes, C., Wynants, B.: Fluctuations and response of nonequilibrium states. Phys. Rev. Lett. **103**(1), 010602 (2009)

Baiesi, M., Maes, C., Wynants, B.: The modified Sutherland-Einstein relation for diffusive nonequilibria. Proc. R. Soc. A **467**(2134), 2792 (2011)

Baiesi, M., Stella, A.L., Vanderzande, C.: Role of trapping and crowding as sources of negative differential mobility. Phys. Rev. E **92**, 042121 (2015)

Barkema, G., Marko, J., Widom, B.: Electrophoresis of charged polymers: simulation and scaling in a lattice model of reptation. Phys. Rev. E **49**(6), 5303–5309 (1994)

Bates, A., Maxwell, A.: DNA Topology. Oxford University Press, Oxford (2005)

Calladine, C.R., Collis, C.M., Drew, H.R., Mott, M.R.: A study of electrophoretic mobility of DNA in agarose and polyacrylamide gels. J. Mol. Biol. **221**(3), 981 (1991)

Calladine, C.R., Drew, H., Luisi, F.B., Travers, A.A.: Understanding DNA: The Molecule and How it Works. Elsevier Academic Press, London (1997)

Cebrián, J., Kadomatsu-Hermosa, M.J., Castán, A., Martínez, V., Parra, C., Fernández-Nestosa, M.J., Schaerer, C., Martínez-Robles, M.-L., Hernández, P., Krimer, D.B., Stasiak, A., Schvartzman, J.B.: Electrophoretic mobility of supercoiled, catenated and knotted DNA molecules., Nucl. Acids Res. **3112**(Ext 4232), 1 (2014)

Cole, K.D., Åkerman, B.: The influence of agarose concentration in gels on the electrophoretic trapping of circular DNA. Separ. Sci. Technol. **38**(10), 2121 (2003)

Di Stefano, M., Tubiana, L., Di Ventra, M., Micheletti, C.: Driving knots on DNA with AC/DC electric fields: topological friction and memory effects. Soft Matter **10**, 6491 (2014)

Dorfman, K.D.: DNA electrophoresis in microfabricated devices. Rev. Mod. Phys. **82**(4), 2903 (2010)
Duke, T.: Tube model of field-inversion electrophoresis. Phys. Rev. Lett. **62**(24), 2877 (1989)
Galajda, P., Keymer, J., Chaikin, P., Austin, R.: A wall of funnels concentrates swimming bacteria. J. Bacteriol. **189**(23), 8704 (2007)
Ghosh, P.K., Hänggi, P., Marchesoni, F., Nori, F.: Giant negative mobility of Janus particles in a corrugated channel. Phys. Rev. E **89**(6), 062115 (2014)
Guenet, J.M., Rochas, C.: Agarose sols and gels revisited. Macromol. Symp. **242**, 65 (2006)
Katritch, V., Bednar, J., Michoud, D., Scharein, R., Dubochet, J., Stasiak, A.: Geometry and physics of knots. Nature **384**, 142 (1996)
Kusner, R., Sullivan, J.: Möbius energies for knots and links, surfaces and submanifolds. Geometric Topology (Proceedings of the 1993 Georgia International Topology Conference) AMS/IP Studies in Advanced Mathematical, pp. 570–604 (1994)
Levene, S.D., Zimm, B.H.: Separations of open-circular DNA using pulsed-field electrophoresis. Proc. Natl. Acad. Sci. USA **84**(12), 4054 (1987)
Maffeo, C., Schöpflin, R., Brutzer, H., Stehr, R., Aksimentiev, A., Wedemann, G., Seidel, R.: DNA-DNA interactions in tight supercoils are described by a small effective charge density. Phys. Rev. Lett. **105**(15), 158101 (2010)
Mickel, S., Arena, V., Bauer, W.: Physical properties and gel electrophoresis behavior of R12-derived plasmid DNAs. Nucl. Acids Res. **4**(5), 1465 (1977)
Mogilner, A., Rubinstein, B.: The physics of filopodial protrusion. Biophys. J. **89**(2), 782 (2005)
Mohan, A., Doyle, P.: Effect of disorder on DNA electrophoresis in a microfluidic array of obstacles. Phys. Rev. E **76**(4), 040903 (2007a)
Mohan, A., Doyle, P.S.: Stochastic modeling and simulation of DNA electrophoretic separation in a microfluidic obstacle array. Macromolecules **40**(24), 8794 (2007b)
Olavarrieta, L., Martínez-Robles, M.L., Sogo, J.M., Stasiak, A., Hernández, P., Krimer, D.B., Schvartzman, J.B.: Supercoiling, knotting and replication fork reversal in partially replicated plasmids. Nucl. Acids Res. **30**(3), 656 (2002)
Pernodet, N., Maaloum, M., Tinland, B.: Pore size of agarose gels by atomic force microscopy. Electrophoresis **18**, 55 (1997)
Piili, J., Marenduzzo, D., Kaski, K., Linna, R.P.: Sedimentation of knotted polymers. Phys. Rev. E **87**(1), 012728 (2013)
Rahong, S., Yasui, T., Yanagida, T., Nagashima, K., Kanai, M., Klamchuen, A., Meng, G., He, Y., Zhuge, F., Kaji, N., Kawai, T., Baba, Y.: Ultrafast and wide range analysis of DNA molecules using rigid network structure of solid nanowires. Sci. Rep. **4**, 5252 (2014)
Rolfsen, D.: Knots and links. AMS Chelsea Publishing, Providence, Rhode Island (2003)
Rubinstein, M.: Discretized model of entangled-polymer dynamics. Phys. Rev. Lett. **59**(17), 1946 (1987)
Stasiak, A., Katritch, V., Bednar, J., Michoud, D., Dubochet, J.: Electrophoretic mobility of DNA knots. Nature **384**, 122 (1996)
Stellwagen, N.C., Stellwagen, E.: Effect of the matrix on DNA electrophoretic mobility. J. Chromatogr. **1216**(10), 1917 (2009)
Sugiyama, J., Rochas, C., Turquois, T., Taravel, F., Chanzy, H.: Direct imaging of polysaccharide aggregates in frozen aqueous dilute systems. Carbohydr. Polym. **23**(4), 261 (1994)
Trigueros, S., Arsuaga, J., Vazquez, M.E., Sumners, D., Roca, J.: Novel display of knotted DNA molecules by two-dimensional gel electrophoresis. Nucl. Acids Res. **29**(13), E67 (2001)
Trigueros, S., Roca, J.: Production of highly knotted DNA by means of cosmid circularization inside phage capsids. BMC Biotechnol. **7**, 94 (2007)
Viovy, J.: Electrophoresis of DNA and other polyelectrolytes: physical mechanisms. Rev. Mod. Phys. **72**(3), 813 (2000)
Viovy, J., Duke, T.: DNA electrophoresis in polymer solutions: Ogston sieving, reptation and constraint release. Electrophoresis **14**, 322 (1993)

Weber, C., Carlen, M., Dietler, G., Rawdon, E.J., Stasiak, A.: Sedimentation of macroscopic rigid knots and its relation to gel electrophoretic mobility of DNA knots. Sci. Rep. **3**, 1091 (2013)
Weber, C., Stasiak, A., De, : Los Rios, P., Dietler, G.: Simulations of electrophoretic collisions of DNA knots with gel obstacles. J. Phys.: Condens. Matter **18**(14), S161 (2006a)
Weber, C., Stasiak, A., De, : Los Rios, P., Dietler, G.: Numerical simulation of gel electrophoresis of DNA knots in weak and strong electric fields. Biophys. J. **90**(9), 3100 (2006b)
Whytock, S., Finch, J.: The substructure of agarose gels as prepared for electrophoresis. Biopolymers **31**(9), 1025 (1991)
Zia, R.K.P., Praestgaard, E.L., Mouritsen, O.G.: Getting more from pushing less: negative specific heat and conductivity in nonequilibrium steady states. Am. J. Phys. **70**(4), 384 (2002)

Chapter 7
Conclusions

What it all boils down to is 1 % inspiration and 99 % perspiration.

T.A. Edison

In light of the results of this Thesis, one could argue that joining the ends of a linear polymer has had an unimaginable effect on the polymer static and dynamic behaviours and it has had a much deeper consequences than one might have naïvely anticipated.

From the change of universality class (Chap. 2) to the possibility of displaying a kinetically arrested state at any temperature (Chap. 4) and to have different interactions with the surrounding environment depending on their knottedness (Chap. 6), ring polymers have been shown to offer a richness of behaviours whose full understanding is possibly one of the main theoretical challenges for the Polymer Physics community in the years to come.

All of this can be summarised by the notion that ring polymers assume well defined topological states, i.e. (un-)knotted and/or (un-)linked, and can interact via three types of inter- and intra-chain topological interactions: threading, linking and knotting. Clearly, these cannot be even defined in systems of linear, or topologically trivial, chains.

These interactions are here investigated in Chaps. 4, 5 and 6, and in each of them I have tried to focus on specific biologically-oriented examples and applications which allowed me to better grasp the meaning and consequences of these topological interactions in real-world problems.

In Chap. 4 I have shown that threadings play a major role in the dynamics of dense solutions of rings. In particular, under some conditions which are not too far (and possibly not far at all!) from experimentally realisable set-ups, the motion of dense solution of rings can be dominated by correlations induced by topological interactions (or "topological correlations") which lead a kinetic arrest, or a "topological glassy" state.

Linking between rings has been explored in Chap. 5, and in particular in the case of the Kinetoplast DNA. The remarkable and unique structure formed by the

D. Michieletto, *Topological Interactions in Ring Polymers*, Springer Theses,
DOI 10.1007/978-3-319-41042-5_7

mitochondrial genome of organisms of the class *Kinetoplastida* offers an exceptional example of how important this topological interaction is even in their bare existence and survival. I showed that the topological regulation of the network of linked rings thereby formed can be understood in terms of simple bio-physical models which, despite their simplicity, can provide us with some fresh insight into this mysterious structure.

Last, but not least, knotting represents one of the most studied and historically important topological (self-)interactions. Despite the enormous effort in characterising the behaviour of knots in various contexts, much is still to be understood. In Chap. 6 I brought my (little) contribution toward the general understanding of this topic by investigating the puzzling and unexplained non-monotonic speed of knotted DNA samples in 2D gel electrophoresis experiments at high fields. This long debated phenomenon has been found to be intimately related to topology as both, the knots' size and their interactions with the gel, are controlled by their knottedness.

Above all, I have here tried to take inspiration from the biological world to ask, and answer, questions which could be relevant and interesting for a broad spectrum of researchers. The scope of the work has always been to provide an accurate, although coarse-grained, description of the systems and to retain the key elements in play. The objective that I set myself was to provide clues toward a deeper understanding of the subjects and I, in particular, aimed to generate experimentally testable predictions and to inform further experiments which are, after all, the final proof of any theory.

Appendix A
Identifying Knots

Identifying unambiguously any knot type is, currently, impossible. The design of an algorithm that will make this possible is one of the biggest challenges for knot theorists in the years to come. Mathematically, knot types are usually identified by analysing the topological properties of the knot complement, i.e. the manifold formed by removing the knot from the space in which it is embedded ($S^3 - \mathcal{K}$), or the topological properties of the Seifert surface $\mathcal{S}$ constructed from a knot diagram representation of a knot (Adams 1994). In practice, these procedures are hardly translated into automated algorithms that can be repeated over thousands of knots. For this reason it is often preferred to use simpler methods, although less reliable. One of these methods is the computation of polynomials, such as the Alexander polynomial.

The construction of the Alexander polynomial starts from a knot diagram a knot (see Fig. A.1a). Being a knot diagram a 2D representation of a 3D object, it is not unique but depends on the perspective chosen for the projection. On the other hand, it can be shown that two knot diagrams of the same knot are equivalent, i.e. can be transformed into one another via a sequence of moves called "Reidemeister moves" (see Fig. A.1). In addition, knot diagrams that cannot be transformed into one another belong to different knot types. There are several quantities that can be calculated from knot diagrams, e.g. the minimal crossing number, the Dowker code, the bridge number or the Alexander and Jones polynomials. Here, I will describe the computation of the Alexander polynomial $\Delta(t)$.

The procedure is the following: (1) Assign a direction to the contour and mark the n crossings and n arcs between crossings (see Fig. A.1a); (2) Determine the sign of the crossings using the standard right-hand rule (see Fig. A.1b); (3) Construct an $n \times n$ matrix M, where the entries of the xth row are

$$M(x,i) = 1 - t;\ M(x,j) = -1;\ M(x,i) = t; \tag{A.1}$$

if the xth crossing is positive, or

$$M(x,i) = 1 - t;\ M(x,j) = t;\ M(x,i) = -1; \tag{A.2}$$

D. Michieletto, *Topological Interactions in Ring Polymers*, Springer Theses,
DOI 10.1007/978-3-319-41042-5

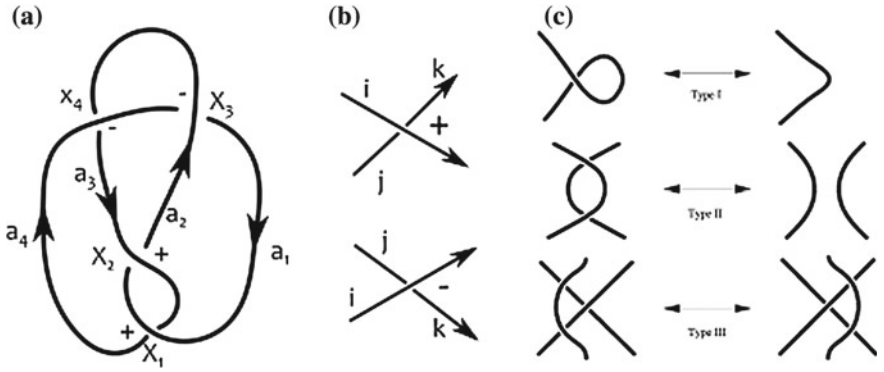

Fig. A.1 **a** Knot diagram of a 4_1 knot. **b** Positive and negative crossings. **c** The three types of Redemeister moves, from Orlandini and Whittington (2007)

if the xth crossing is negative, and where i, j, k are the strands forming the crossing such that i passes over j and k. (4) Delete one row and one column, i.e. take one minor of the matrix, and (5) compute its determinant $\Delta(t)$.

From the knot represented in Fig. A.1 one gets:

$$M(t) = \begin{pmatrix} 1-t & 0 & -1 & t \\ -1 & t & 1-t & 0 \\ -1 & 1-t & 0 & t \\ 0 & t & -1 & 1-t \end{pmatrix} \rightarrow M'(t) = \begin{pmatrix} t & 1-t & 0 \\ 1-t & 0 & t \\ t & -1 & 1-t \end{pmatrix} \tag{A.3}$$

whose determinant is $\Delta(t) = -t^2 + 3t - 1$: the Alexander polynomial of a figure of eight (4_1) knot.

Because Alexander polynomials of different knot diagrams of the same knot can differ up to $\pm t^m$ with $m \in \mathbb{Z}$, it is common practice to compute $\Delta(-1)$ (and identify $\Delta(-1)$ with $-\Delta(-1)$) so to avoid ambiguities. The Alexander polynomial is a good knot invariant for a number of practical applications, in particular when dealing with many randomly generated configurations. On the other hand, it cannot distinguish between, for instance, the 8_{20} knot and the Granny $3_1\#3_1$ knot or between a knot and its mirror image and it is, therefore, to be used with caution.

References

Adams, C.C.: The Knot Book: An Elementary Introduction to the Mathematical Theory of Knots. W.H. Freeman and Company, New York (1994)

Orlandini, E., Whittington, S.G.: Statistical topology of closed curves: some applications in polymer physics. Rev. Mod. Phys. **79**(2), 611 (2007)